NASA TECHNICAL MEMORANDUM

NASA TM X-2693

NASA TM X-2693

LONGITUDINAL AERODYNAMIC AND PROPULSION CHARACTERISTICS OF A PROPULSIVE-WING V/STOL MODEL AT HIGH SUBSONIC SPEEDS

by Leland B. Salters, Jr., and James W. Schmeer

Langley Research Center
Hampton, Va. 23365

NATIONAL AERONAUTICS AND SPACE ADMINISTRATION • WASHINGTON, D. C. • JANUARY 1973

1. Report No.	2. Government Accession No.	3. Recipient's Catalog No.
NASA TM X-2693		

4. Title and Subtitle	5. Report Date
LONGITUDINAL AERODYNAMIC AND PROPULSION CHARACTERISTICS OF A PROPULSIVE-WING V/STOL MODEL AT HIGH SUBSONIC SPEEDS	January 1973
	6. Performing Organization Code
7. Author(s)	8. Performing Organization Report No.
Leland B. Salters, Jr., and James W. Schmeer	L-8500
	10. Work Unit No.
9. Performing Organization Name and Address	501-17-01-10
NASA Langley Research Center Hampton, Va. 23365	11. Contract or Grant No.
	13. Type of Report and Period Covered
12. Sponsoring Agency Name and Address	Technical Memorandum
National Aeronautics and Space Administration Washington, D.C. 20546	14. Sponsoring Agency Code

15. Supplementary Notes

16. Abstract

The aerodynamic and propulsion characteristics of a 1/6-scale propulsive-wing V/STOL air-powered model was investigated over the Mach number range from 0.40 to 0.96 and at angles of attack from -5° to 15° for several fan rotational speeds. Three fan-duct-exit configurations were tested, including two exit areas. The model with 25-percent-thick wing had a drag-rise Mach number of 0.85, which is typical of aircraft with thinner, conventional, unswept wings.

17. Key Words (Suggested by Author(s))	18. Distribution Statement
V/STOL Propulsive wing Aerodynamic characteristics Subsonic cruise	Unclassified – Unlimited

19. Security Classif. (of this report)	20. Security Classif. (of this page)	21. No. of Pages	22. Price*
Unclassified	Unclassified	74	$3.00

*For sale by the National Technical Information Service, Springfield, Virginia 22151

LONGITUDINAL AERODYNAMIC AND PROPULSION CHARACTERISTICS OF A PROPULSIVE-WING V/STOL MODEL AT HIGH SUBSONIC SPEEDS

By Leland B. Salters, Jr., and James W. Schmeer
Langley Research Center

SUMMARY

The aerodynamic and propulsion characteristics of a 1/6-scale propulsive-wing V/STOL air-powered model have been investigated at Mach numbers from 0.40 to 0.96. The 1.049-meter-span model was powered by four (14-cm-diam) tip-turbine fans located in the thick wings. The fans induced air into the leading edge of the wing and exhausted it from the trailing edge. Three fan-duct-exit configurations were investigated, including two exit areas. The investigation covered a range of angles of attack from -5° to 15° for several fan rotational speeds.

The results of the investigation indicated that the model with a 25-percent-thick propulsive wing had a drag-rise Mach number of 0.85, which is typical of aircraft with thinner, conventional, unswept wings. Significant changes in longitudinal stability characteristics resulted from changes in the fan-duct-exit configurations and fan rotational speeds. For a given fan rotational speed a larger fan-duct exit area increased mass flow through the system but decreased net thrust.

INTRODUCTION

The need for efficient V/STOL high-speed aircraft has been recognized by the aircraft industry and military services for some time. The ability of these type aircraft to operate from small airports and small unprepared landing areas becomes increasingly important in view of the present trend in modern aircraft requirements for larger landing areas and stronger hard-surfaced runways. Because of the growing needs for V/STOL aircraft, NASA, as well as industry, has investigated a number of different concepts; such as, deflected slipstream (ref. 1), tilt-wing-propeller (refs. 2 and 3), fan-in-wing (ref. 4), lift-thrust fans (refs. 5 and 6), and lift-thrust jets (refs. 7, 8, and 9).

Another V/STOL concept is the propulsive-wing type (ref. 10) in which the turbine-driven fans are located in thick wings. The wing fans, oriented in the axial-thrust direction, induce air into the leading edge of the wing and exhaust it through the trailing edge. Either lift and/or axial thrust are obtained by means of a slipstream deflection and modu-

lation system. In the cruise mode, variable angle flaps aid in the control of the fan flow direction as well as provide expansion surfaces for the two-dimensional turbine exhaust flow from the gas generator (similar to jet-flap concept).

The purpose of this exploratory investigation, conducted in the Langley 16-foot transonic tunnel, was to determine some of the aerodynamic performance characteristics of the propulsive-wing model in the high-speed and cruise modes. The 1/6-scale model was powered by compressed air which was used to drive four tip-turbine fans and to simulate the turbine (gas-generator) exhaust flow. The model incorporated outboard horizontal tails and a central vertical tail. Two flap fairings and fan efflux areas were investigated.

A six-component strain-gage balance was used to measure the model forces and moments, including thrust components. Internal flow characteristics from the fan and flap jet are also included. Data were obtained through a Mach number range of 0.40 to 0.96 at angles of attack from -5° to 15° for several power settings (rpm) of the tip-turbine fans.

A study of the interference effects due to a protuberance (knuckle simulator) on the sting immediately downstream of the fuselage is presented in the appendix.

SYMBOLS

The aerodynamic coefficients in this paper are referenced to the stability axes and include internal force and moments due to the propulsive systems.

A_i fan-duct inlet area at rake station, m^2

C_D drag coefficient, $\frac{D}{qS}$

$\frac{dC_D}{dM}$ slope of drag-rise curve

C_L lift coefficient, $\frac{L}{qS}$

C_{L_α} lift-curve slope, $\frac{dC_L}{d\alpha}$

C_m pitching-moment coefficient, $\frac{M_Y}{qS\bar{c}}$

$C_{p,c}$ fuselage-cavity pressure coefficient, $\frac{p_c - p_\infty}{q}$

$C_{T,n}$ net-thrust coefficient, $\frac{F_t - D_r}{qS}$

$C'_{T,n}$ net-thrust coefficient for single fan, $\frac{F_f - \dot{m}_i V_\infty}{qS}$

$C_{p,s}$ afterbody-shell pressure coefficient, $\frac{p_s - p_\infty}{q}$

C_μ momentum- or gross-thrust coefficient, $\frac{F_t}{qS}$

C'_μ gross-thrust coefficient for single fan or flap jet, $\frac{F_f}{qS}$ or $\frac{F_j}{qS}$

c local chord, m

$\bar{c}$ mean geometric chord, 0.5990 m

D drag, including thrust component, positive downstream, N

D_r ram drag, $\sum_{k=1}^{4} (\dot{m}_i)_k V_\infty$, N

F_f fan gross thrust, N

F_j flap-jet thrust, N

F_t total gross thrust, $\sum_{k=1}^{4} (F_f)_k + \sum_{l=1}^{2} (F_j)_l$, N

k designation number for fans

L lift, including thrust component, N

l designation number for jet flaps

M free-stream Mach number

M_Y pitching moment, including thrust component, m-N

$\dot{m}_d$ fan-drive-air mass flow, kg/sec

$\dot{m}_{d,ref} = \dot{m}_d \frac{\sqrt{\theta}}{\delta}$, kg/sec

$\dot{m}_f$ fan-duct-exit mass flow, kg/sec

$\dot{m}_{f,ref} = \dot{m}_f \frac{\sqrt{\theta}}{\delta}$, kg/sec

$\dot{m}_i$ fan-duct-inlet mass flow (see eq. (4)), kg/sec

$\dot{m}_j$ flap-jet mass flow, kg/sec

$\dot{m}_{j,ref} = \dot{m}_j \frac{\sqrt{\theta}}{\delta}$, kg/sec

n fan rotational speed, rpm

$n_{ref} = \frac{n}{\sqrt{\theta}}$, rpm

p static pressure, N/m^2

p_c fuselage-cavity static pressure, N/m^2

p_∞ free-stream static pressure, N/m^2

p_s afterbody-shell average static pressure, N/m^2

p_t total pressure, N/m^2

q free-stream dynamic pressure, N/m^2

R gas constant for air, 287.3 $\frac{N\text{-}m}{kg\text{-}K}$

r/R fractional radius to rake probe, where R is radius of duct

S reference wing area, 0.675 m^2

T_t total temperature, K

V_f fan-duct-exit equivalent velocity (see eq. (3)), m/sec

V_j flap-jet-exit equivalent velocity (see eq. (6)), m/sec

V_∞ free-stream velocity, m/sec

x axial wing coordinates

y vertical wing coordinates

α model angle of attack with reference to waterline, deg

γ ratio of specific heats for air, 1.4

δ ratio of free-stream static pressure to sea-level standard pressure, $p_\infty/101.325$, kN/m^2

θ ratio of total temperature to sea-level standard temperature, $T_t/288.2$, K

Subscripts:

f fan-duct exit

i fan-duct inlet

j flap jet

ref referred to sea-level standard conditions

t total

∞ free-stream conditions

APPARATUS AND METHODS

Wind Tunnel

The investigation was conducted in the Langley 16-foot transonic tunnel which is a single-return, atmospheric wind tunnel with an octagonal test section and continuous air exchange. The tunnel has a continuously variable speed range from Mach number 0.20 to 1.30.

Model and Support System

Photographs of the 1/6-scale V/STOL model mounted on a sting in the test section are shown in figure 1. A three-view drawing showing the principal dimensions is given in figure 2(a). The significant geometric properties of the model are indicated in table 1. A cross-sectional side view of the body indicating the compressed-air passages is shown in figure 2(b), and cross-sectional side views showing typical fan-duct and flap-jet configurations are shown in figure 2(c). The removable fan exit fairings permitted testing with two different fan-duct exit areas. The flap fairings could only be used when the fan exit fairings were off and were designed to make the flap lower surface parallel to the wing-chord plane. Configuration identification is listed in table 2.

The air was brought into the model through the sting and the hollow tubular-shaped force balance to a bellows-plenum-chamber arrangement which bridged the metric and nonmetric parts of the model (fig. 2(b)). A schematic diagram of the model internal airflow and propulsion system is shown in figure 2(d). The fan-drive air was heated to 305 K to prevent moisture in the inlet air from freezing on the duct walls. A small amount of air was bled from the plenum chamber to the oil-mist lubrication system for the fan bearings (fig. 2(b)).

For boundary-layer transition, 0.25-cm strips of No. 120 carborundum grit were located on the fuselage and wing-tip booms 10.16 cm from the respective noses. The strips were placed on the wings 2.92 cm from the leading edge, on the horizontal tail 18 percent of the chord from the leading edge, and on the vertical tail 14 percent of the chord from the leading edge.

Instrumentation

Sixteen-tube cruciform inlet rakes with eight adjacent static orifices and a thermocouple installed in the fan ducts were used to calculate the mass flow of air entering each fan duct (see fig. 2(c)). Twenty-tube cruciform efflux rakes in the fan ducts and twelve-tube rakes in each of the flap-jet exits were used to evaluate exit momentums (gross thrust).

A vane-type turbine flowmeter was used to measure the total supply airflow to the model, as shown in figure 2(d). The airflow to the two flap jets providing engine-turbine exhaust simulation was measured by means of calibrated metering orifices. The drive airflow rate to each fan was determined from static calibrations of mass flow as a function of static-pressure measurements in the fan-drive air-supply pipes downstream of the individual remote-control valves.

A six-component strain-gage balance was used to measure overall model forces and moments, including both external and internal components. Three static orifices

located in the fuselage base were used to correct base force to a condition of free-stream static pressures. Model angle of attack was determined by means of a strain-gage-type attitude transmitter located in the fuselage. Rotational speed of the four fans was measured by electromagnetic pickups mounted in the fan hubs.

Tests

Six-component balance data, flowmeter, thermocouple, pressure, and fan-rotational-speed data were recorded simultaneously by means of a magnetic tape system over a Mach number range from 0.40 to 0.96, an angle-of-attack range from -5° to 15°, and fan rotational speeds from 24 000 to 36 000 rpm. Reynolds number based on wing-chord length (not including flap) of 0.5990 m ranged from 4.73×10^6 to 7.75×10^6.

Data Reduction

These data are referred to the stability-axis system with the moments referenced to the mean geometric quarter-chord. The aerodynamic coefficients include the components of internal thrust forces.

Gross thrust was calculated for each fan and flap-jet exit using the respective total-pressure rakes and thermocouples located near their exits and assuming that the flow was fully expanded to free-stream static pressure. The following equations were applied to each fan or flap jet and the resulting thrusts were summed to give the model total gross-thrust coefficient C_μ: For fan gross thrust,

$$F_f = \dot{m}_f V_f \tag{1}$$

where

$$\dot{m}_f = \dot{m}_i + \dot{m}_d \tag{2}$$

$$V_f = \sqrt{\frac{2\gamma}{\gamma - 1} RT_{t,f}\left[1 - \left(\frac{p_\infty}{p_{t,f}}\right)^{\frac{\gamma-1}{\gamma}}\right]} \tag{3}$$

$$\dot{m}_i = p_i A_i \sqrt{\frac{2}{RT_{t,i}}\left(\frac{\gamma}{\gamma - 1}\right)\left(\frac{p_{t,i}}{p_i}\right)^{\frac{\gamma-1}{\gamma}}\left[\left(\frac{p_{t,i}}{p_i}\right)^{\frac{\gamma-1}{\gamma}} - 1\right]} \tag{4}$$

and $\dot{m}_d$ is obtained from static calibrations of mass flow as a function of static pressure in the supply line. For flap-jet thrust,

$$F_j = \dot{m}_j V_j \tag{5}$$

where $\dot{m}_j$ is obtained from calibrated metering orifices and

$$V_j = \sqrt{\frac{2\gamma}{\gamma - 1} RT_{t,j}\left[1 - \left(\frac{p_\infty}{p_{t,j}}\right)^{\frac{\gamma-1}{\gamma}}\right]} \tag{6}$$

RESULTS

The results of the investigation are presented in the following figures:

DISCUSSION

Longitudinal Aerodynamic Characteristics

The basic data presented in figures 3 to 8 were obtained from two different wind-tunnel test procedures: (1) constant angle of attack of 0° with variable Mach number (figs. 3(a), 7, 8(a), and 8(c)) and (2) variable angle of attack at constant Mach numbers of 0.40, 0.60, 0.80, and 0.90 (figs. 3(b), 3(c), 4, 5, 6, 8(b), and 8(d)). It should be noted that all of the data presented herein are for untrimmed flight conditions.

Variation with Mach number, $\alpha = 0^\circ$.- The lift curves, together with the pitching-moment curves in figures 3(a), 7, 8(a), and 8(c), show decreases in C_L with accompanying increases in C_m. The variations in lift and pitching moments indicate that the areas on the model experiencing these changes in lift are located downstream of the moment center. One of the most significant variations was the rather sudden loss in lift and increase in pitching moment with increase in Mach number from about $M = 0.93$ to 0.95. The decrease in lift was caused by a rapid decrease in static pressure on the bottom of the flap and adjacent surfaces, as indicated by static-pressure measurements made during a previous (unpublished) investigation. This pressure change was probably associated with the rearward movement of the model shock waves with increasing Mach number in

the transonic regime. The shape of the undersurface of the flap and adjacent surfaces apparently influenced this phenomenon, as indicated by a comparison of figures 3(a), 7, and 8(c).

The effect of fan-duct configuration on the aerodynamic characteristics may be noted by a comparison of figures 3(a), 7, and 8(c). The removal of the fan exit fairing, as in changing from configuration 1 to configuration 5, caused a small increase in lift but decreased the moment coefficient. The addition of the flap fairing, as in changing from configuration 5 to configuration 6, increased the lift considerably and decreased the moment significantly. Dividing the lift increment into the moment increment to determine the effective moment arm indicates that the change in lift for each configuration occurred near the fan-duct exit. A possible explanation for the change in model lift at the fan-duct exit is that the deflection of the jet, as it was exhausted into the free stream, was different for each configuration. A large lift increase occurred due to the addition of the wedge to the bottom surface of the flap, as in changing from configuration 5 to configuration 6. This 2.5° wedge rotated the upper boundary of the emerging jet downward 2.5° which in turn deflected the entire jet downward an unknown amount. The reaction on the model due to the deflection of the jet downward appeared as an increase in lift. The location of the lift increment behind the model moment center added a negative increment to the pitching-moment coefficient.

Variation with lift coefficient.- The pitching-moment coefficient versus lift coefficient curves for Mach numbers 0.40, 0.60, 0.80, and 0.90 for various configurations are shown on the variable angle-of-attack figures (figs. 3(b), 3(c), 4, 5, 6, 8(b), and 8(d)). These data indicate that the model was stable over most of the range of angle of attack for configurations incorporating the horizontal tail and for power-on conditions. For power-off conditions (windmilling fans), configuration 6 (fig. 8(b)) was unstable at low lift coefficients for Mach numbers less than 0.90. At moderate lift coefficients, all configurations, including horizontal tail-off configurations (2 and 3), exhibited a strong, sometimes abrupt, increase in stability.

The aerodynamic phenomena causing the changes in slope of the pitching-moment curves may be identified by referring to references 11 and 12 in which the same type curves occur for an unswept-wing-fuselage combination (with no horizontal tail). As indicated by the wing pressure distributions in these references, the changes in slopes occurred at the angle of attack at which leading-edge separation (with reattachment) occurred. At that point the pressure distributions lost the peak leading-edge pressures, which were replaced by a plateau of higher pressure, the downstream edge of the plateau extending further downstream. This caused the center of pressure to move downstream, producing a more negative pitching moment and a stable slope. The same phenomena were observed in wing pressure distributions (unpublished) of the present model.

The effect of the horizontal tail on the longitudinal aerodynamic characteristics may be seen in figure 9(a), where data for configurations 1 and 2 are compared at fan rotational speed of 28 000 rpm. The strong stabilizing effect of the tail is clearly evident at all Mach numbers. The figure also shows that the presence of the tail increased the slope of the lift curves. This is more clearly shown in figure 9(b) where the lift-curve slopes C_{L_α}, taken near $\alpha = 0^\circ$, are plotted against Mach number for two fan rotational speeds. The lift-curve slopes were increased by from 0.012 to 0.014 by the presence of the horizontal tail which increased the wing effective aspect ratio. Because of this increase in effective aspect ratio, the rate of increase of C_D with C_L (induced drag) was smaller for the tail-on configuration (fig. 9(a)).

Effect of fan rotational speed.- A comparison of figure 8(b) (power-off) and figure 8(d) (36 000 rpm) indicates that for configuration 6 an increase in fan rotational speed increases the lift and decreases pitching moment over the entire range of angle of attack covered in this paper. This was apparently caused by the downward deflection of the jet at the jet exit, as mentioned previously. However, for configurations incorporating the fan exit fairing (configurations 1, 2, 3, and 4), change in fan rotational speed did not influence the lift and pitching moment greatly or consistently, as shown for instance in figure 3(a), which seems to indicate that the deflection of the jet at the jet exit was small.

In comparing figures 8(b) and 8(d) it may also be observed that fan rotational speed affected the stability characteristics for configuration 6. Under power-off conditions the model was unstable at negative and low positive angles of attack but was stable at higher angles of attack. However, at 36 000 rpm fan rotational speed, the configuration was stable over the entire angle-of-attack range. A physical mechanism by which the fan rotational speed might affect the model stability would be its influence on the wing upper-surface leading-edge flow separation characteristics. The rotational speed of the fan determined the mass-flow ratio at the fan-duct inlet, and the mass-flow ratio controlled the location of the stagnation line on the inlet and, thereby, the spillage flow. Since part of the leading edge of the inlet was also the leading edge of the wing upper surface, the location of the stagnation line and spillage flow would also affect the flow over the wing upper surface, especially near the leading edge, and, as a consequence, the leading-edge separation characteristics. Evidence of these effects is shown in reference 13 where pressure distributions near nose inlet leading edges for bodies of revolution indicate that negative pressure peaks near the inlet leading edges which usually exist at low mass-flow ratios may be eliminated by increasing the mass-flow ratio.

Figure 9(b) also indicates that the increase in fan rotational speed from 24 000 to 28 000 rpm increased C_{L_α}, especially at the lower Mach numbers. This increase in C_{L_α} is probably due to the increase in thrust.

Effect of vertical tail.- The effect of the vertical tail on model drag is shown in figure 10 to be small and on the order of the balance accuracy. The effect of the vertical tail on pitching-moment coefficient and lift coefficient was insignificant and therefore not presented.

Drag-rise Mach number.- In figure 11 is shown the variation of the drag of configuration 6 with tunnel Mach number at 0° angle of attack. The curve with square symbols represents cross-plotted data at a net-thrust coefficient of zero and simulates the condition where sufficient power is applied to the fans to overcome and exactly balance the internal drag of the model. As ordinarily defined $\left(dC_D/dM = 0.1\right)$, the drag rise for the model at zero net-thrust coefficient occurred at about Mach number 0.85 which is considered very good for a thick wing, especially in combination with a blunt fuselage with a relatively low fineness ratio of 6.5.

Internal Aerodynamic Characteristics

In order to give some indication of the internal flow characteristics of the propulsive wing, data for a typical fan and fan-duct system (left outboard, fan 1) are presented in figures 12 to 15 and for a typical flap jet (left flap jet) in figure 16. Because the investigation was terminated by failure of the model bellows before the test program had been completed, the data for configurations 5 and 6 are incomplete; therefore, only data points, rather than complete curves, could be presented on these plots. Configurations 1 to 4 incorporated the small fan-duct exit area (102.58 cm^2) and configurations 5 and 6 the large area (134.84 cm^2). The term "windmill" refers to power-off conditions where the rotation of the fan was produced by the local air velocity through the fan blades. It should be noted that for configurations 1 to 4 the minimum cross-sectional area of the fan duct occurred at the exit but for configurations 5 and 6 at the fan rotor. In the latter case the exit area was about 21 percent larger than the minimum cross-sectional area of the fan duct.

Effect of fan rotational speed.- The effect of fan rotational speed on the gross-thrust coefficient C'_{μ} is shown in figure 12(a). Since the gross-thrust coefficient is based on the momentum of the air at the fan-duct exit, a positive thrust coefficient is indicated for windmill conditions of the fan, the momentum in this case being produced by flow induced through the duct by tunnel free-stream velocity. Gross thrust increased fairly linearly with increase in fan rotational speed for each Mach number.

Figure 12(a) indicates that for a given fan rotational speed, enlarging the fan-duct exit cross-sectional area from the small to the large areas (31-percent increase), in general, decreased the gross-thrust coefficient. Although the mass flow increased slightly (see fig. 12(c)), it was not a sufficient increase to negate the effects of the larger

decrease in velocity at the exit, causing a decrease in momentum. The restriction to the flow at the minimum cross-sectional area probably limited the mass-flow increase.

The effect of fan rotational speed on the net-thrust coefficient is shown in figure 12(b). The net-thrust coefficient $C'_{T,n}$ was obtained by subtracting the ram drag coefficient from the gross-thrust coefficient C'_{μ}. It therefore represents the change in momentum of the air from free-stream conditions upstream of the fan-duct inlet to the exit. The change in momentum was produced by the inlet, the fan, the exhaust air from the tip turbine, and the internal aerodynamic drag of the duct and fan. Due to the introduction of tip-turbine exhaust air into the fan duct, the mass flow of air at the fan-duct exit was greater than that at the inlet except for power-off conditions. The ram drag was based on the mass flow at the inlet only and does not include the mass flow of the tip-turbine exhaust air. The negative net-thrust-coefficient values for power-off conditions represent the loss in momentum from free-stream conditions to the fan-duct exit and are indicative of the internal drag of the fan duct, including the windmilling fan.

The data in figure 12(b) show that increasing the fan-duct exit area from that of configurations 1 to 4 to that of configurations 5 and 6 decreased the values of net-thrust coefficient for a given fan rotational speed. The effect of changes in duct-exit area on the net thrust of the fan-duct system is related to the fan performance characteristics. Standard bench tests for fans show a large effect of discharge-air volume on total pressure at the fan discharge, and from fan-performance curves obtained in these tests, an ideal fan-discharge area may be determined for maximum thrust. Any departure from this ideal discharge area, one way or the other, decreases thrust. The same principles apply to the present case except for the addition of external flow. The effect of external flow on ideal fan-discharge area for this model would not be expected to be large. The data would indicate that the small exit area was closer to the ideal-maximum-thrust area than the larger exit area.

The variation of mass flow of air through the fan duct with fan rotational speed is shown in figure 12(c). The mass flow was referred to standard conditions by correcting free-stream static pressure and temperature to standard sea-level conditions. Increasing the exit area evidently decreased the back pressure on the fan, resulting in an increase in mass flow. Under power-off conditions, the windmilling fan acted as a moving-van-type flowmeter and indicated an increase in fan rotational speed with increase in mass flow for the larger exit area. Although other studies have indicated choking conditions near the fan-duct exit at the higher Mach numbers, the regularity of the curves, specifically at the higher Mach numbers, seems to indicate no adverse effects due to compressibility or choke.

The effect of fan rotational speed on the pressure ratio (ratio of total pressure in the fan-duct exit to the free-stream static pressure) is presented in figure 12(d). This

figure indicates that increasing the fan-duct exit area by about 31 percent decreased the pressure ratio in the exit by about 15 percent for Mach numbers 0.90 and 0.80, 9 percent for $M = 0.60$, and about 4 percent for $M = 0.40$. In order to maintain a pressure ratio of 1.7 in the fan-duct exit at Mach number 0.90, a fan rotational speed of about 22 000 rpm was required for the smaller area and about 35 000 rpm for the larger area.

The fan was designed for a total-pressure ratio $p_{t,f}/p_{t,i}$ of 1.25 at static conditions; but the highest total-pressure ratio for data from figure 12(d) was about 1.18, which indicates that the fan was operating well within design limits. This probably accounts for the smoothness and regularity of the curves.

Effect of fan efflux pressure ratio.- The variation of the fan-duct-exit pressure ratio with the gross-thrust coefficient and the net-thrust coefficient is shown in figure 13. These curves were included mainly for correlation with jet-exit data where pressure ratio is the primary parameter.

The variation of net-thrust coefficient for fan 1 with the mass-flow rate of air used to power the tip turbine is presented in figure 14. This figure also indicates that power requirements to produce a given thrust were greater for the large fan-duct exit area (configurations 5 and 6) than for the small exit area (configurations 1 to 4). These results may appear inconsistent with the principles involved where efficiency increases and power requirements decrease with increase in mass flow and reduced velocity. In the present case, however, the jet exit only, and not the entire fan-duct area, was increased, and the mass flow did not increase in proportion to the exit-area increase.

The effect of fan rotational speed on the total-pressure distribution in the fan duct, downstream of fan 1, is shown in figure 15 for Mach numbers 0.40 and 0.90 and for configurations 1 and 6. Both horizontal and vertical rakes indicate a significant decrease in total pressure in the central portions of the rakes for both configurations and both Mach numbers. This loss in total pressure was apparently associated with the bluntness of the fan-afterbody shape and resulting flow separation. The design of the fan afterbody incorporated a series of three concentric ring airfoils designed to decrease flow separation on the downstream end of the afterbody. The loss in total head in the central portion of the fan duct would probably have been much greater without the ring airfoils; however, the effectiveness of the ring airfoils was not determined in this investigation. The bluntness of the fan afterbody was necessitated by the location of the slipstream deflection system, used in the hovering and transition modes of flight, immediately downstream of the fan.

Data from a previous investigation (unpublished) obtained from total pressure rakes at the fan-duct exit indicate that the total-pressure distribution in the exit had less distortion than at the present location of the rakes. These results would be expected for two reasons: (1) the flow at the fan-duct exit had a greater time and distance to recover from

the distortion at the afterbody and (2) the contraction ratio, the cross-sectional area being less at the exit than at the present location of the rake, produced more uniformity in the flow distribution.

The vertical part of the rake showed a lack in symmetry in the total-pressure distributions about the duct center line (r/R = 0), the total-pressure values being greater above the center line than below. Apparently, this resulted from the curvature of the fan-duct center line slightly downward, downstream of the fan afterbody.

The pressure ratios were, in general, higher on the left side of the fan duct than on the right side; the reason for this is not known. However, the location of the wing boom on the left side of the fan duct may have produced an unsymmetrical flow distribution in the lateral direction.

The loss in total pressure due to the afterbody wake, in general, covered the r/R range from about 0.70 to -0.70, which represents about 50 percent of the cross-sectional area of the fan duct.

Variation of flap-jet flow characteristics with fan-duct-exit pressure ratio.- The effect of pressure ratio in the flap-jet exit on the thrust coefficient is shown in figure 16(a) for a typical (left) flap jet. The total pressures in the flap jets were usually set equal to that of the fan-duct exit except for some data of configurations 5 and 6. In contrast to the flow conditions for the fan-duct exit, where the flow was a combination of inlet air from the tunnel free stream and exhaust air from the tip turbine, the flap-jet air was supplied completely from the compressed air supply. There was, therefore, no ram air associated with the flap-jet flow. Figure 16(b) indicates the variation of mass flow in the left flap jet with the pressure ratio in the exit. Mass flow was measured by supercritical sharp-edged metering orifices in the air-supply tubes, instead of the pressure-temperature relationships in the exit.

The fact that the data for Mach numbers 0.40 to 0.90 fall on the same line indicates that the Mach number and the external-flow variations had no significant effect on the mass flow through the flap jet.

CONCLUSIONS

An investigation of the propulsion and aerodynamic characteristics of a 1/6-scale propulsive-wing V/STOL air-powered model in the cruise mode indicated the following conclusions:

1. Although the propulsive wing was geometrically thick (thickness-to-chord ratio of 25 percent), aerodynamically it was relatively thin, as indicated by the drag rise which occurred at a Mach number of about 0.85.

2. Significant changes in pitching moment and model stability occurred at Mach numbers above 0.85. These changes were greatly influenced by flap undersurface modifications and fan rotational speed.

3. The presence of the outboard horizontal tail increased the effective aspect ratio of the model, as indicated by the significant increase in the slopes of the lift curves and decrease in induced drag.

4. Increasing the fan-duct exit area 31 percent increased the mass flow of air for both power-on and power-off conditions but decreased the net thrust. Power requirements to produce a given thrust were also increased.

Langley Research Center,
National Aeronautics and Space Administration,
Hampton, Va., November 30, 1972.

APPENDIX

INTERFERENCE EFFECTS OF KNUCKLE ON MODEL AERODYNAMIC CHARACTERISTICS

In a previous (unpublished) investigation of the model, an articulated sting was used to obtain a large angle-of-attack range. This articulated sting incorporated a knuckle located near the downstream end of the fuselage (fig. 17(a)). The basic sting was cylindrical in shape, diameter of 10.80 cm, and cross-sectional area of 91.7 cm^2. The maximum cross-sectional area of the knuckle was 507 cm^2 and represented a sudden enlargement in the sting cross-sectional area which, from an aerodynamic point of view, presented the possibility of significant interference effects on the model.

In the present investigation, a cylindrical sting of 10.80-cm diameter was used. In order to evaluate the interference effects of the knuckle, a knuckle simulator (fig. 17(b)) was installed on the sting for some of the wind-tunnel tests. The locations of the static orifices on the afterbody are shown in figures 17(b) and 17(c).

The presence of the knuckle decreased model drag fairly consistently over the whole Mach number range covered in this investigation, as indicated in figure 18. The mechanism by which model drag was decreased was the increase in static pressure on the rearward sloping surfaces of the fuselage. This was indicated by the increase in static pressure in the body cavity, as shown in figure 19, and the increase in static pressure on the afterbody surfaces, as shown in figures 20 and 21.

The effects of knuckle interference on lift and pitching moment, also shown in figure 18, are generally small and not particularly significant.

In figure 22 is shown the effect of the presence of the knuckle on the drag-rise characteristics of the model at zero angle of attack. The presence of the knuckle decreased model drag significantly over the Mach number range covered in the investigation but did not affect the drag-rise Mach number.

REFERENCES

1. Kuhn, Richard E.; and Grunwald, Kalman J.: Lateral Stability and Control Characteristics of a Four-Propeller Deflected-Slipstream VTOL Model Including the Effects of Ground Proximity. NASA TN D-444, 1961.

2. Kuhn, Richard E.; and Draper, John W.: Investigation of the Aerodynamic Characteristics of a Model Wing-Propeller Combination and of the Wing and Propeller Separately at Angles of Attack Up to 90°. NACA Rep. 1263, 1956. (Supersedes NACA TN 3304 by Draper and Kuhn.)

3. Goodson, Kenneth W.: Comparison of Wind-Tunnel and Flight Results on a Four-Propeller Tilt-Wing Configuration. Conference on V/STOL and STOL Aircraft, NASA SP-116, 1966, pp. 51-62.

4. Chambers, Joseph R.; and Grafton, Sue B.: Static and Dynamic Longitudinal Stability Derivatives of a Powered 0.18-Scale Model of a Fan-in-Wing VTOL Aircraft. NASA TN D-4322, 1968.

5. Hall, Leo P.; Hickey, David H.; and Kirk, Jerry V.: Aerodynamic Characteristics of a Large-Scale V/STOL Transport Model With Lift and Lift-Cruise Fans. NASA TN D-4092, 1967.

6. Spreemann, Kenneth P.: Wind-Tunnel Investigation of Longitudinal Aerodynamic Characteristics of a Powered Four-Duct-Propeller VTOL Model in Transition. NASA TN D-3192, 1966.

7. Schmeer, James W.; Cassetti, Marlowe D.; and Simonson, Albert J.: Transonic Aerodynamic Characteristics of a Model of a Single-Engine Four-Jet V/STOL Airplane. NASA TM SX-528, U.S. Air Force, 1961.

8. Vogler, Raymond D.: Wind-Tunnel Investigation of a VTOL Jet-Transport Model With Powered Lift Engines in Pods at Wing Midspan or Inboard. NASA TN D-5770, 1970.

9. Winston, Matthew M.: Wind-Tunnel Data From a 0.16-Scale V/STOL Model With Direct-Lift and Lift-Cruise Jets. NASA TM X-1758, 1969.

10. Havey, C. Todd: ADAM-II Propulsion System and Internal Aerodynamics. [Preprint] 670353, Soc. Automot. Eng., Apr. 1967.

11. Hieser, Gerald; Henderson, James H.; and Swihart, John M.: Transonic Aerodynamic and Loads Characteristics of a 4-Percent-Thick Unswept-Wing—Fuselage Combination. NACA RM L54B24, 1954.

12. Schmeer, James W.: Effect of Leading-Edge Droop on the Aerodynamic and Loading Characteristics of a 4-Percent-Thick Unswept-Wing—Fuselage Combination at Transonic Speeds. NACA RM L56C14, 1956.

13. Pendley, Robert E.; Milillo, Joseph R.; and Fleming, Frank F.: An Investigation of Three NACA 1-Series Nose Inlets at Subsonic and Transonic Speeds. NACA RM L52J23, 1953.

TABLE 1.- GEOMETRIC PROPERTIES OF MODEL

Wing (not including flaps):	
Area (tip to tip), m^2	0.6284
Area (boom center line to boom center line plus horizontal tails), m^2	0.6751
Span (tip to tip), m	1.0490
Span (including horizontal tails), m	1.3469
Mean geometric chord (not including flap), m	0.5990
Aspect ratio (wing only)	1.755
Aspect ratio (including horizontal tails)	2.645
Taper ratio	1.0
Sweep, deg	0
Twist, deg	0
Incidence angle, deg	0
Dihedral, deg	0
Flap (one surface):	
Area (configurations 1 to 5), m^2	0.0459
Area (configuration 6), m^2	0.0547
Span, m	0.3099
Chord (configurations 1 to 5), m	0.1481
Chord (configuration 6), m	0.1764
Fuselage:	
Length, m	2.0650
Height (maximum), m	0.4045
Width (maximum), m	0.2540
Vertical tail:	
Area (exposed), m^2	0.0975
Span, m	0.3667
Taper ratio	0.308
Sweep (c/4)	$43^{\circ}50'$
Aspect ratio	1.38
Airfoil section	NACA 65A010
Horizontal tail (one surface):	
Area (exposed), m^2	0.0383
Area (total), m^2	0.0492
Span (each), m	0.1921
Taper ratio	0.316
Sweep (c/4)	$54^{\circ}11'$
Aspect ratio	0.752
Dihedral, deg	0
Airfoil section	NACA 65A010

TABLE 1.- GEOMETRIC PROPERTIES OF MODEL – Concluded

Nozzle inlet areas (per fan):

Inlet capture area, cm^2	206.43
Inlet area at rake, cm^2	153.81

Nozzle exit areas:

Fan duct (per fan for configurations 1 to 4), cm^2	102.58
Fan duct (per fan for configurations 5 and 6), cm^2	134.84
Flap jet (each), cm^2	57.42

Fans (each):

Diameter, cm	14.00
Hub-tip radius ratio	0.35
Number of blades	16

Wing coordinates (not including flap):

x, percent $\bar{c}$	y, percent $\bar{c}$	
	Exterior surfaces	Inlet interior surfaces
0	±11.14	±11.14
1.00	±11.99	±10.25
2.00	±12.28	±9.78
4.00	±12.67	±9.20
6.00	±13.00	±8.82
10.00	±13.65	±8.82
15.00	±14.20	±9.62
20.00	±14.61	±10.93
30.00	±15.25	-----
40.00	±15.38	-----
60.00	±14.57	-----
80.00	±14.28	-----
[a] 81.20	±14.25	-----
[b] 100.00	±13.43	-----
Leading-edge radii 0.53 percent $\bar{c}$		

[a] Trailing-edge bottom surface.

[b] Trailing-edge top surface.

TABLE 2.- CONFIGURATION IDENTIFICATION

Configuration	Horizontal tail	Vertical tail	Fan exit fairing	Flap fairing	Fan efflux area
1	On	On	On	Off	Small
2	Off	On	On	Off	Small
3	Off	Off	On	Off	Small
4	On	Off	On	Off	Small
5	On	On	Off	Off	Large
6	On	On	Off	On	Large

Fan	Location
1	Left outboard
2	Left inboard
3	Right inboard
4	Right outboard

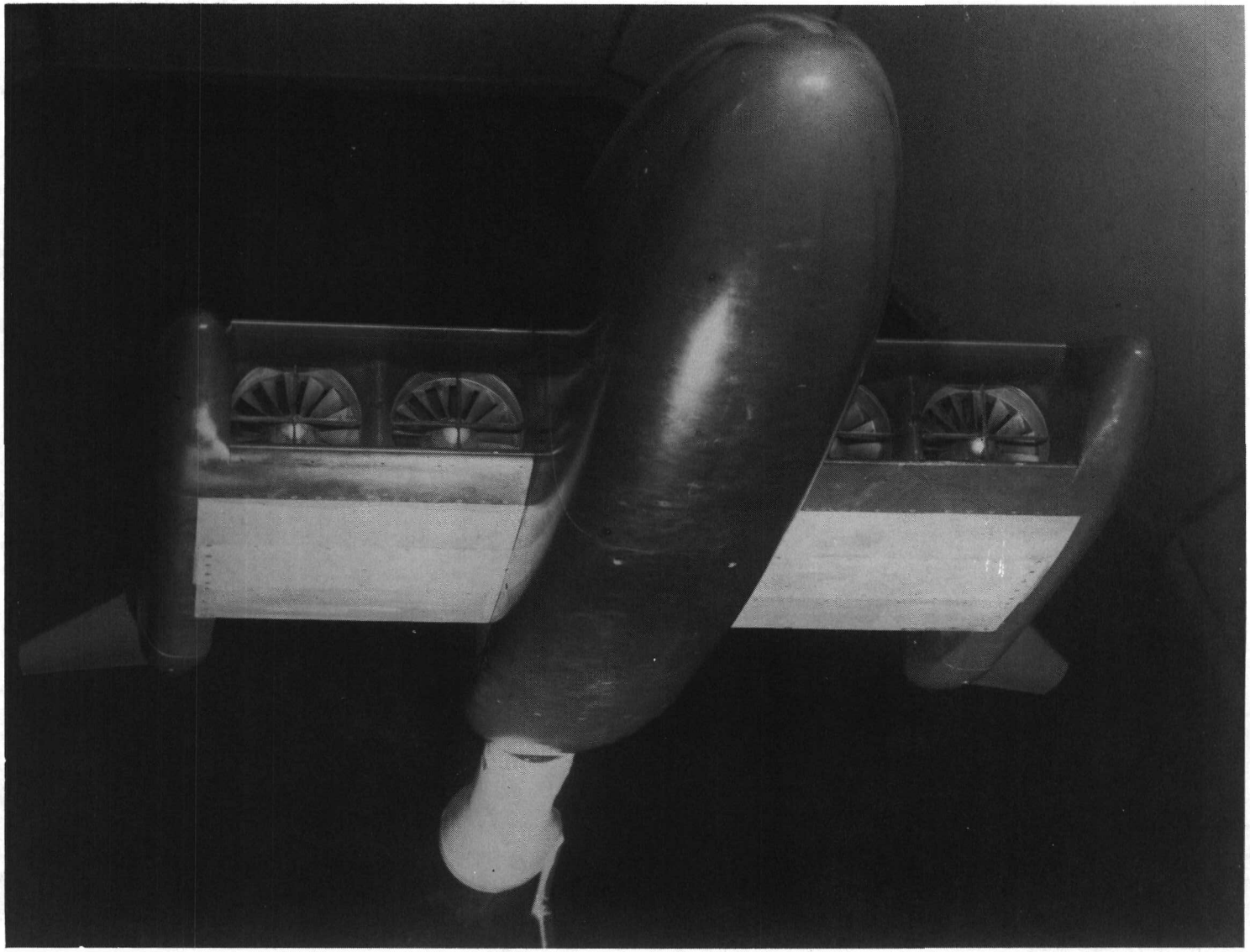

L-70-1839

(a) Front view.

Figure 1.- Photograph of model.

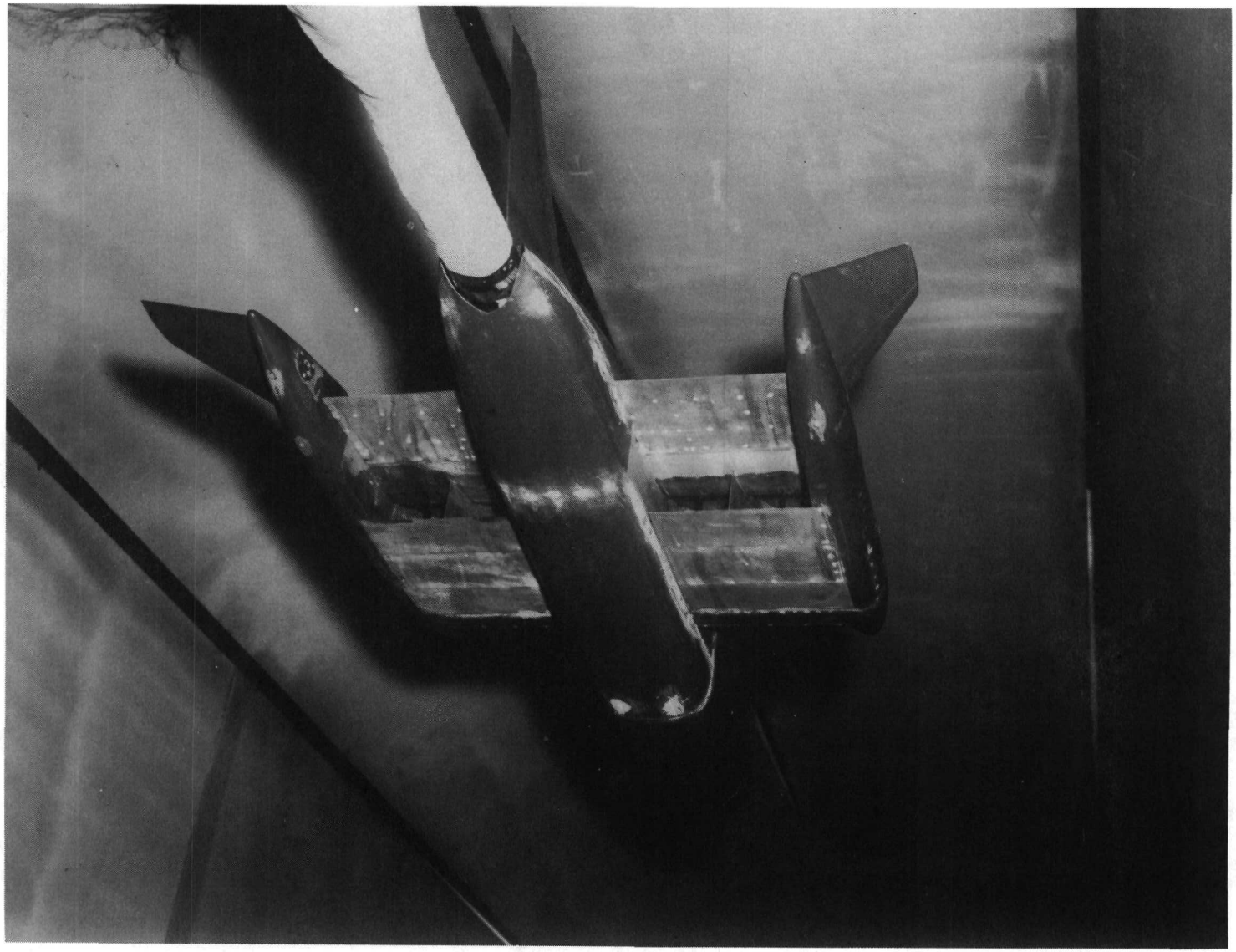

L-70-2074

(b) Rear view.

Figure 1.- Concluded.

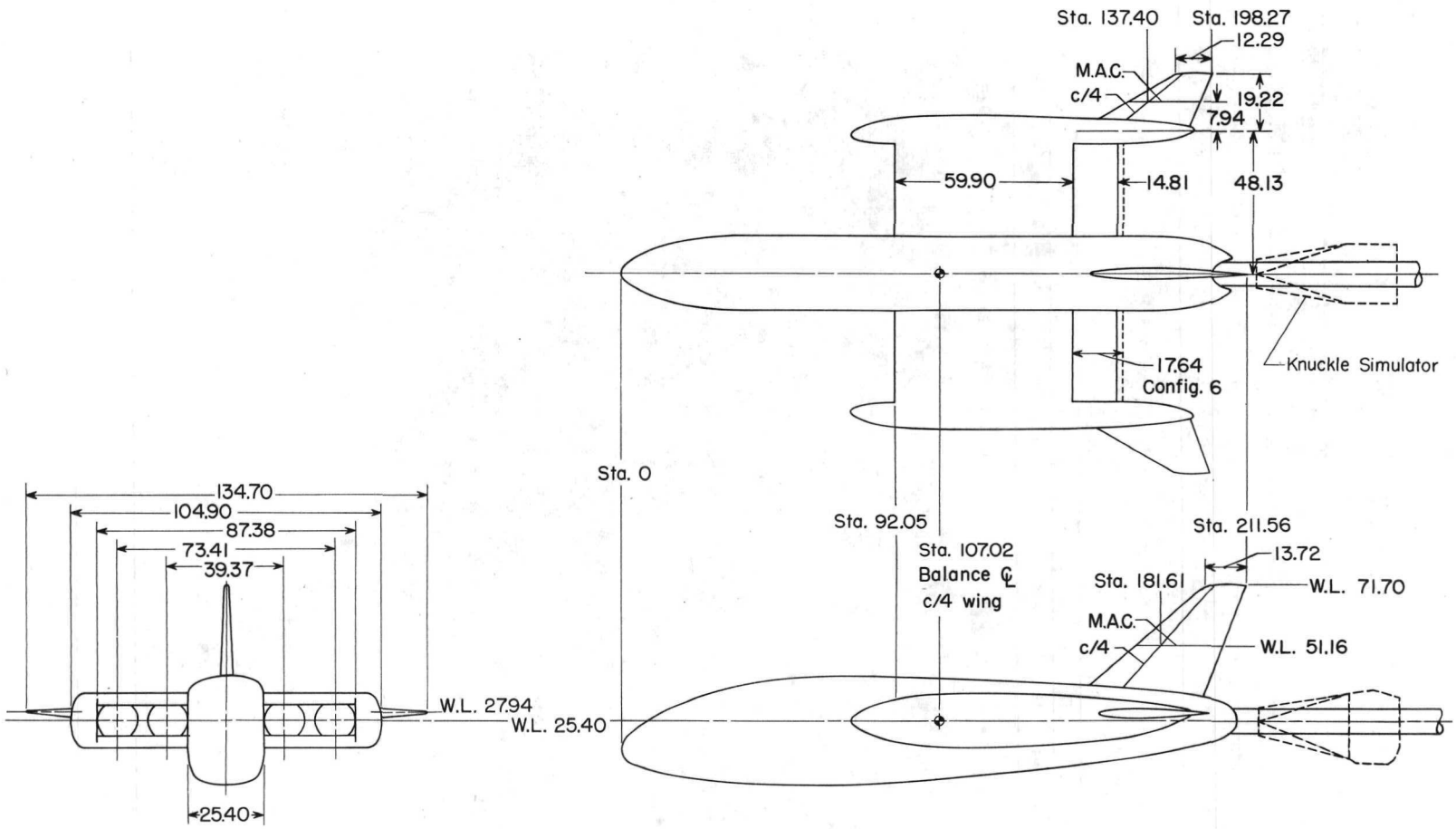

(a) Three-view drawing of model. All dimensions are in centimeters.

Figure 2.- Details of model.

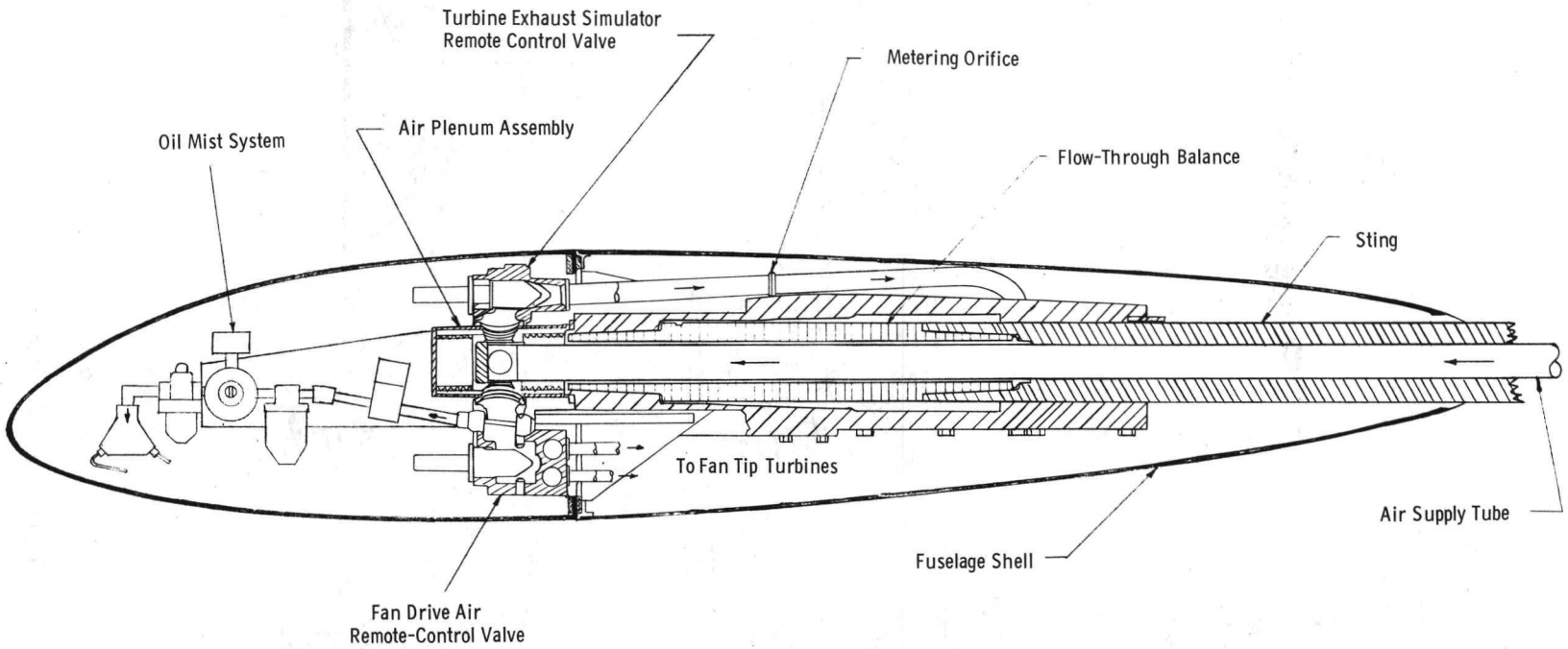

(b) Sectional view of fuselage and wing showing compressed-air route.

Figure 2.- Continued.

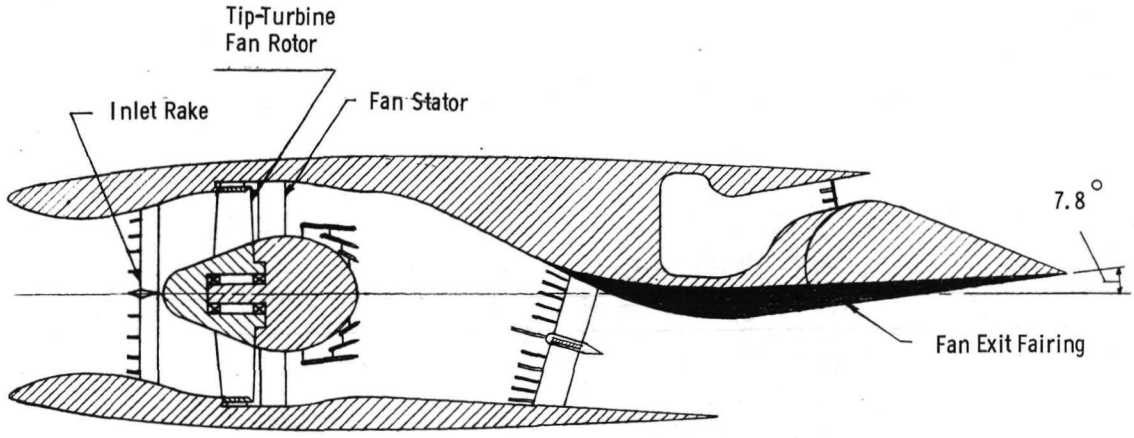

Configurations 1-4

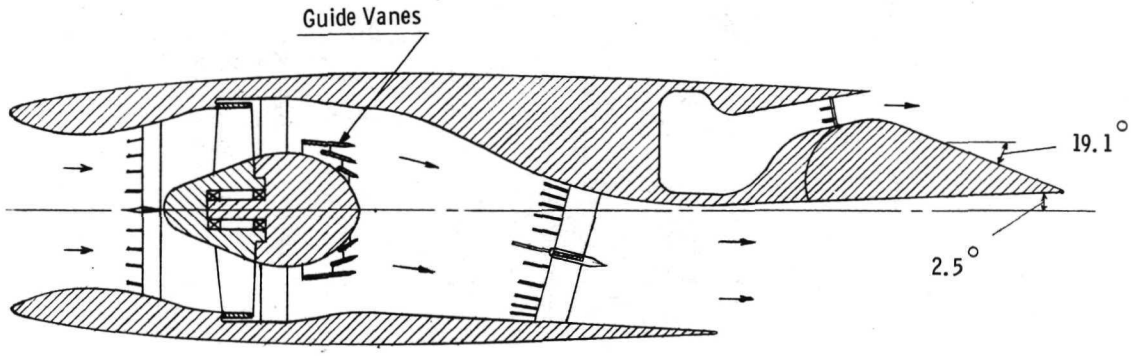

Configuration 5

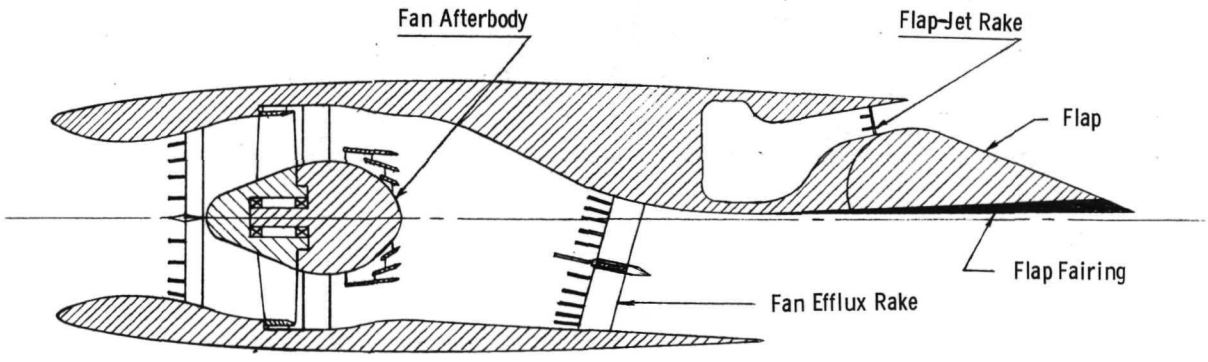

Configuration 6

(c) Details of the propulsive wing.

Figure 2.- Continued.

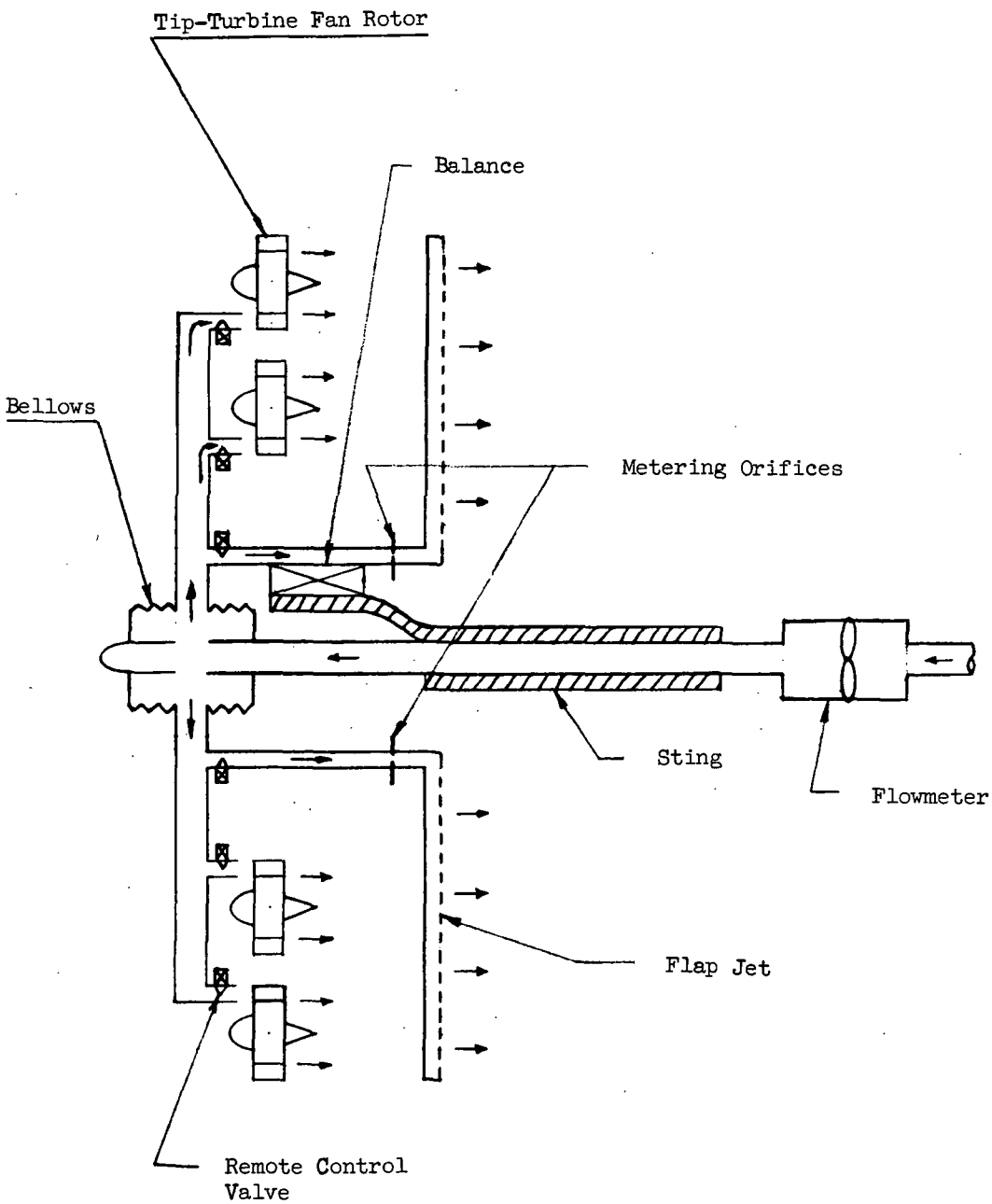

(d) Schematic diagram of model compressed-air propulsion system.

Figure 2.- Concluded.

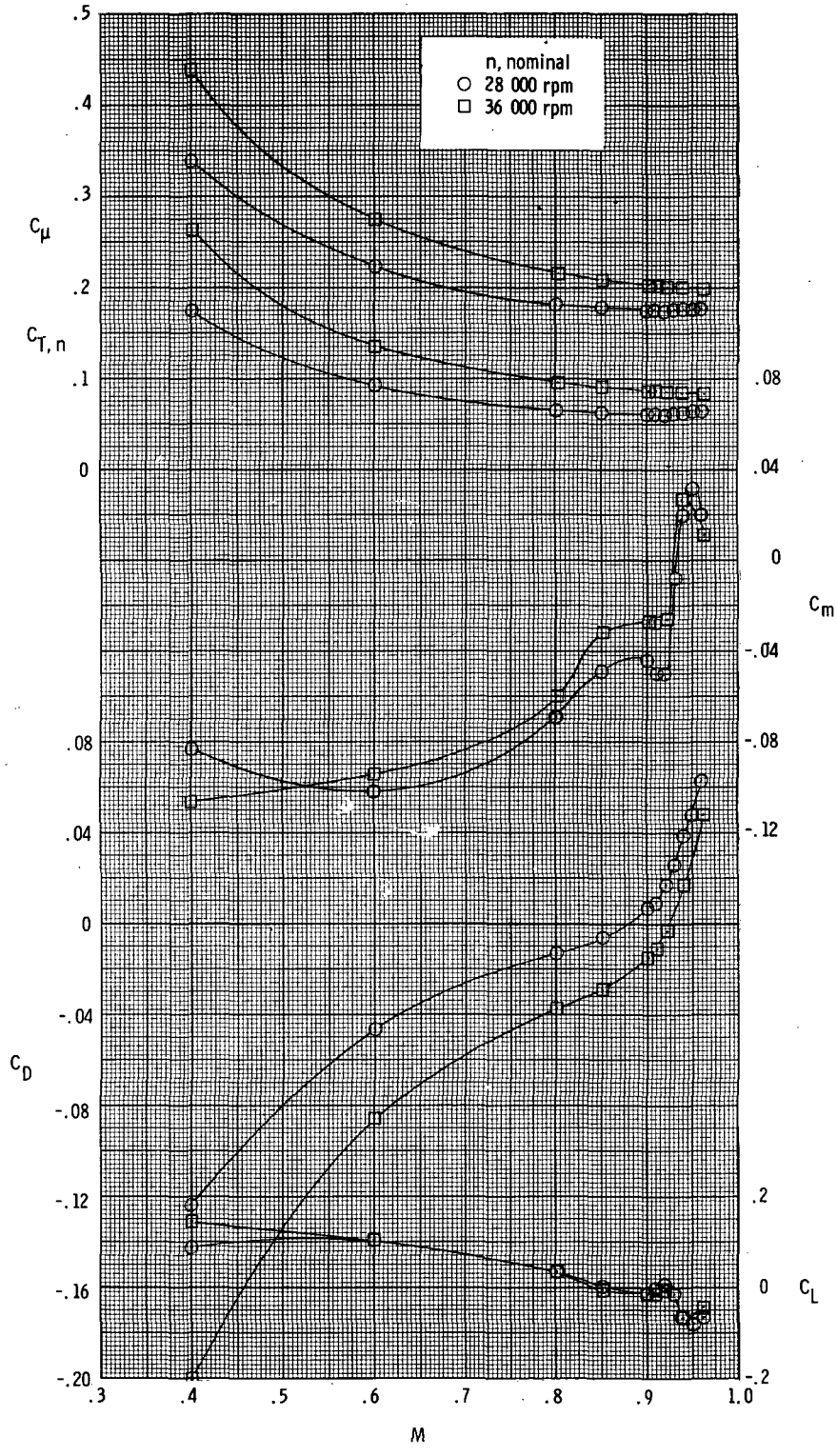

(a) Variation with Mach number; $\alpha = 0^{\circ}$.

Figure 3.- Longitudinal aerodynamic characteristics, configuration 1.

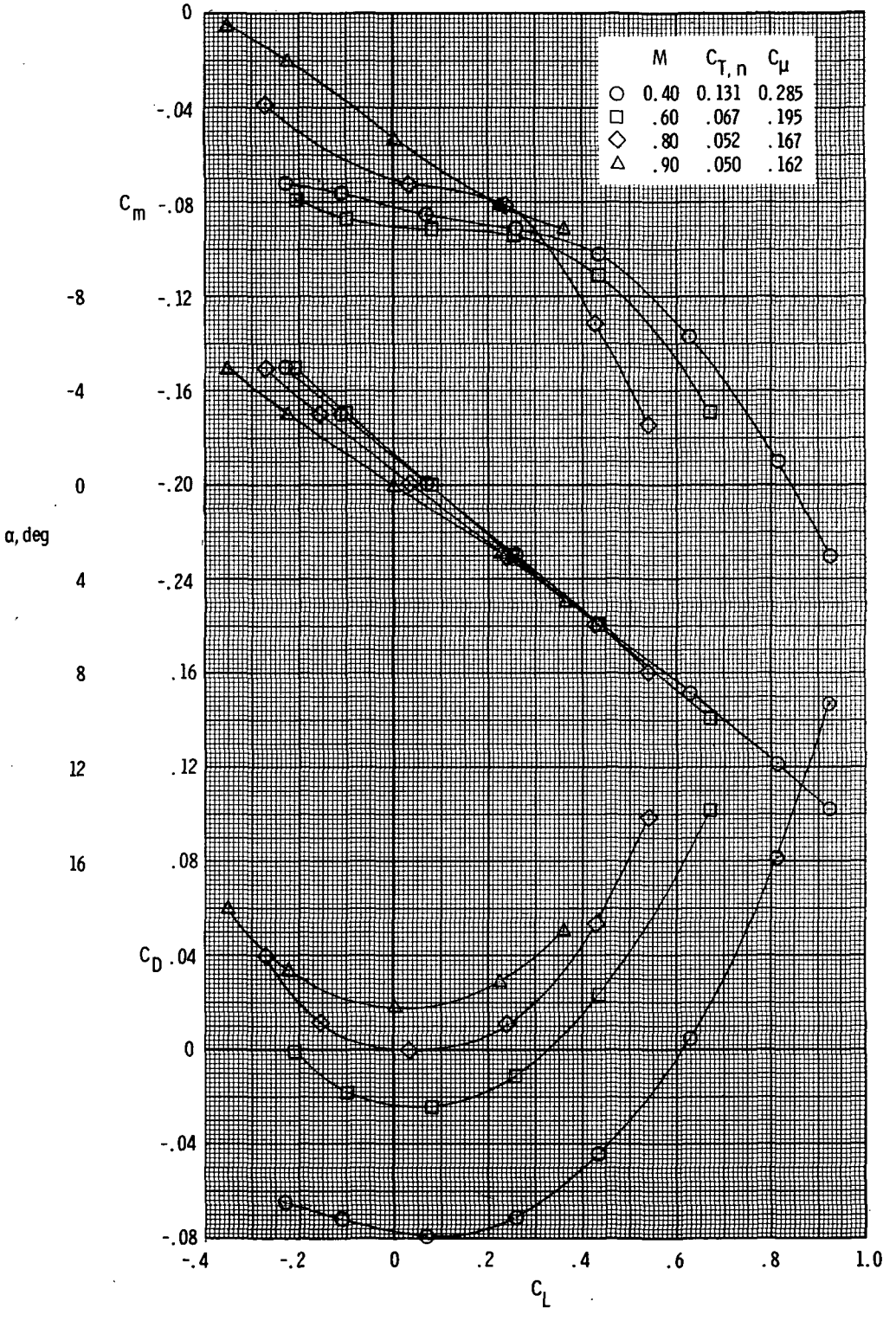

(b) Variation with α; n = 24 000 rpm, nominal.

Figure 3.- Continued.

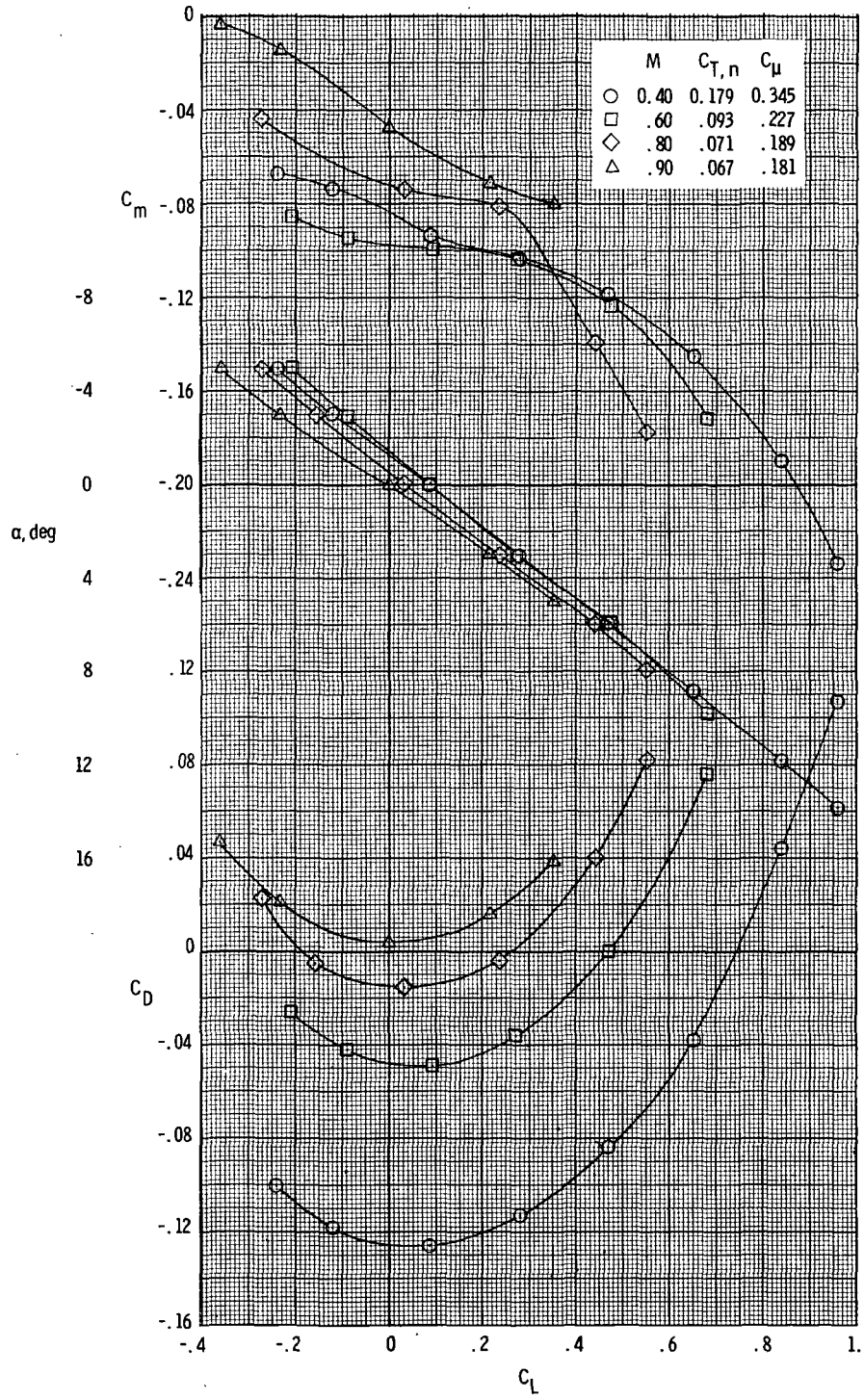

(c) Variation with α; n = 28 000 rpm, nominal.

Figure 3.- Concluded.

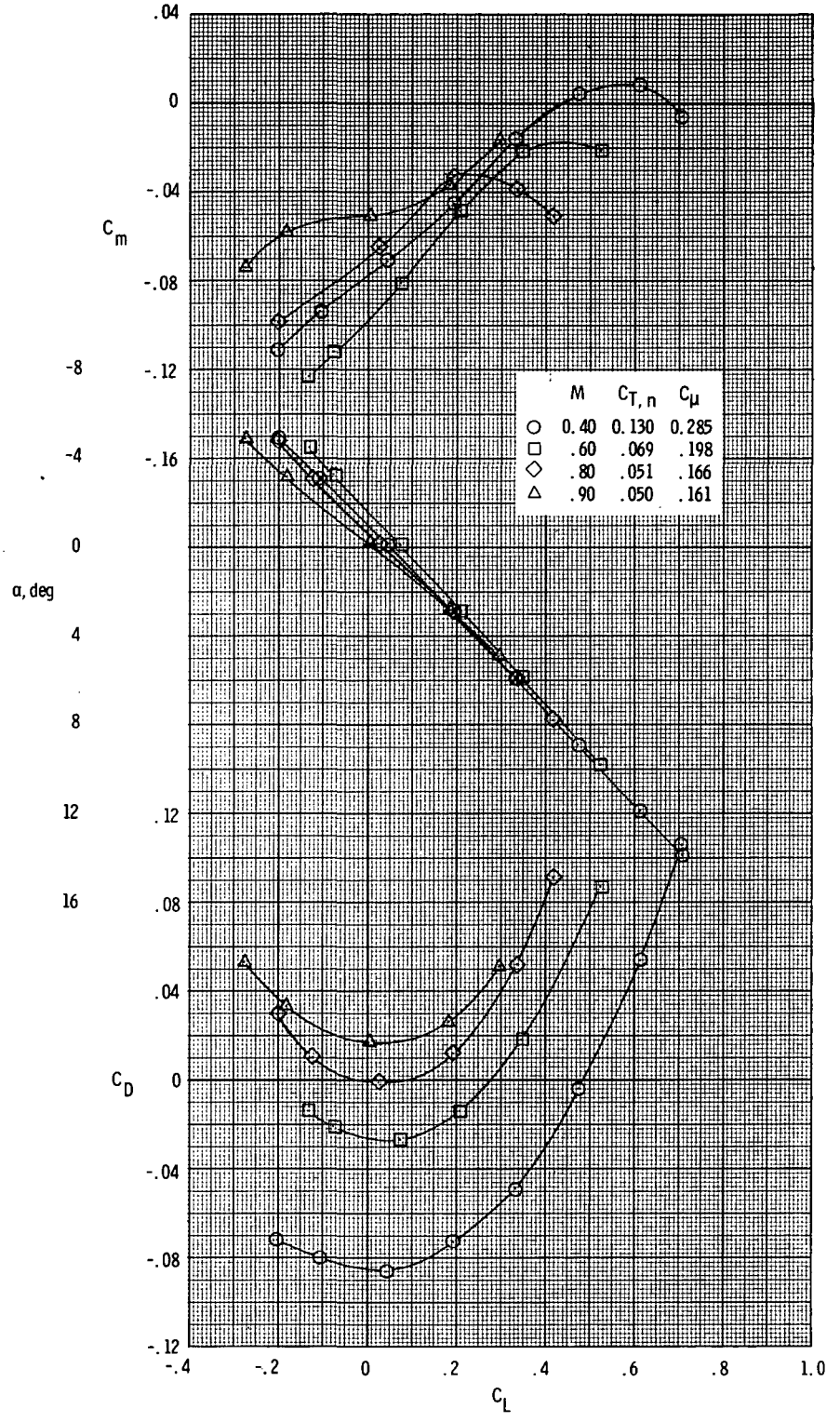

(a) n = 24 000 rpm, nominal.

Figure 4.- Variation of longitudinal aerodynamic characteristics with α, configuration 2.

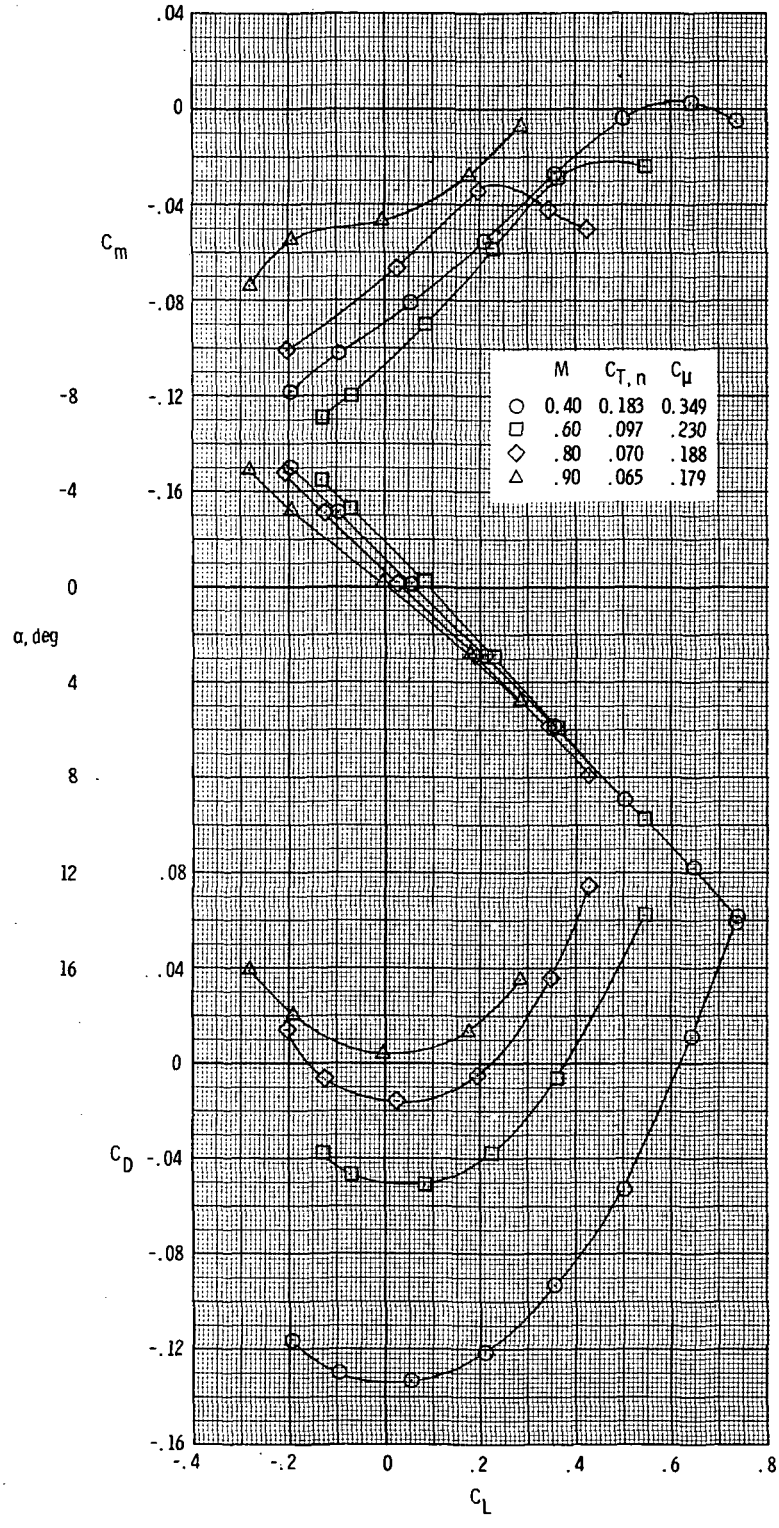

(b) n = 28 000 rpm, nominal.

Figure 4.- Concluded.

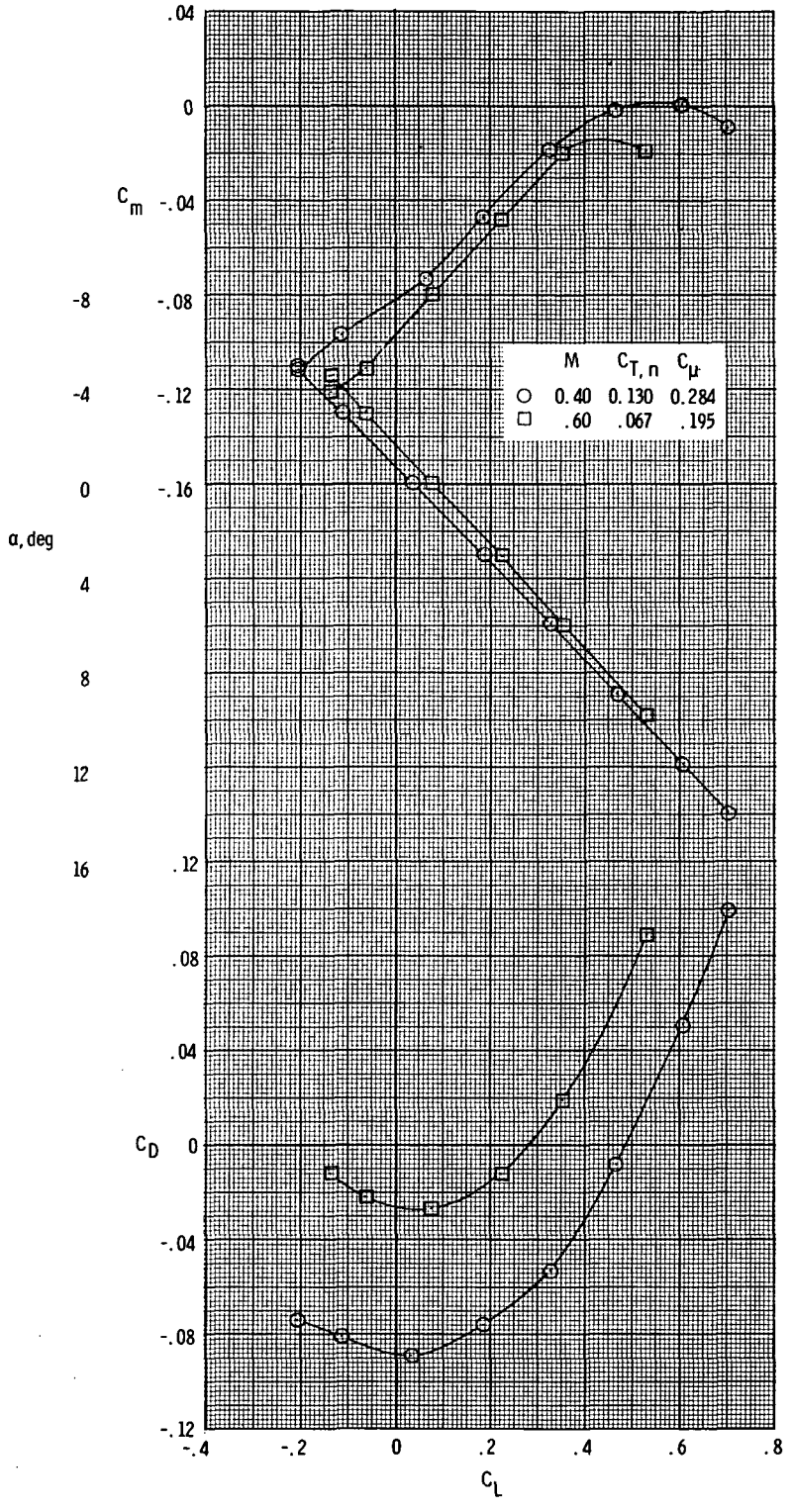

(a) n = 24 000 rpm, nominal.

Figure 5.- Variation of longitudinal aerodynamic characteristics with α, configuration 3.

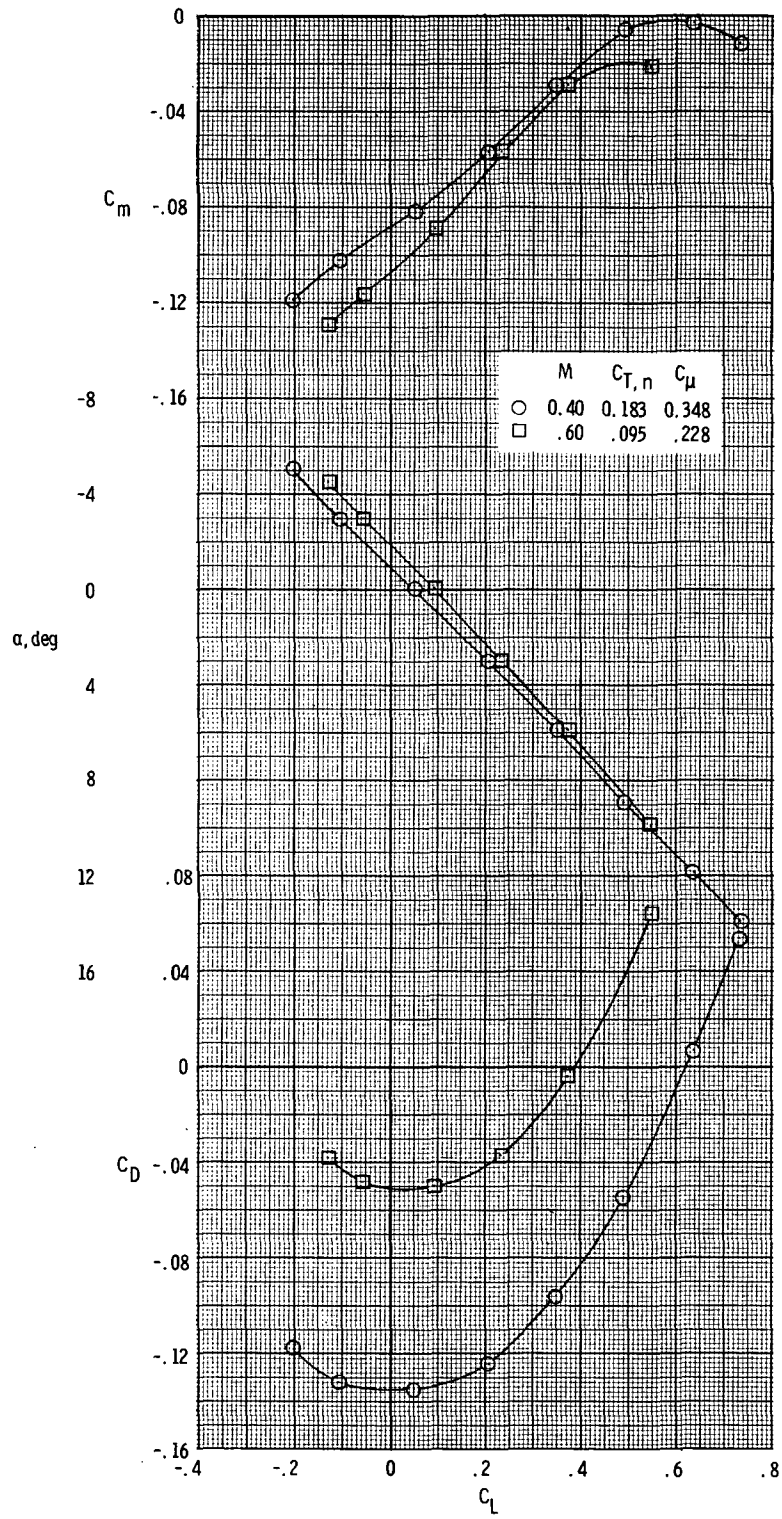

(b) n = 28 000 rpm, nominal.

Figure 5.- Continued.

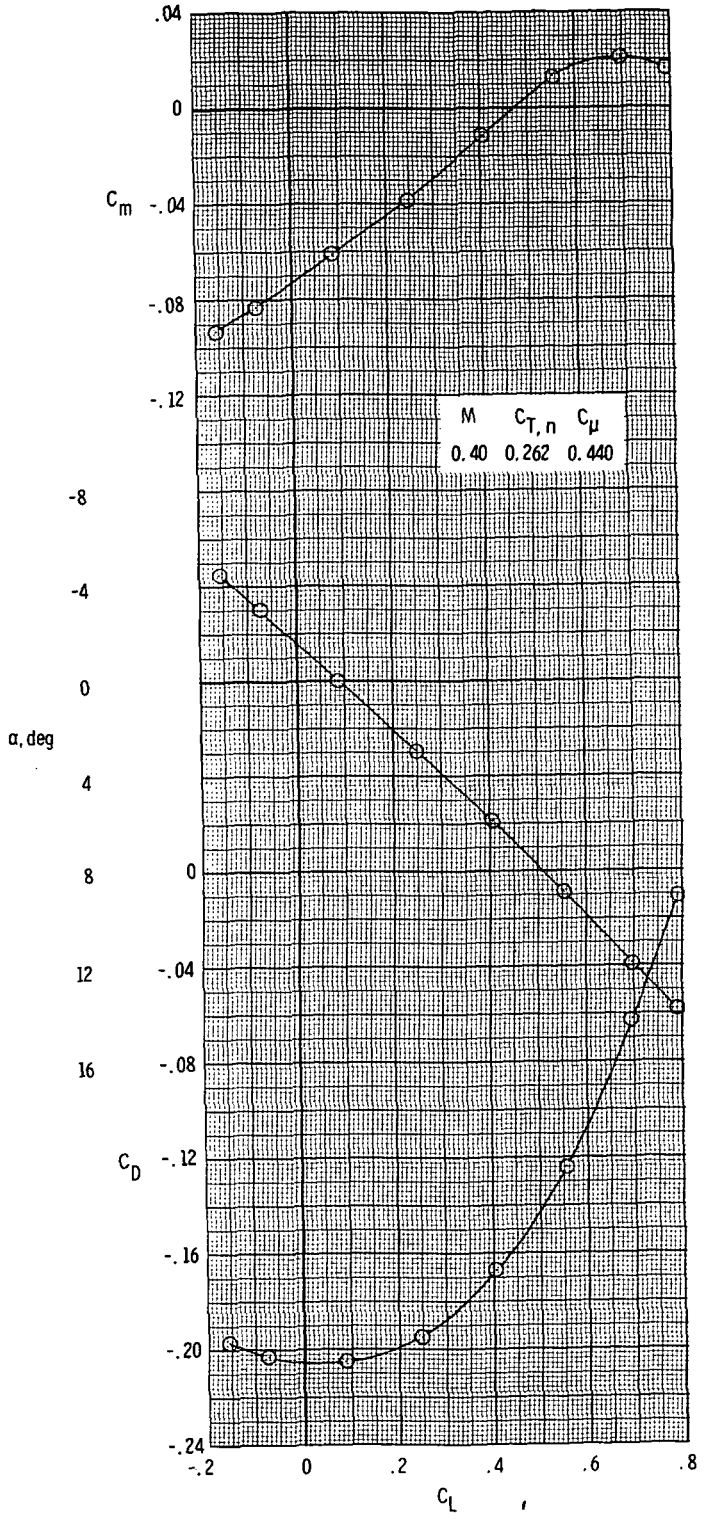

(c) n = 36 000 rpm, nominal.

Figure 5.- Concluded.

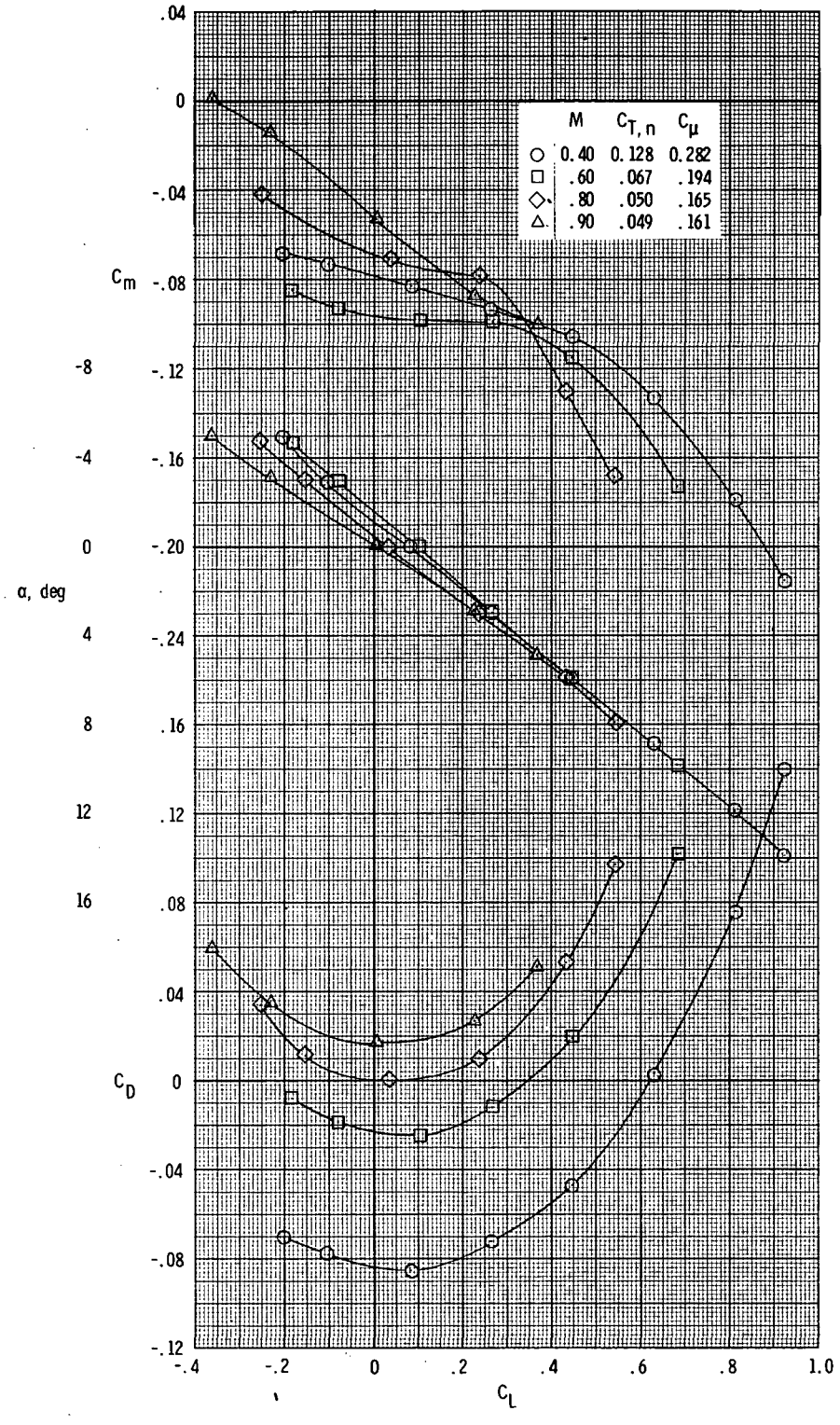

(a) n = 24 000 rpm, nominal.

Figure 6.- Variation of longitudinal aerodynamic characteristics with α, configuration 4.

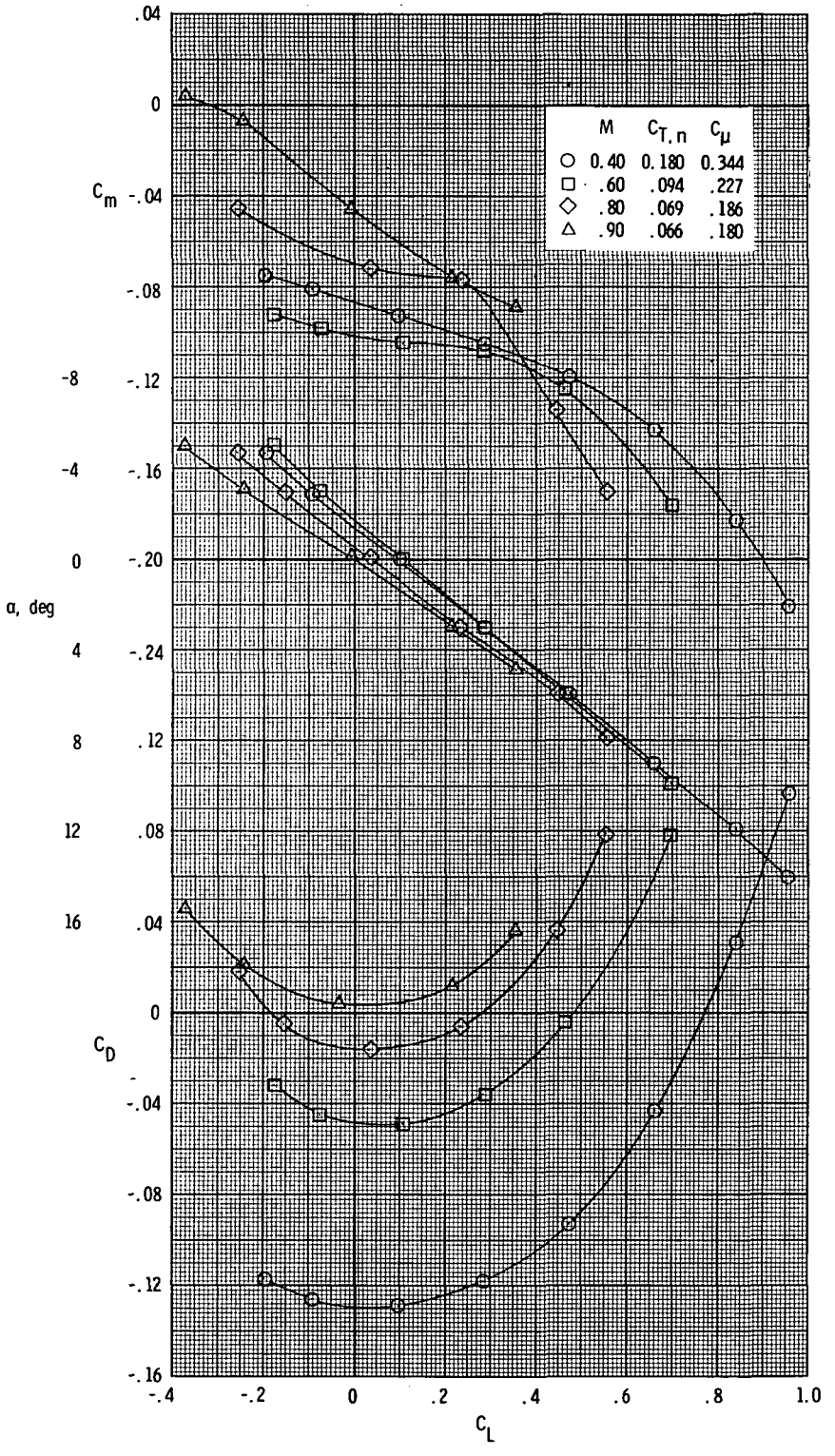

(b) n = 28 000 rpm, nominal.

Figure 6.- Concluded.

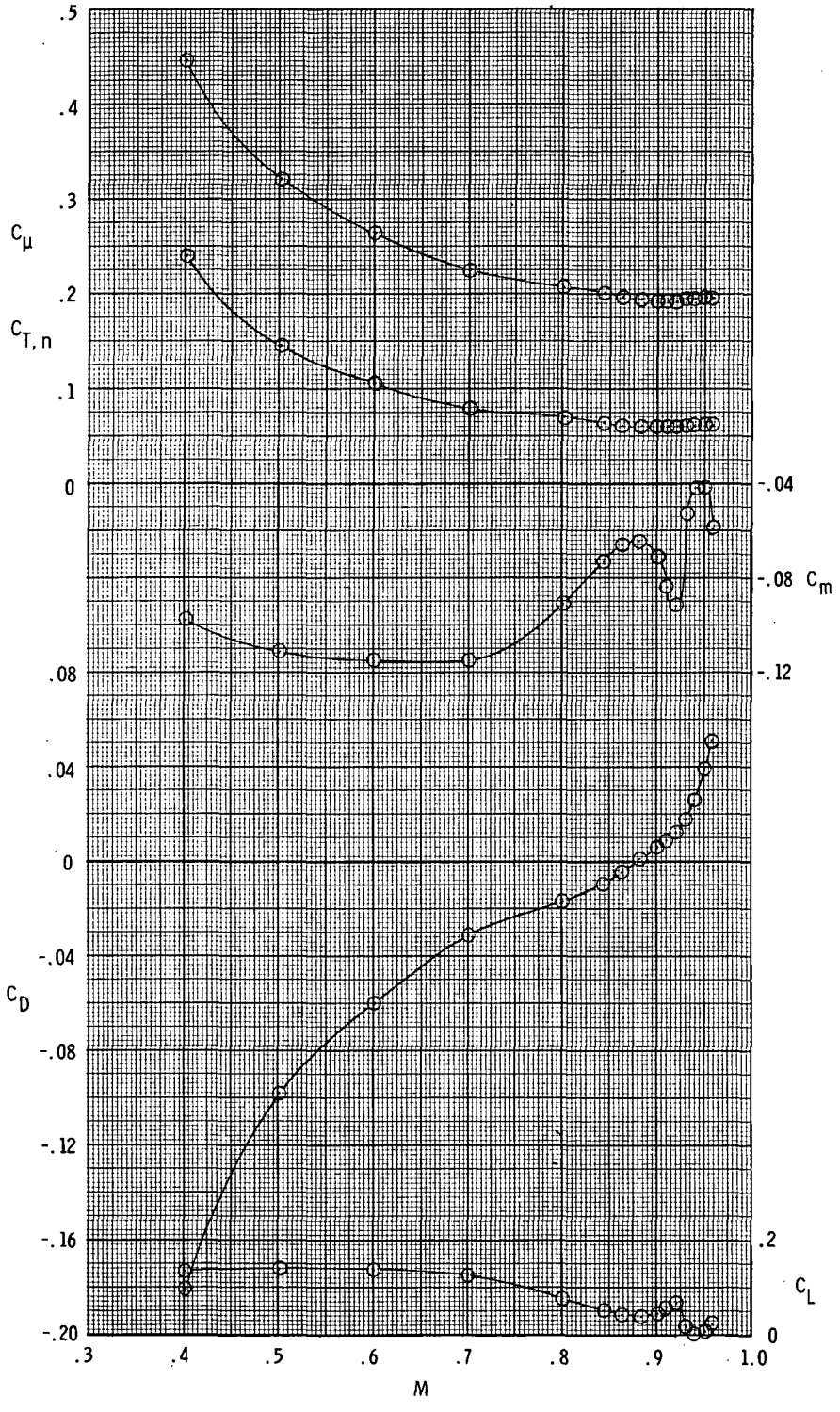

Figure 7.- Variation of longitudinal aerodynamic characteristics with Mach number, configuration 5; $\alpha = 0^{o}$; n = 36 000 rpm, nominal.

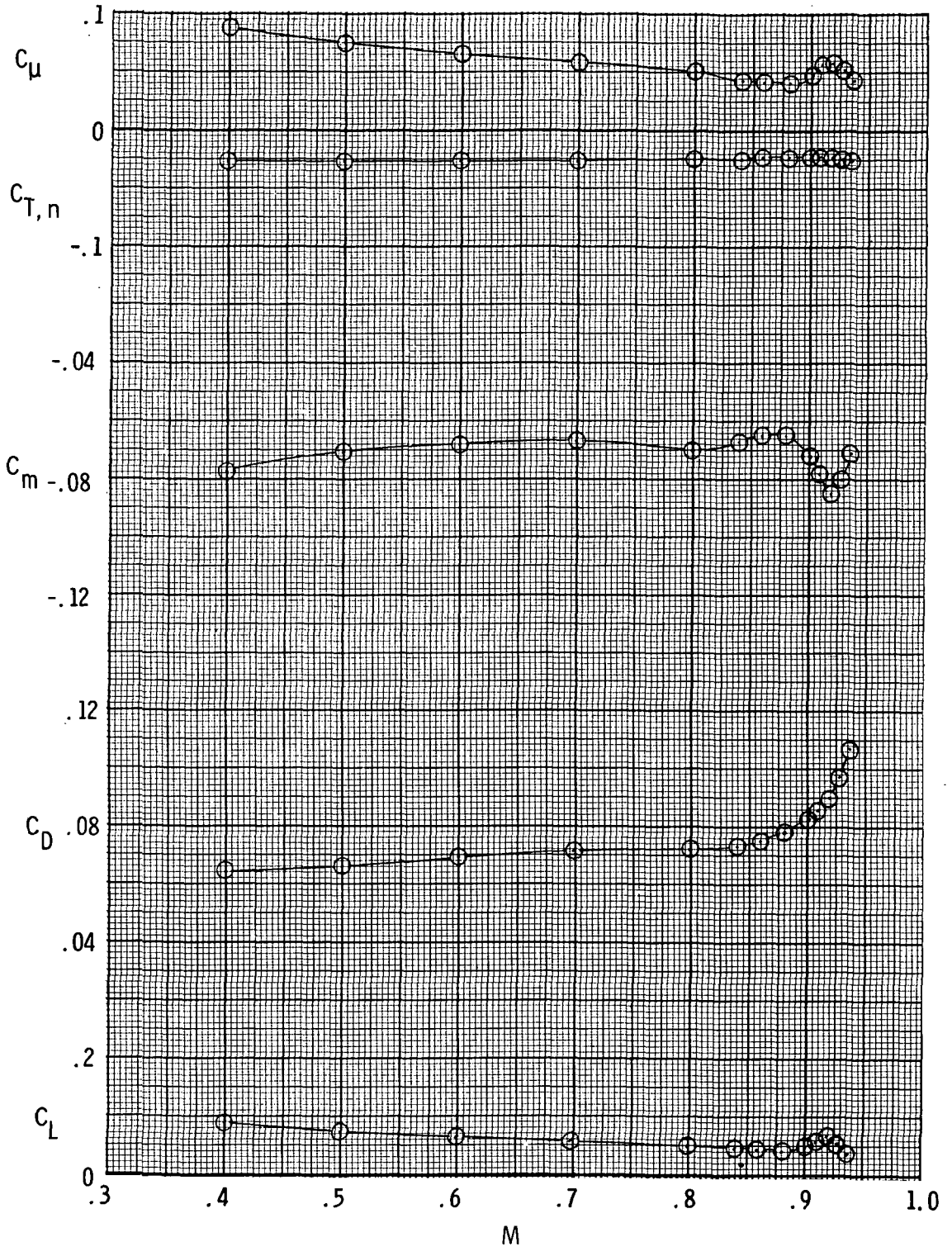

(a) Variation with Mach number; windmilling fans; $\alpha = 0^{\circ}$.

Figure 8.- Longitudinal aerodynamic characteristics, configuration 6.

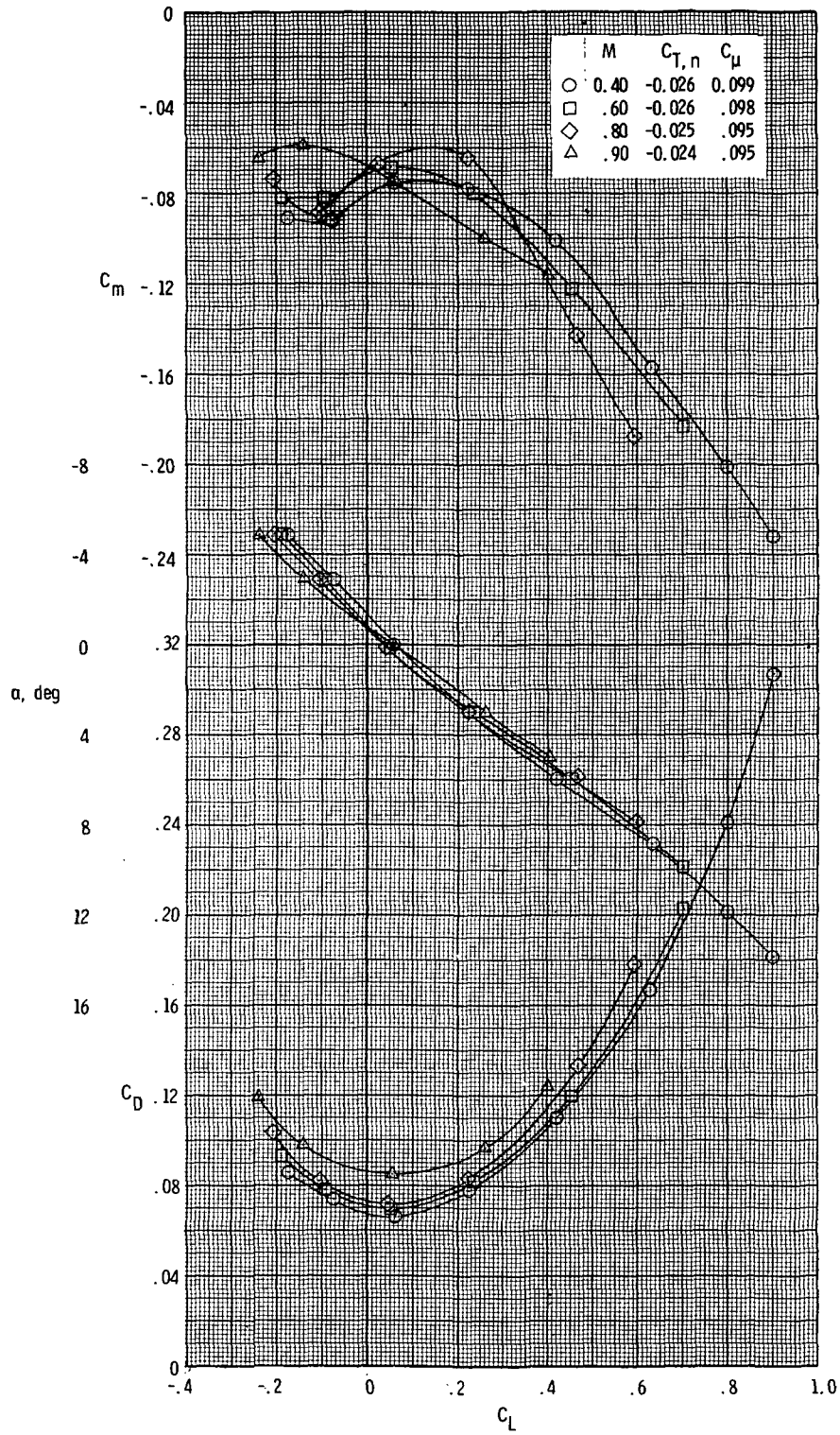

(b) Variation with α; windmilling fans.

Figure 8.- Continued.

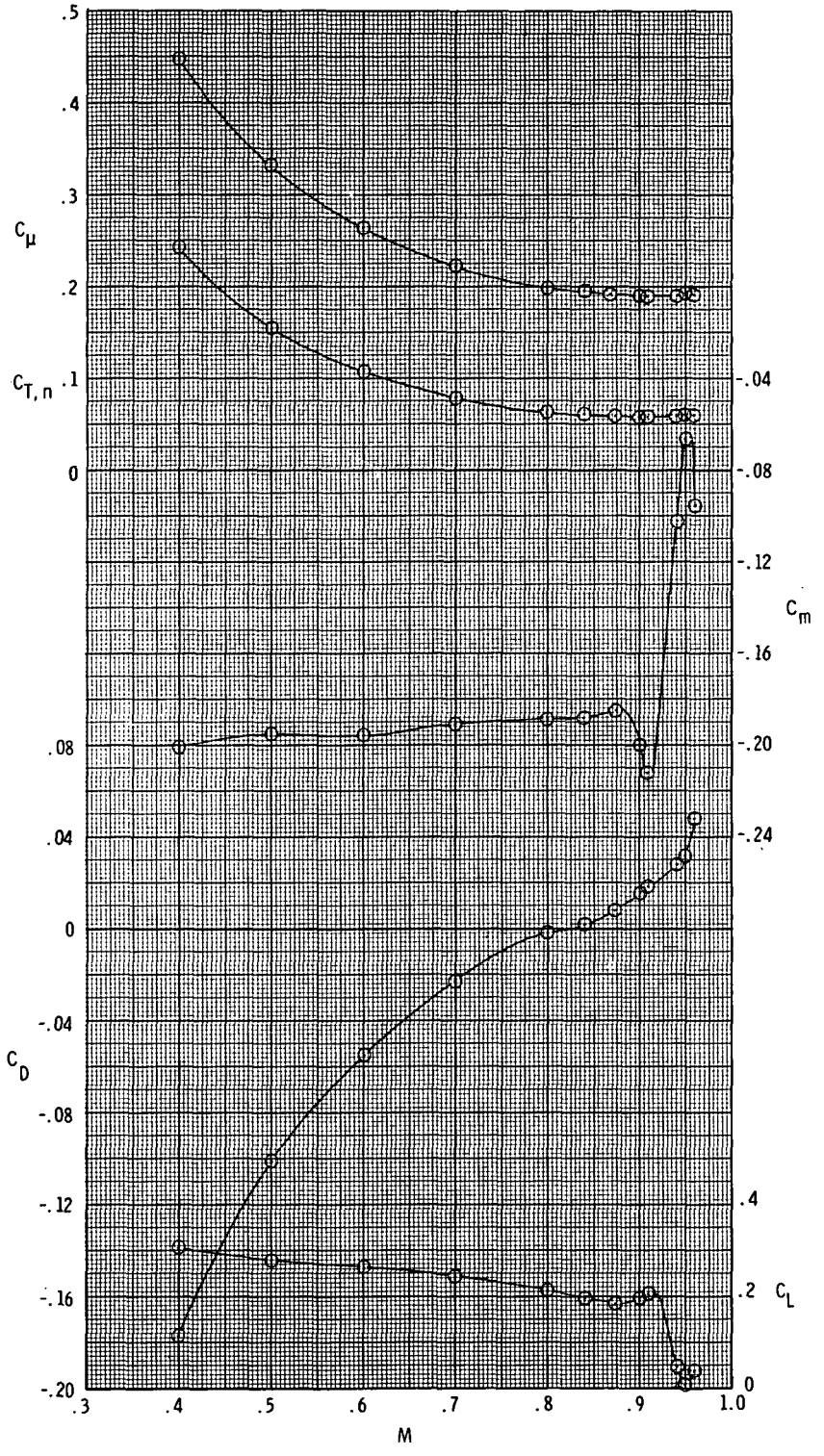

(c) Variation with Mach number; n = 36 000 rpm, nominal; $\alpha = 0^{o}$.

Figure 8.- Continued.

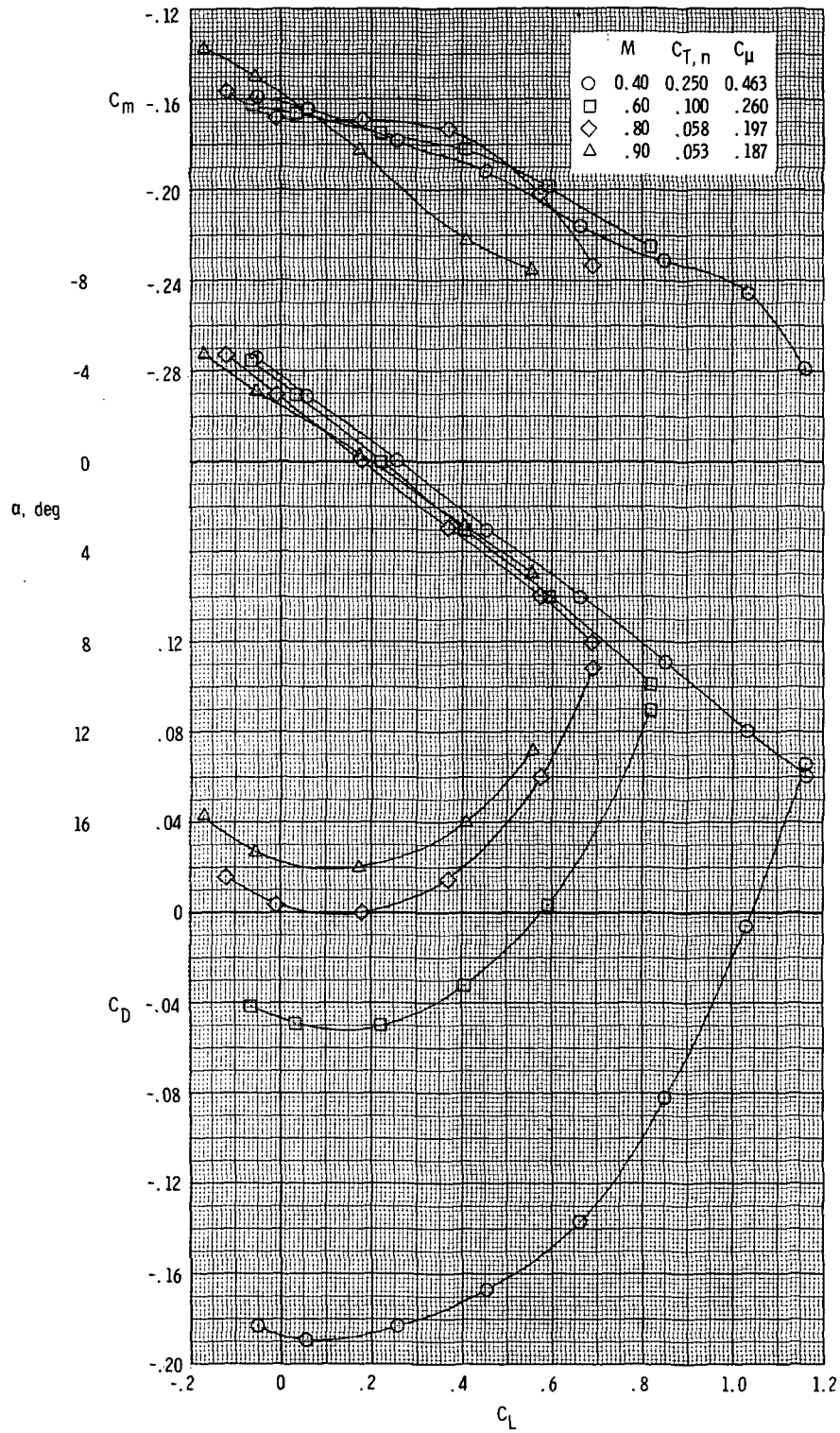

(d) Variation with α; n = 36 000 rpm, nominal.

Figure 8.- Concluded.

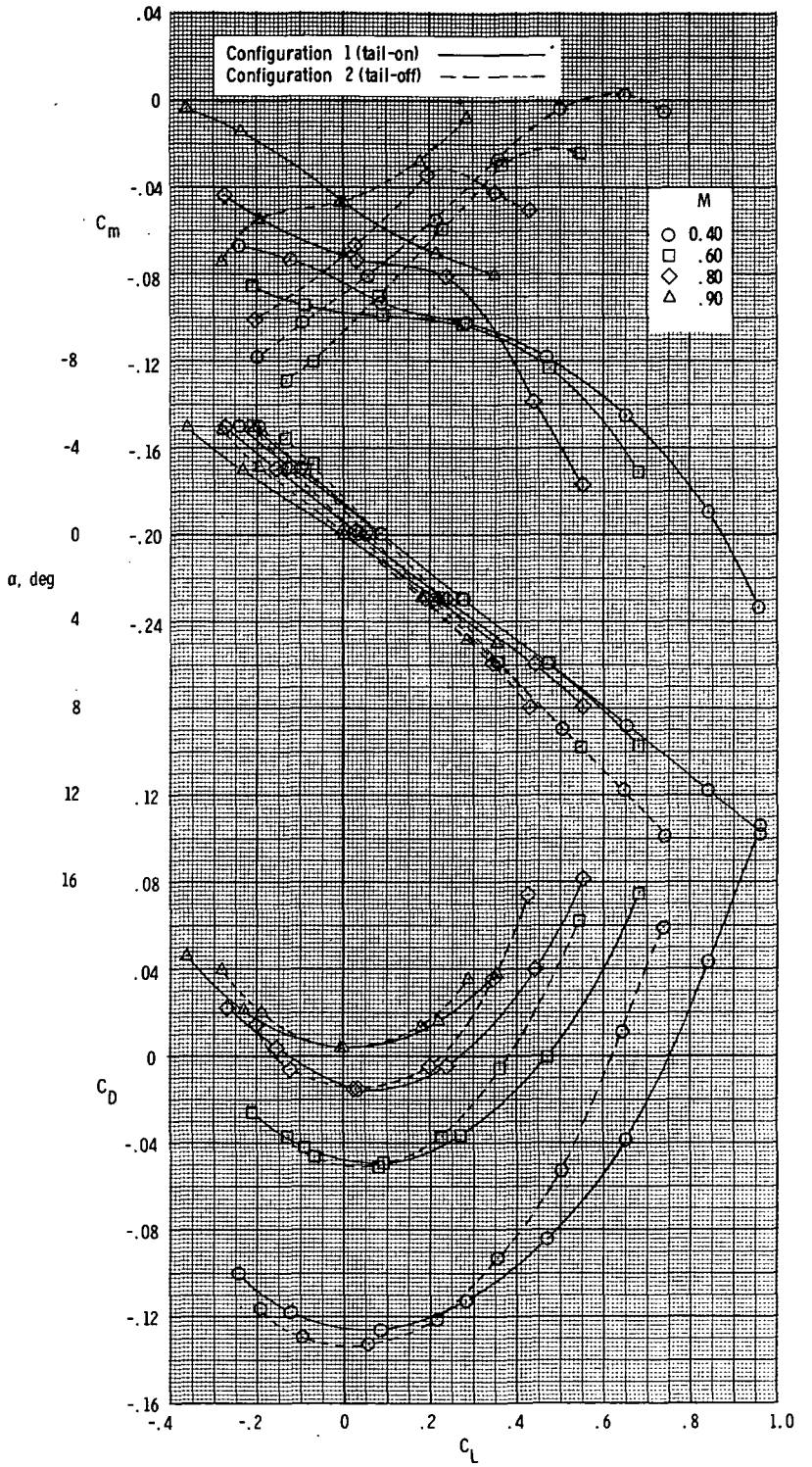

(a) Variation of C_D, α, and C_m with C_L; n = 28 000 rpm, nominal.

Figure 9.- Effect of horizontal tail on longitudinal aerodynamic characteristics.

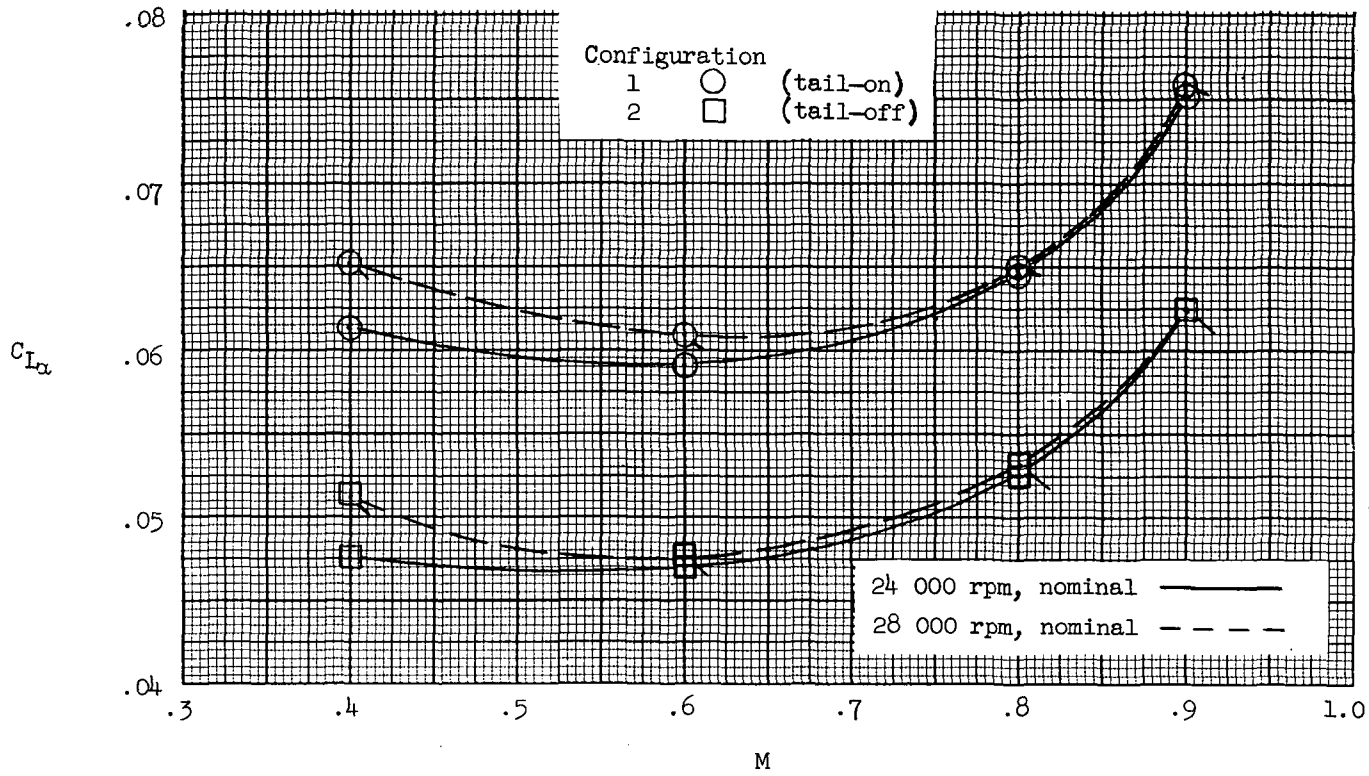

(b) Variation of C_{L_α} with M.

Figure 9.- Concluded.

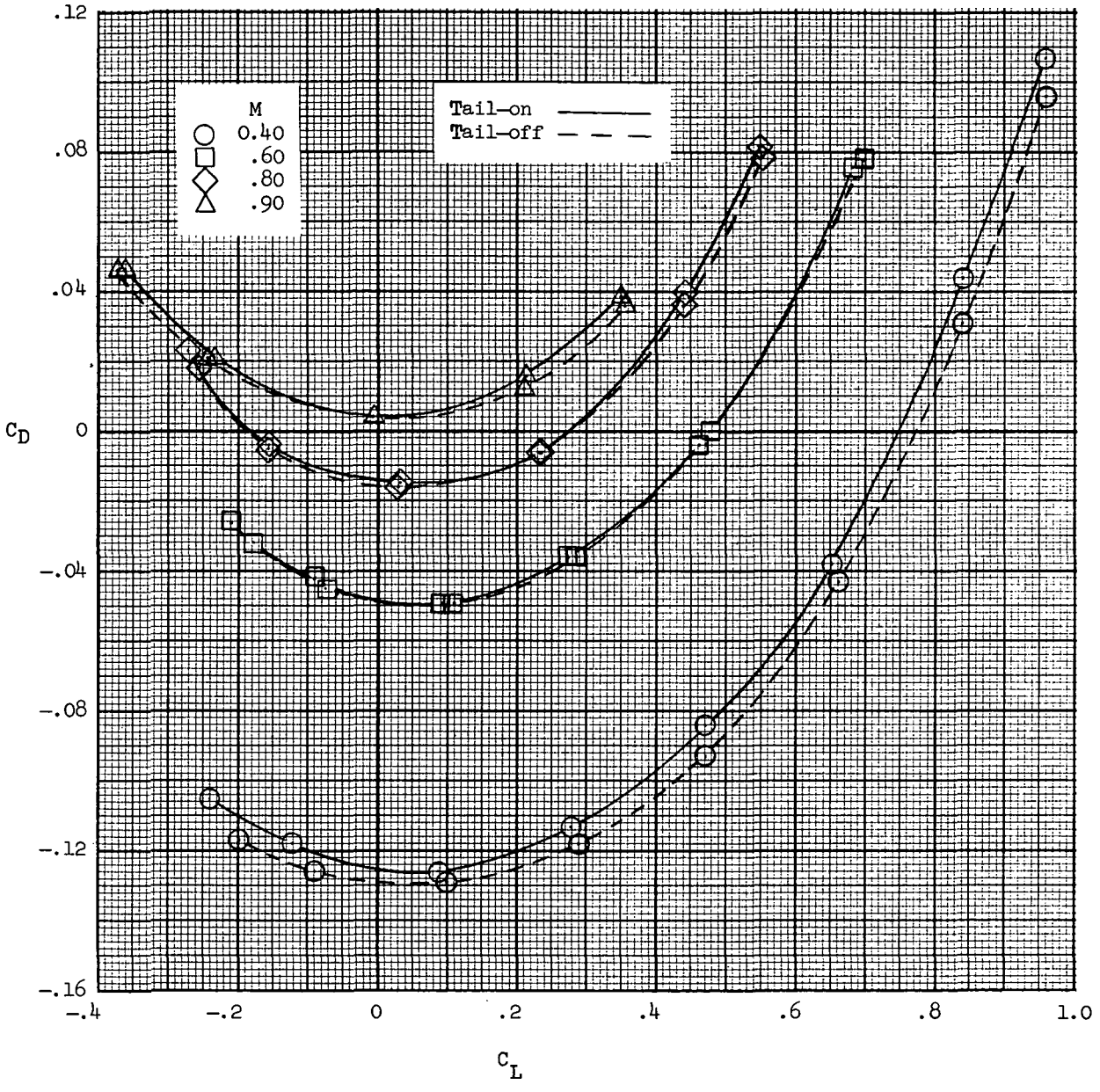

Figure 10.- Effect of vertical tail on drag; n = 28 000 rpm, nominal.

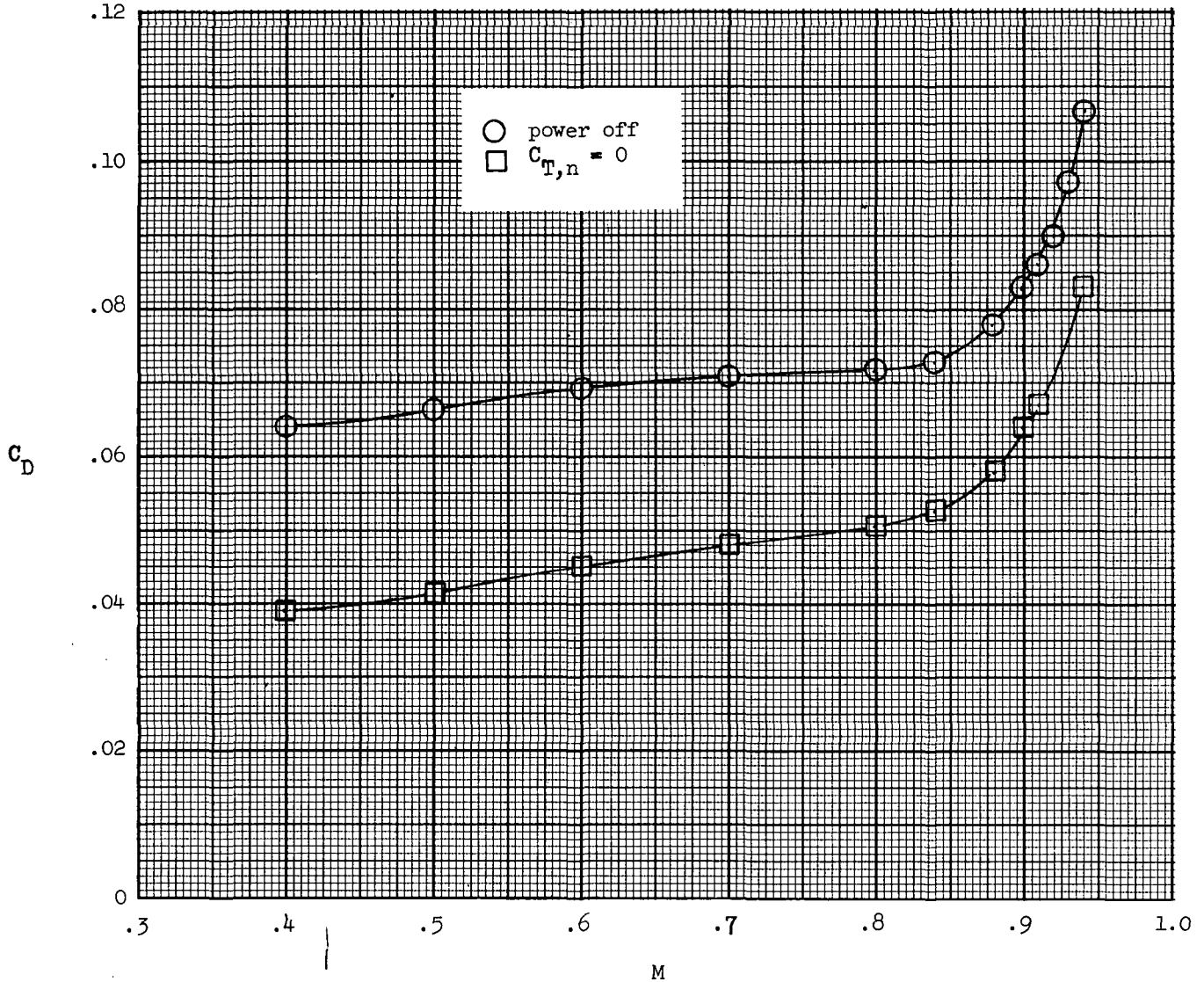

Figure 11.- Variation of C_D with M, configuration 6; $\alpha = 0^o$.

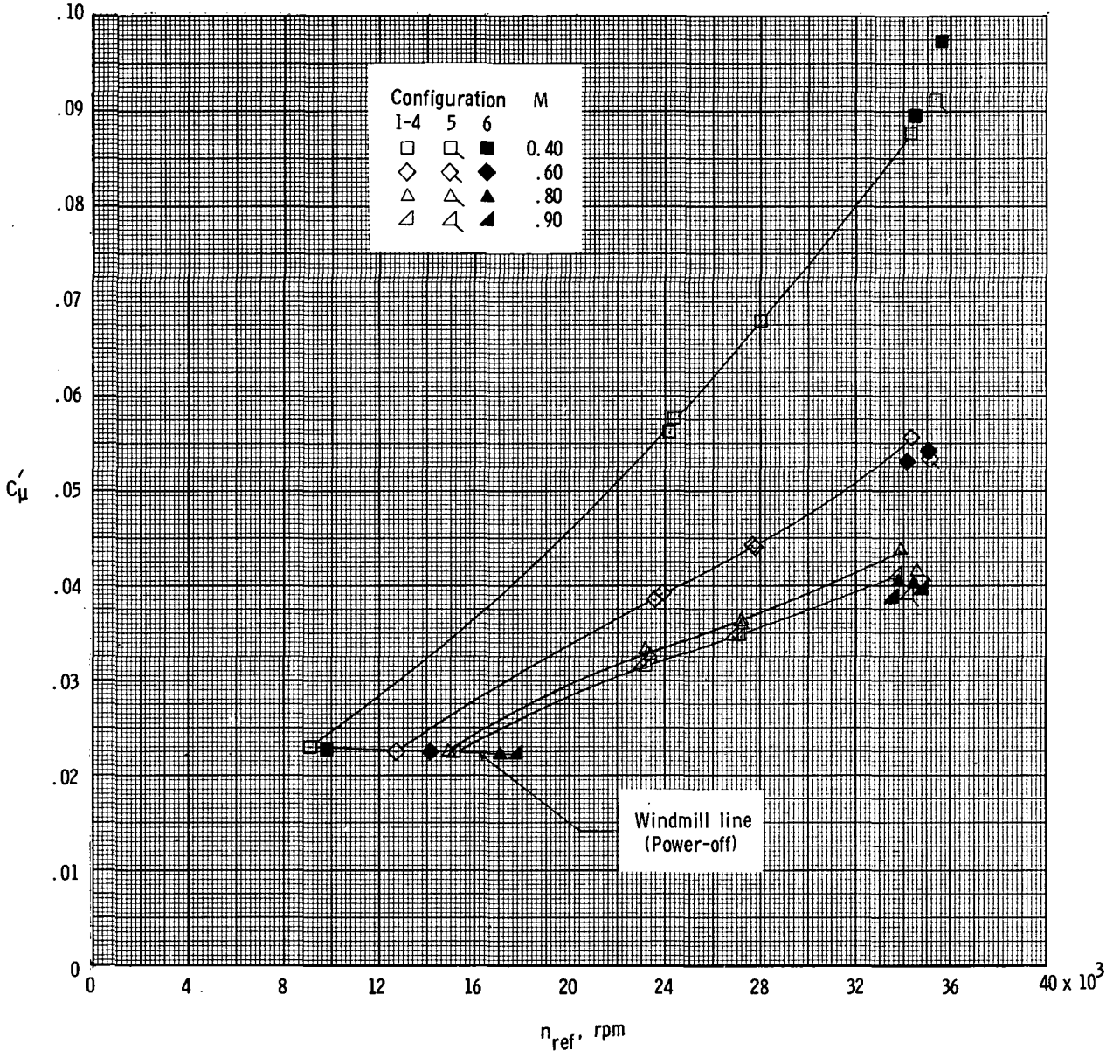

(a) Gross-thrust coefficient C'_μ.

Figure 12.- Effect of fan rotational speed on internal aerodynamic characteristics at $\alpha = 0^o$, fan 1.

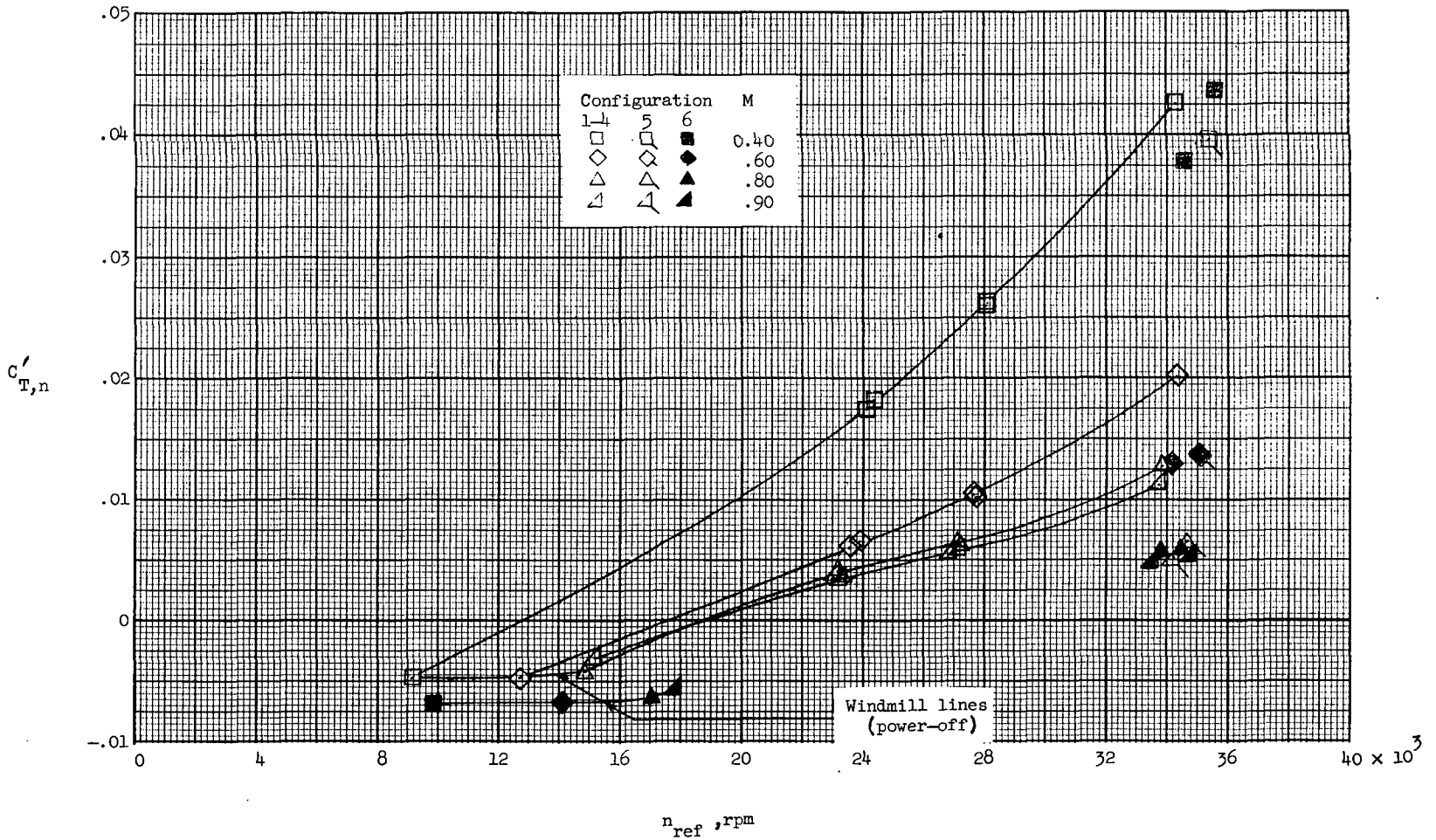

(b) Net-thrust coefficient $C'_{T,n}$.

Figure 12.- Continued.

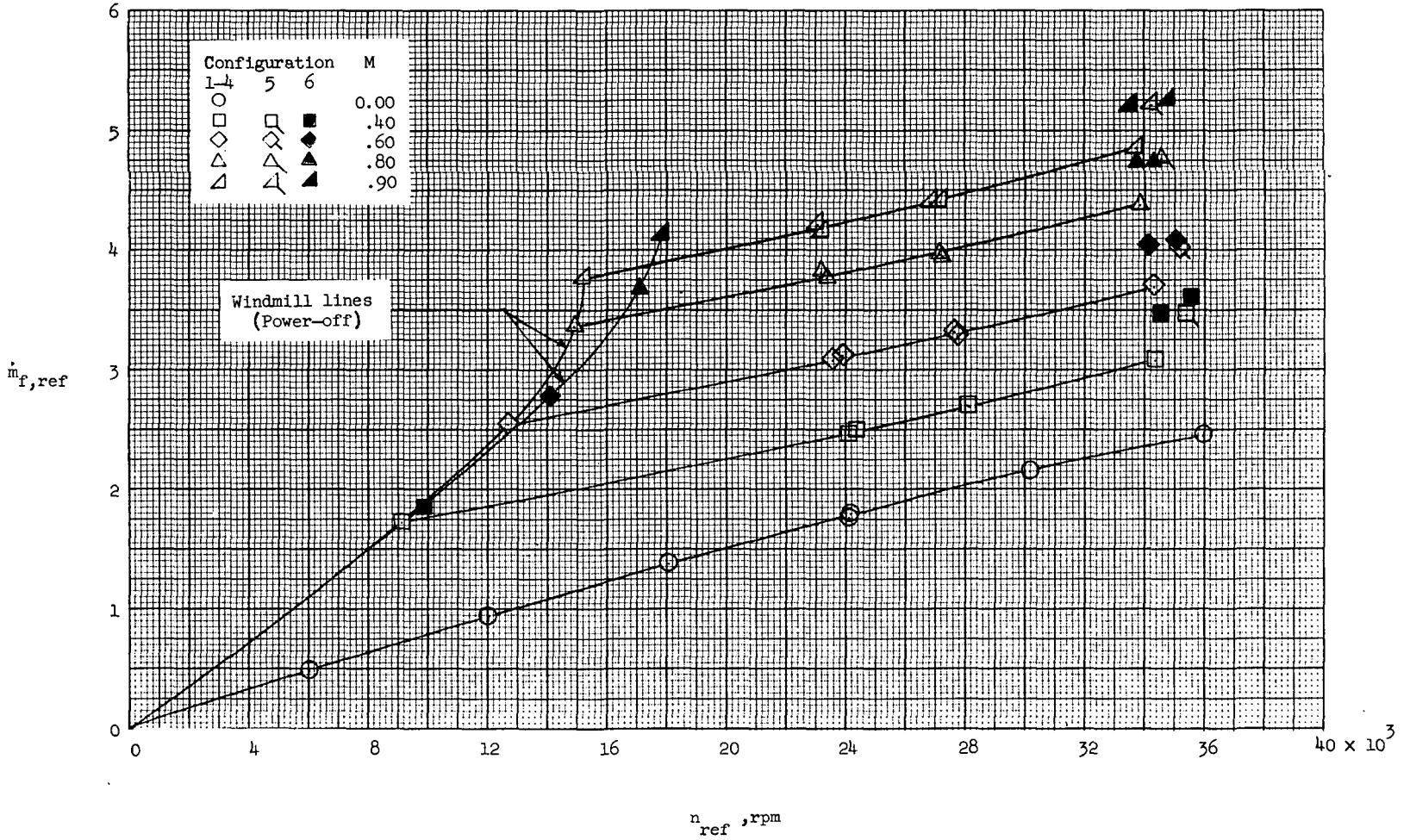

(c) Mass flow $\dot{m}_{f,ref}$.

Figure 12.- Continued.

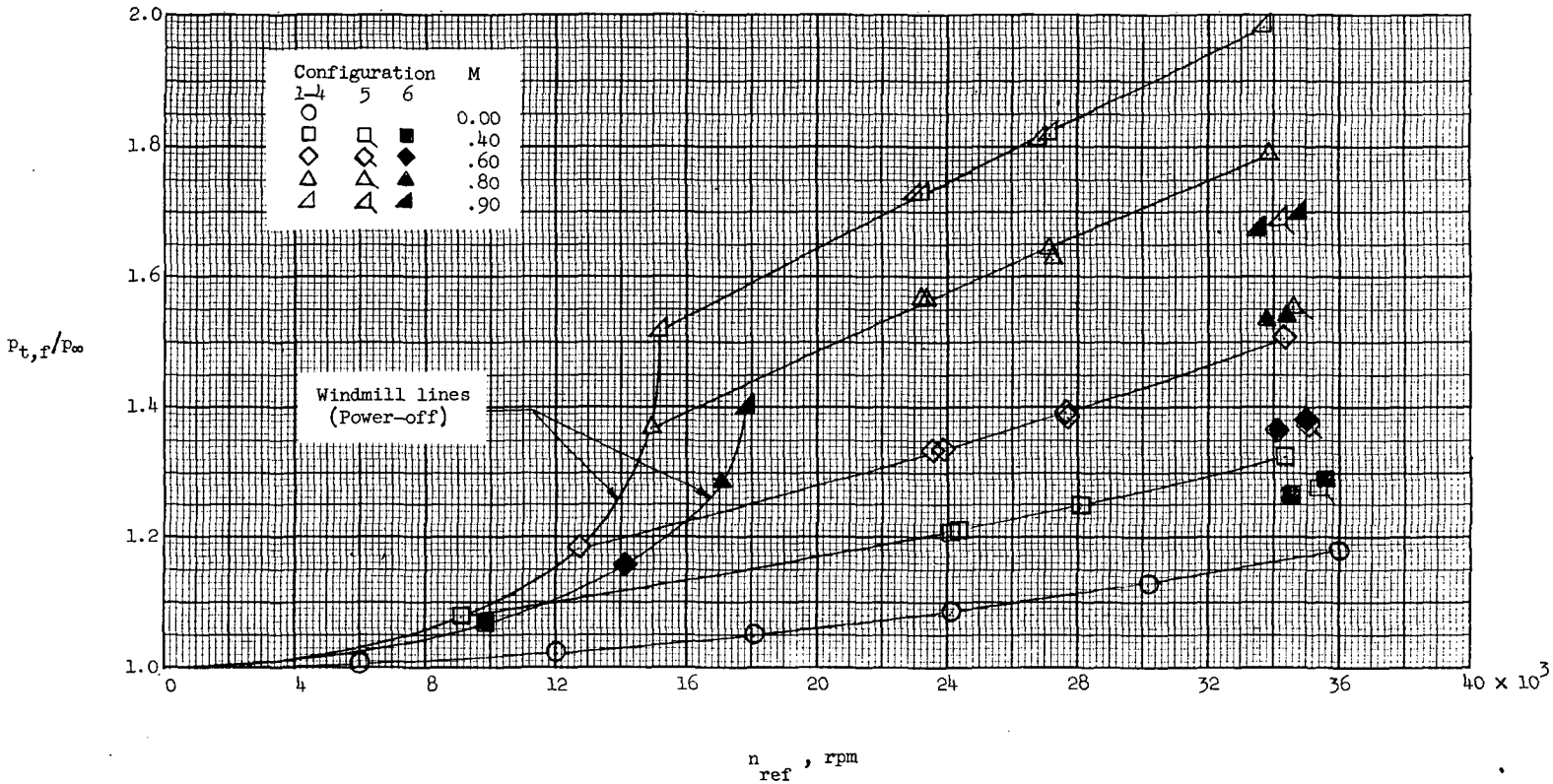

(d) Pressure ratio $p_{t,f}/p_\infty$.

Figure 12.- Concluded.

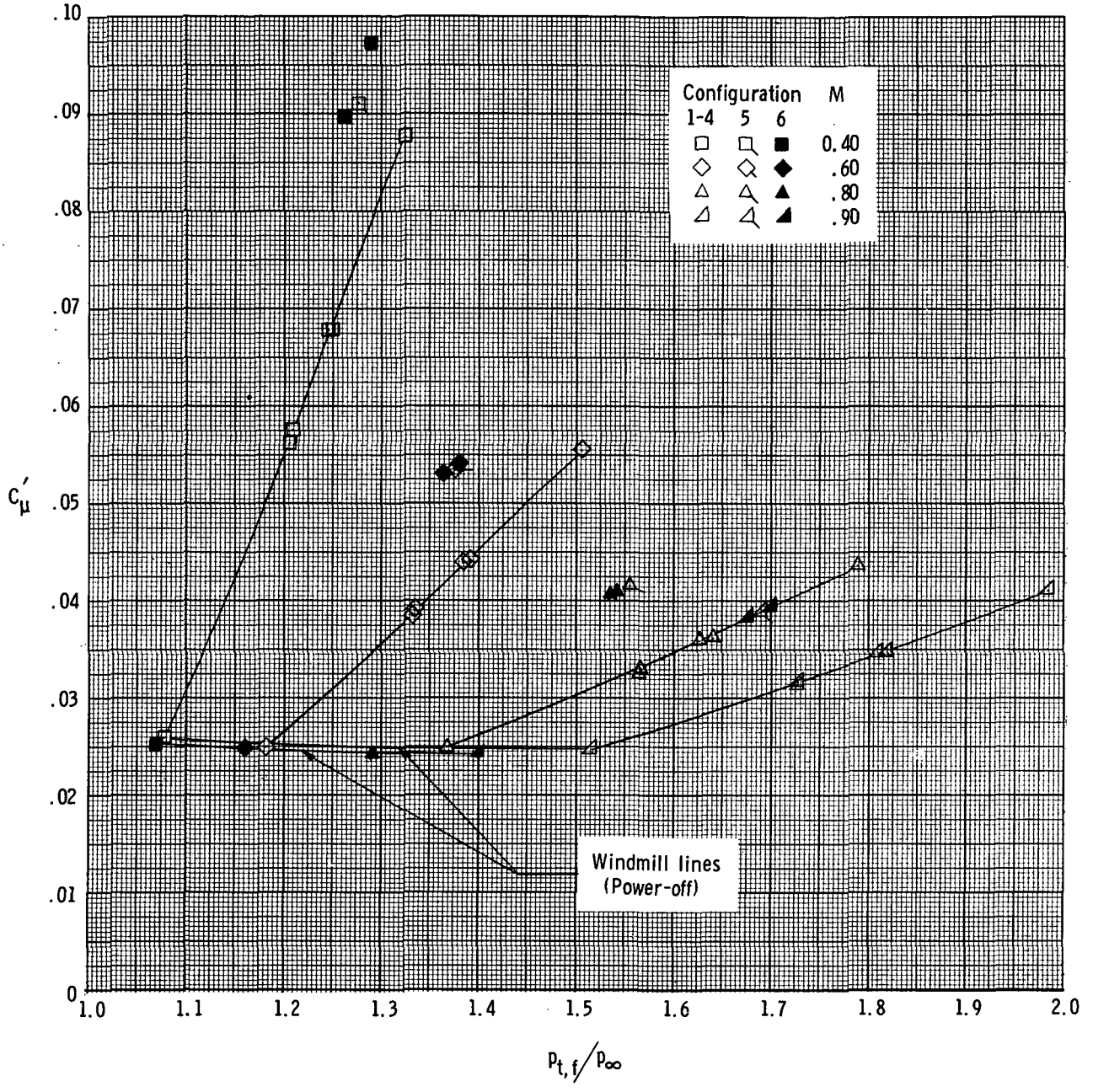

(a) Gross-thrust coefficient C'_μ.

Figure 13.- Effect of fan efflux pressure ratio on internal aerodynamic characteristics at $\alpha = 0^{\circ}$, fan 1.

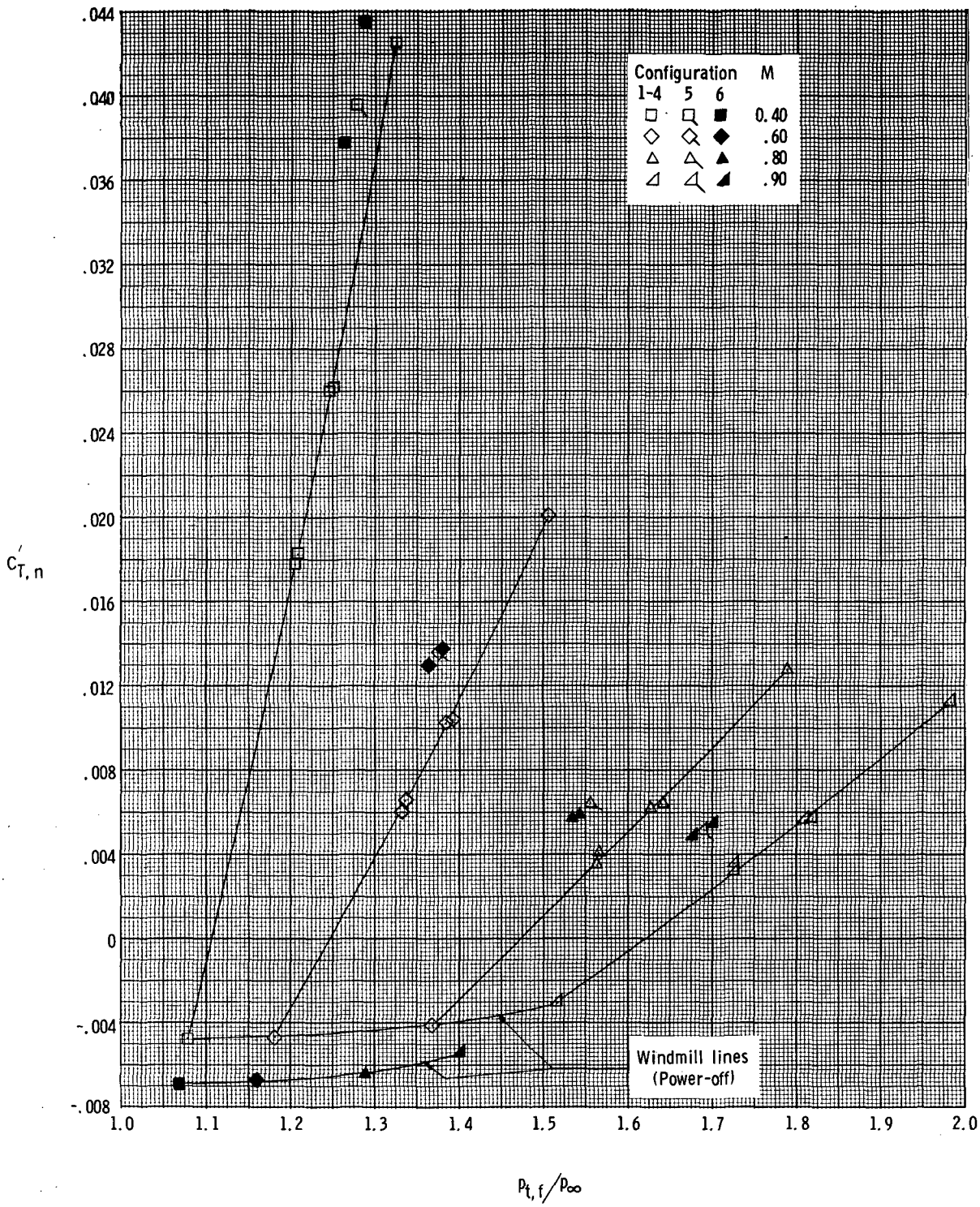

(b) Net-thrust coefficient $C'_{T,n}$.

Figure 13.- Concluded.

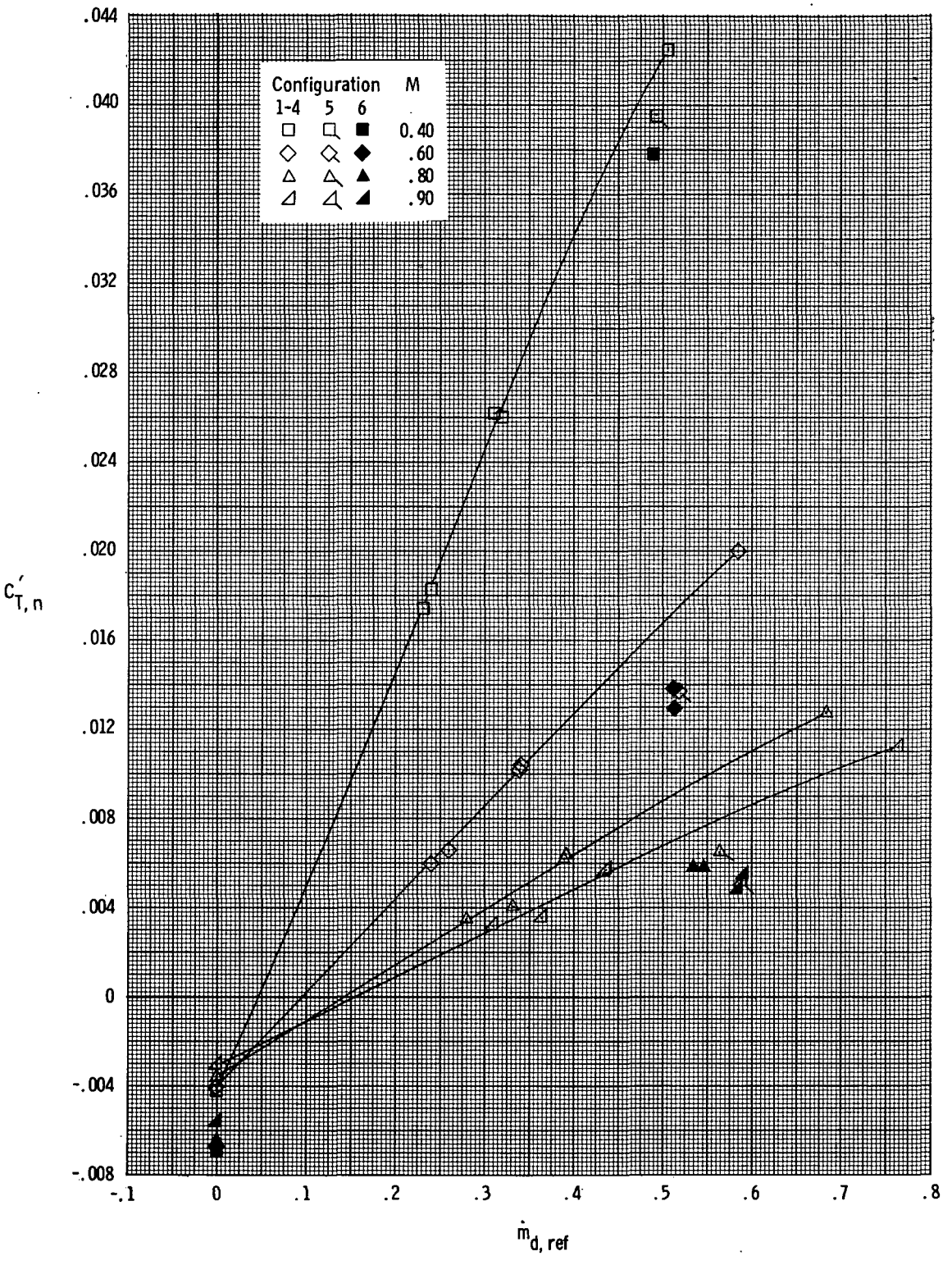

Figure 14.- Variation of net-thrust coefficient with fan-drive-air mass flow, fan 1; $\alpha = 0^{o}$.

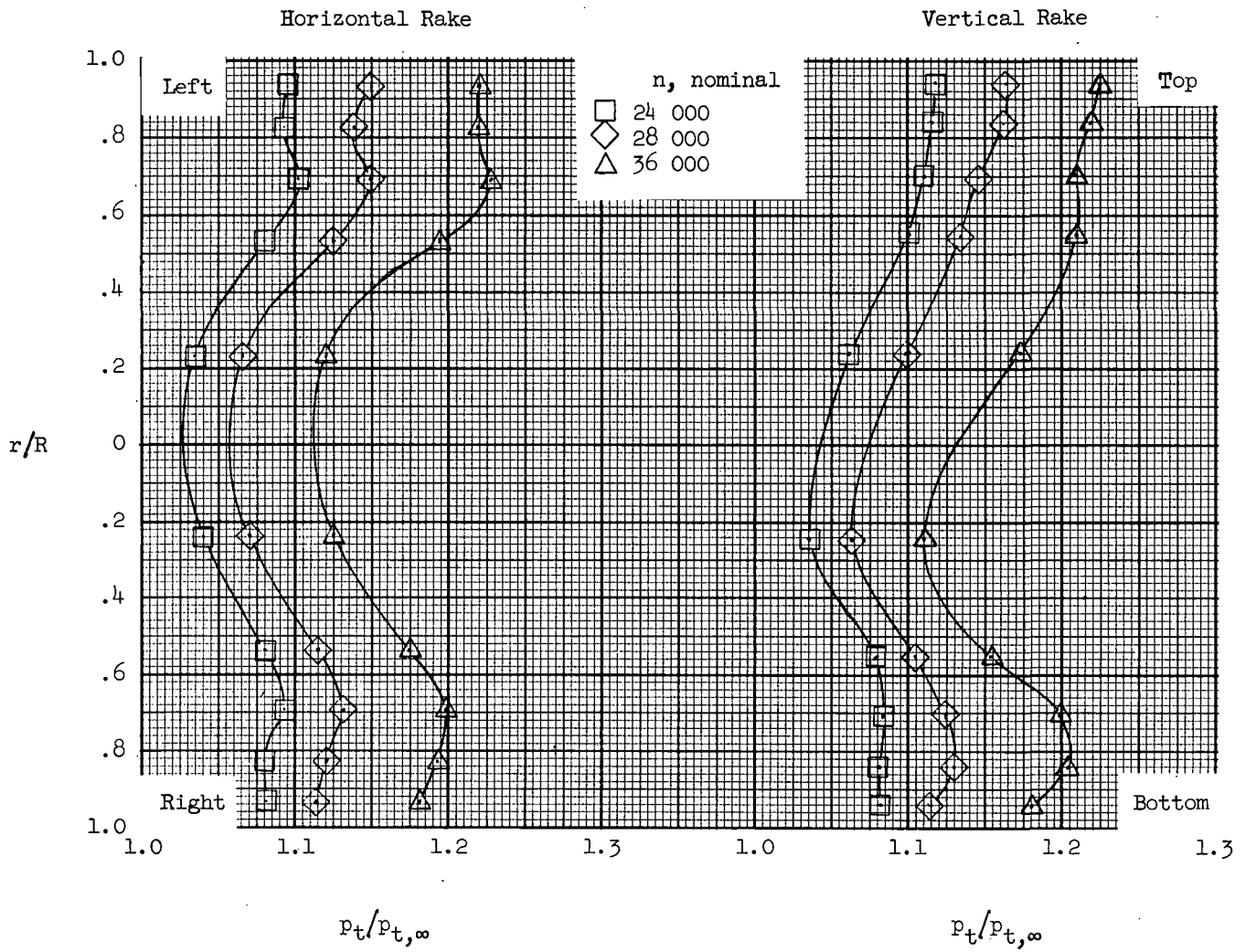

(a) Configuration 1, M = 0.40.

Figure 15.- Efflux rake total-pressure distributions at $\alpha = 0^o$, fan 1.

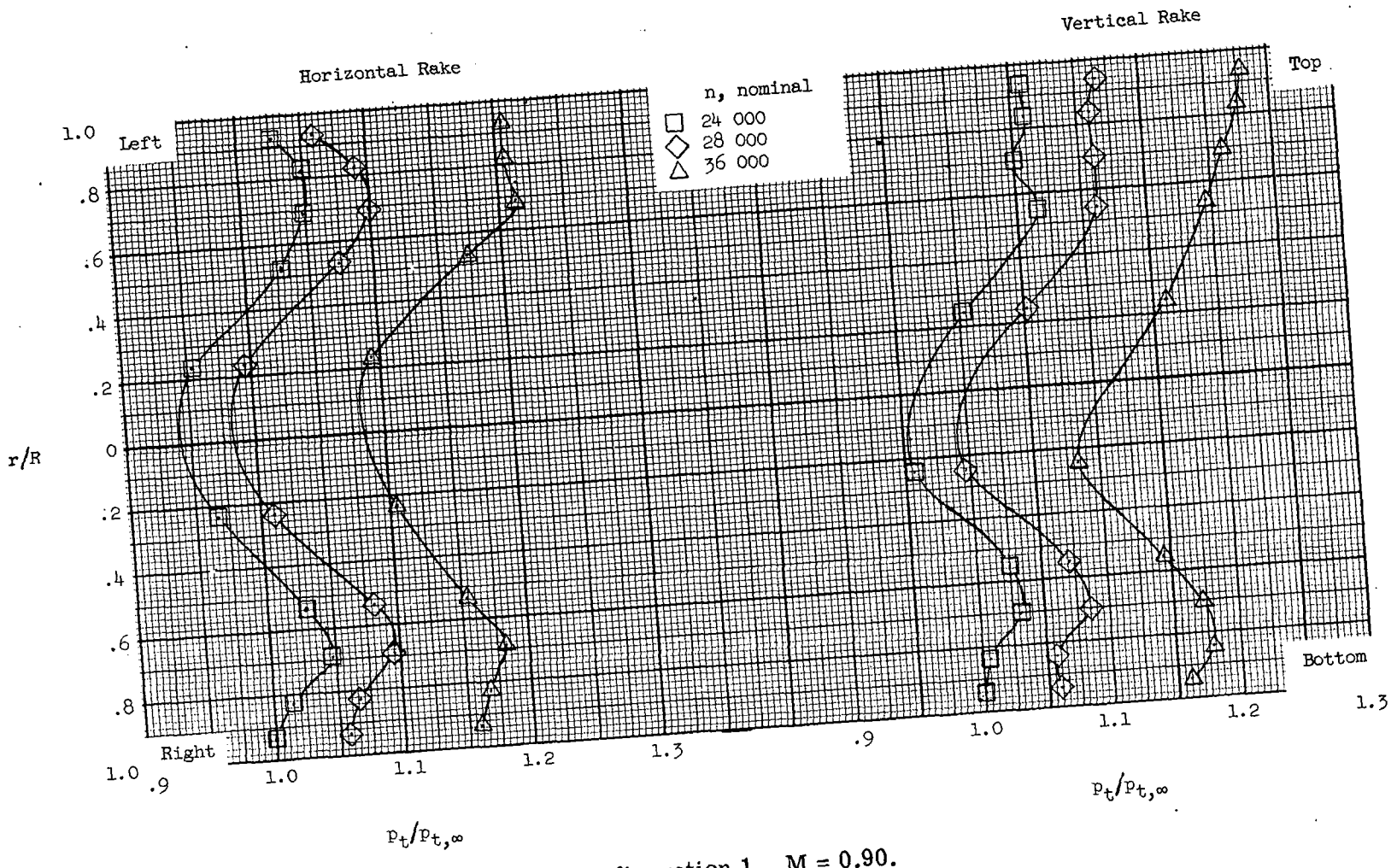

(b) Configuration 1, M = 0.90.

Figure 15.- Continued.

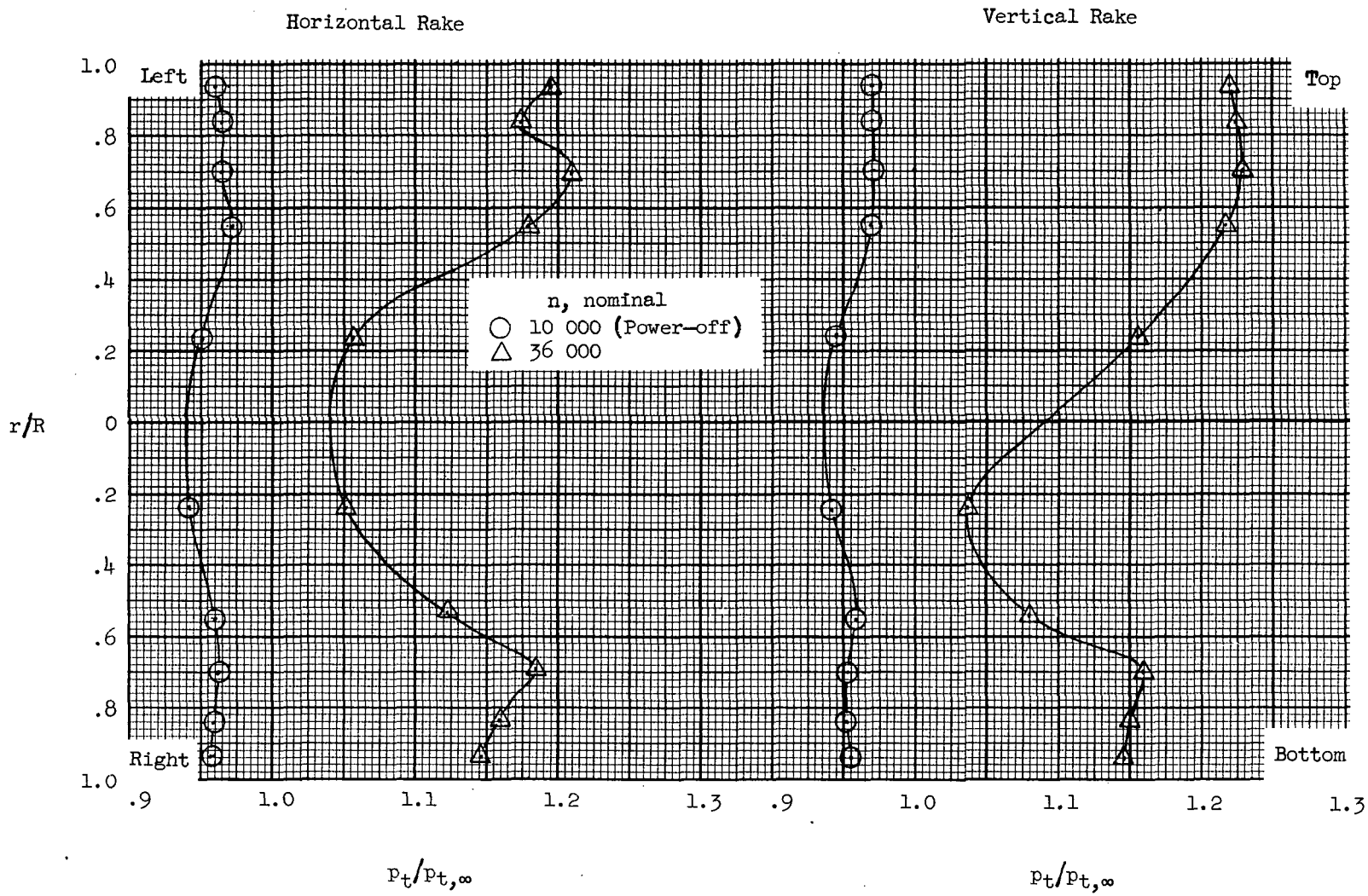

(c) Configuration 6, M = 0.40.

Figure 15.- Continued.

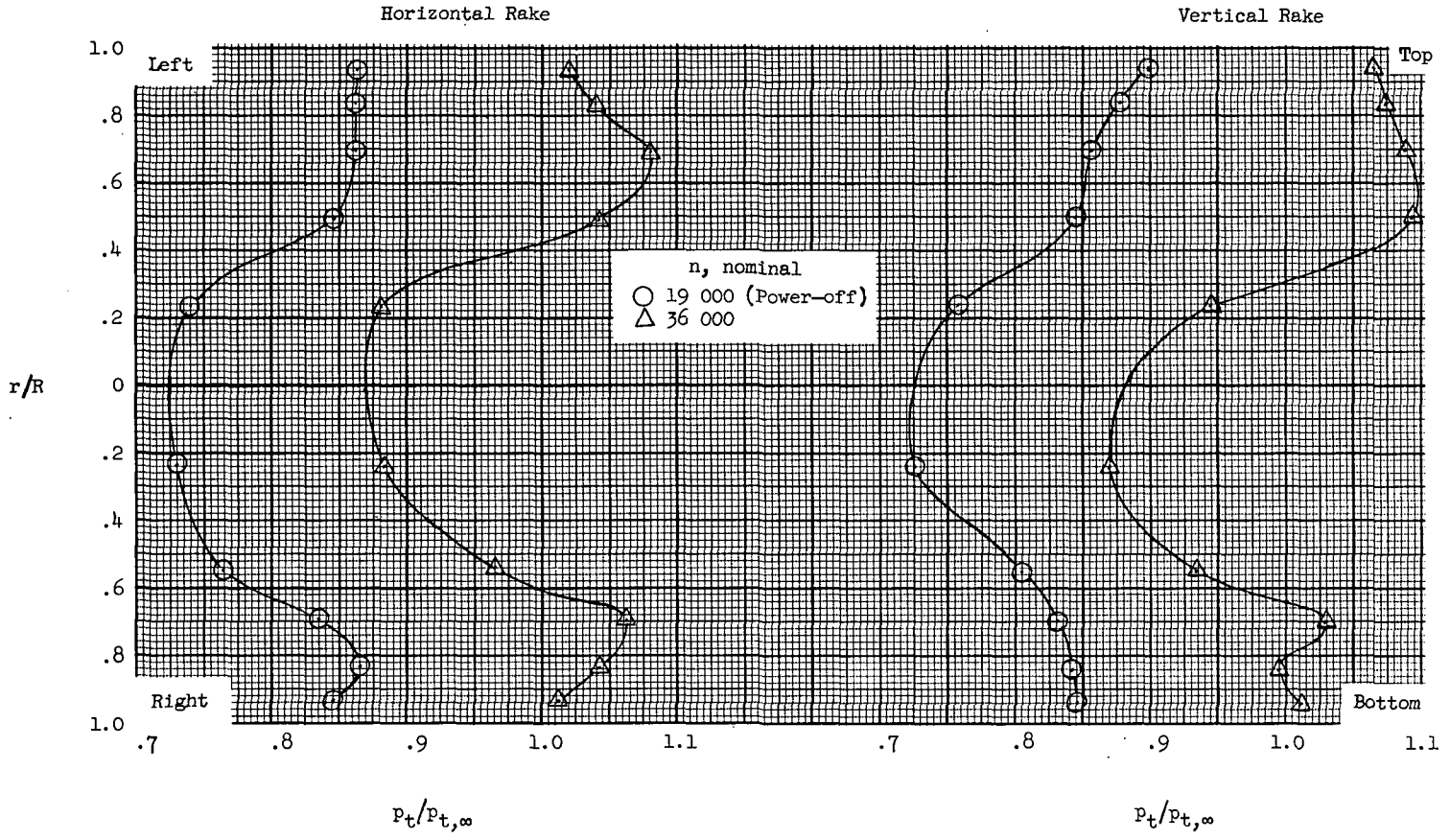

(d) Configuration 6, M = 0.90.

Figure 15.- Concluded.

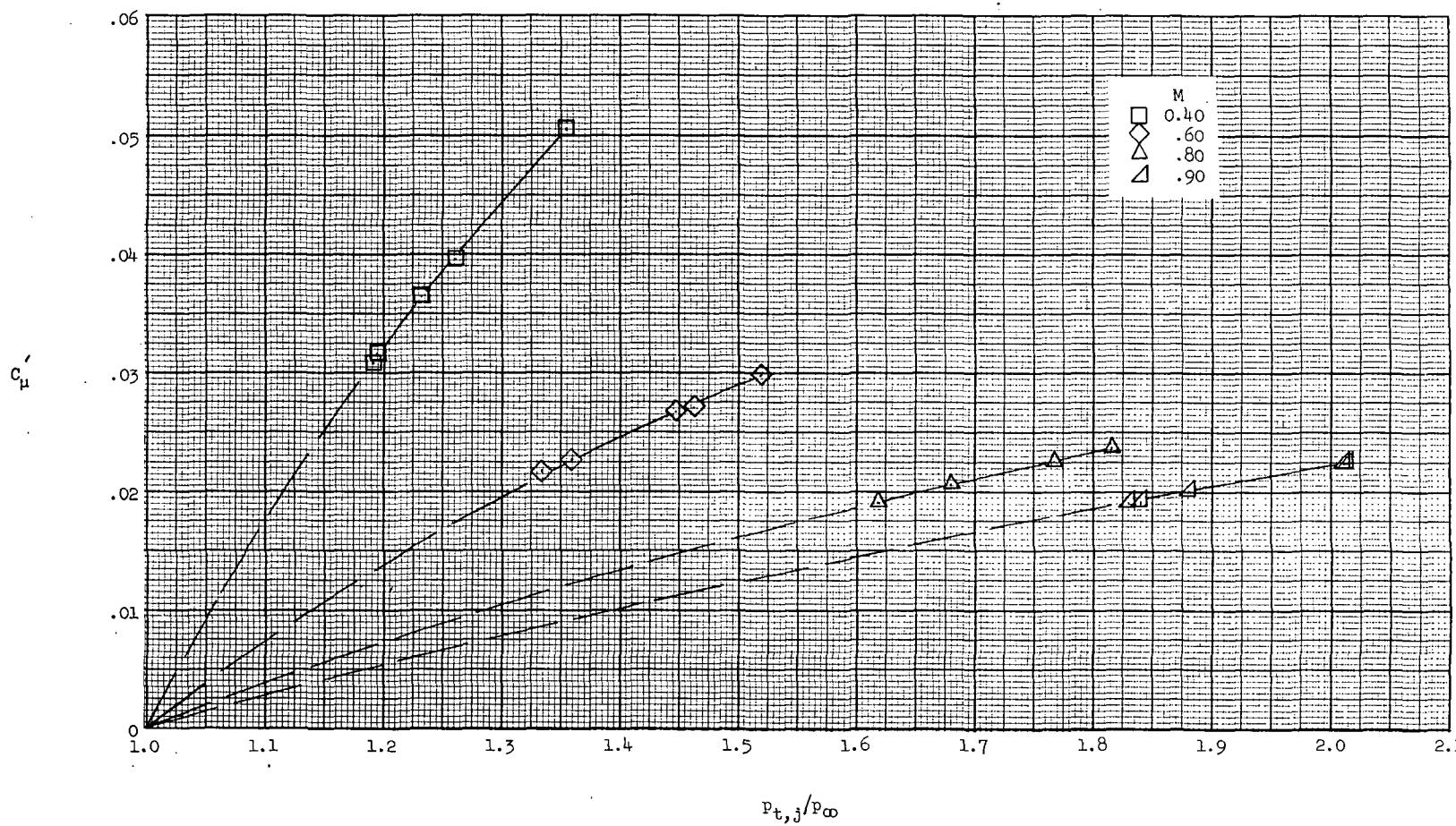

(a) Variation of C_μ'.

Figure 16.- Effect of efflux pressure ratio on left-flap-jet flow characteristics at $\alpha = 0^o$.

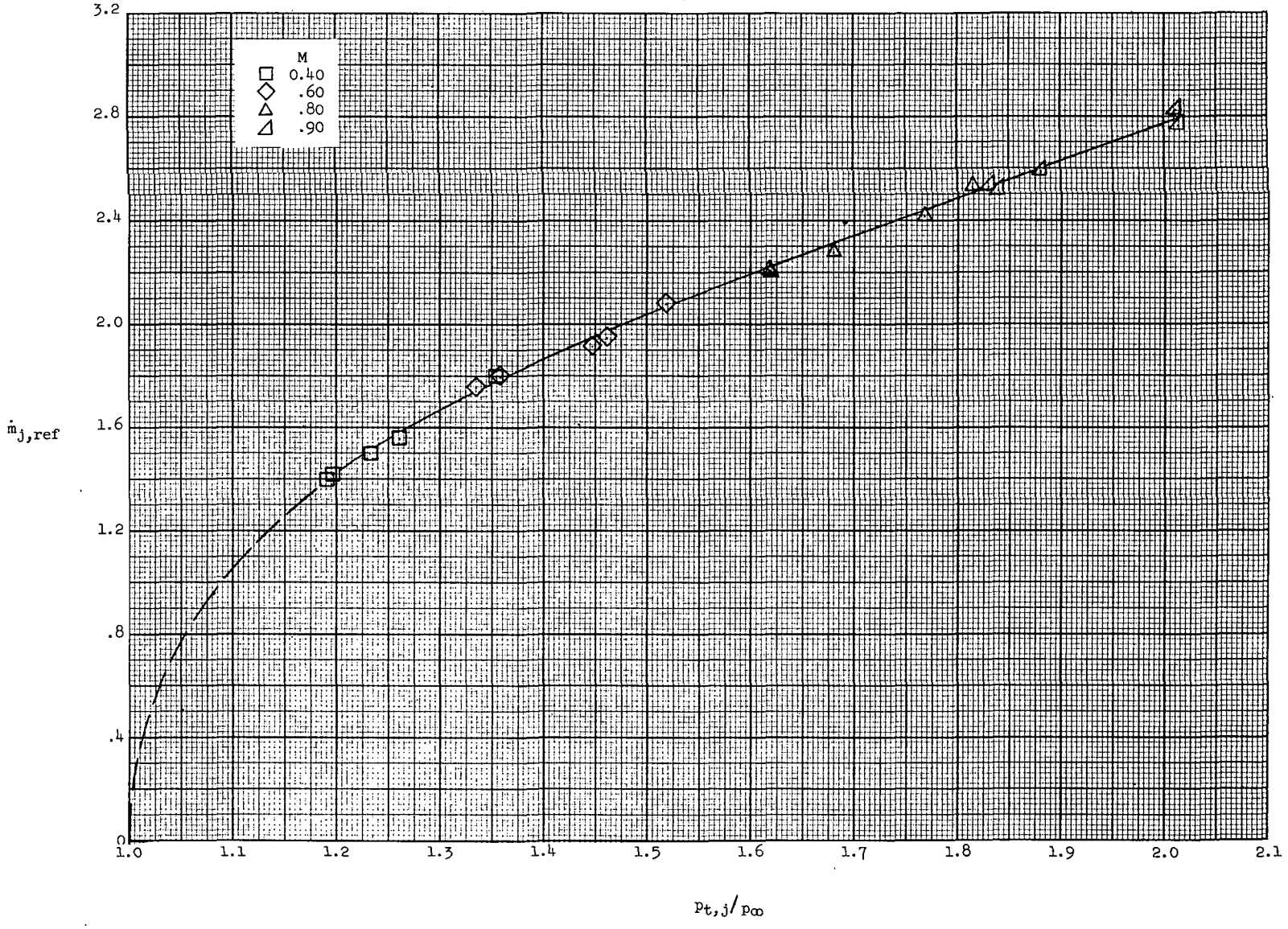

(b) Variation of mass flow.

Figure 16.- Concluded.

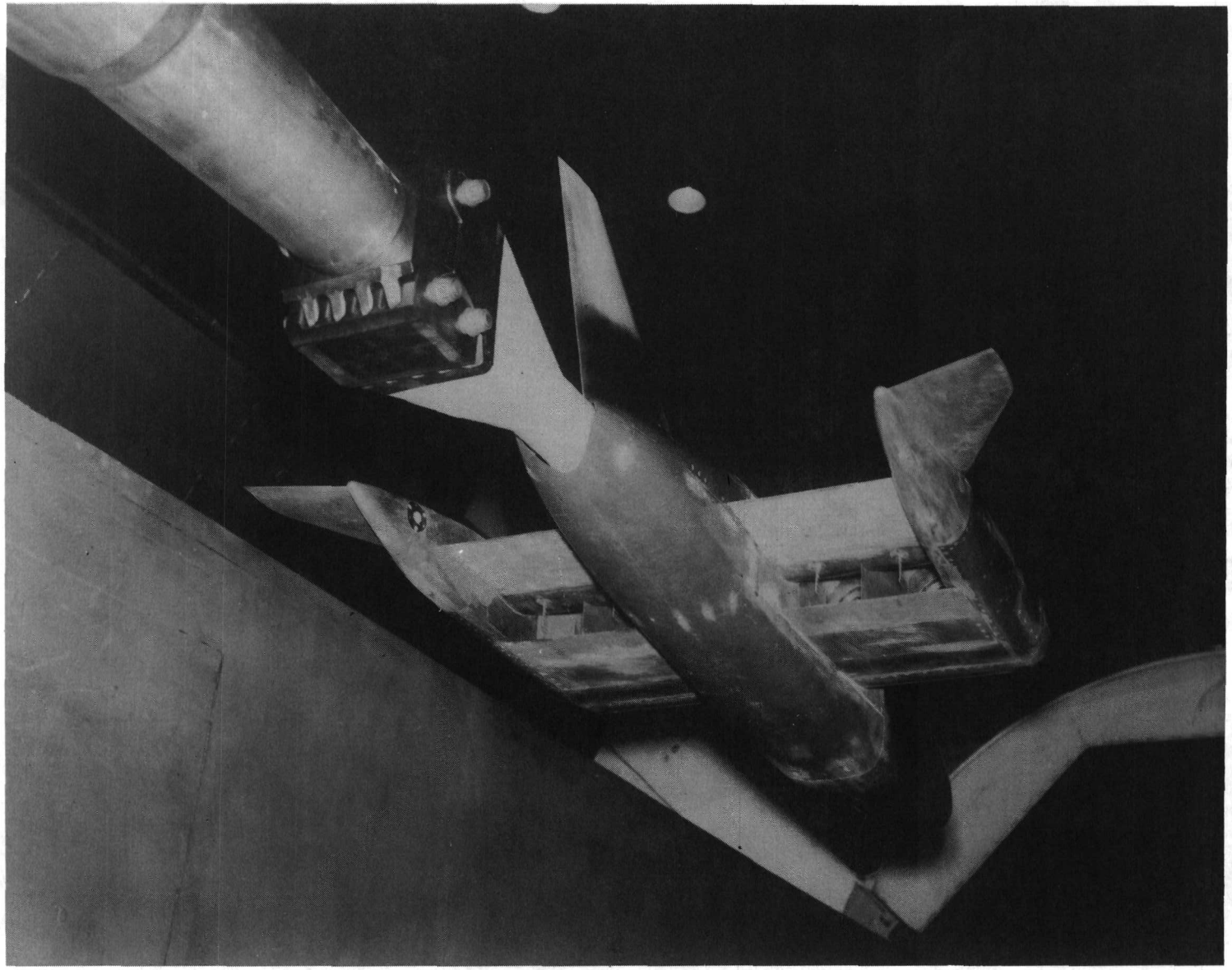

L-67-5321

(a) Photograph of sting-knuckle installed.

Figure 17.- Sting-knuckle details and location of aft-fuselage static pressure orifices.

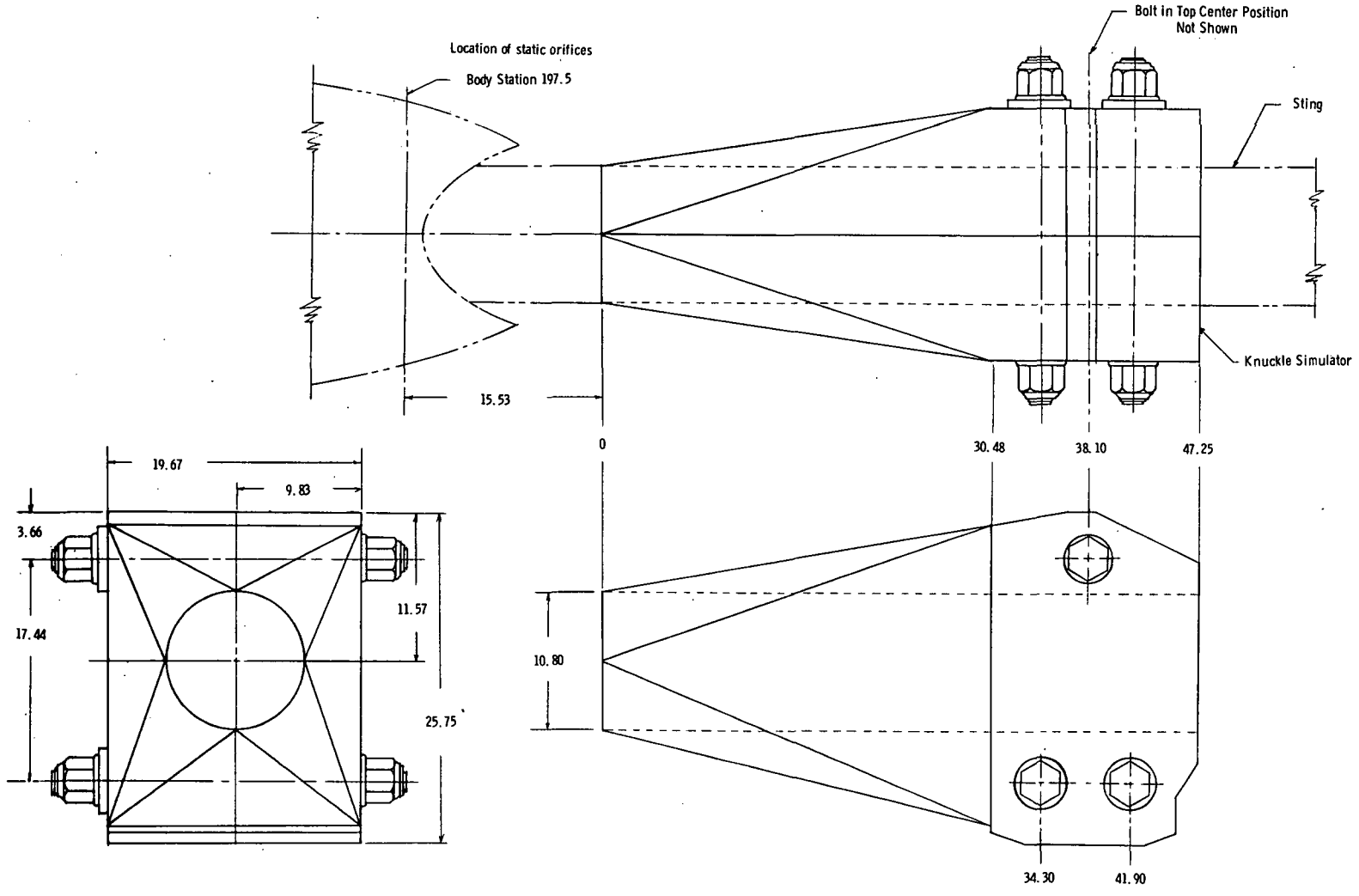

(b) Sketch of sting-knuckle simulator. All dimensions in cm.

Figure 17.- Continued.

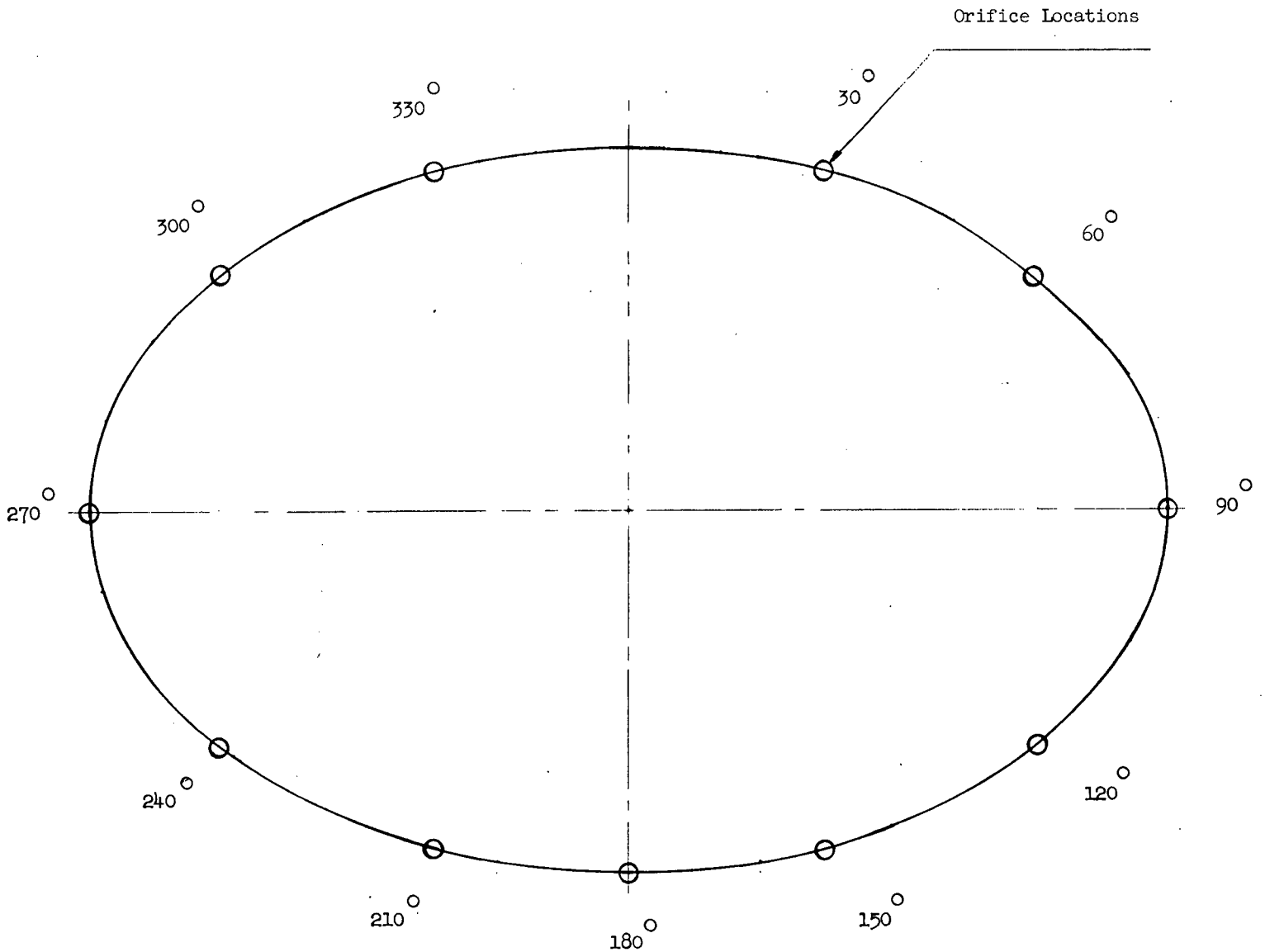

(c) Location of aft-fuselage static pressure orifices at station 197.5, looking forward.

Figure 17.- Concluded.

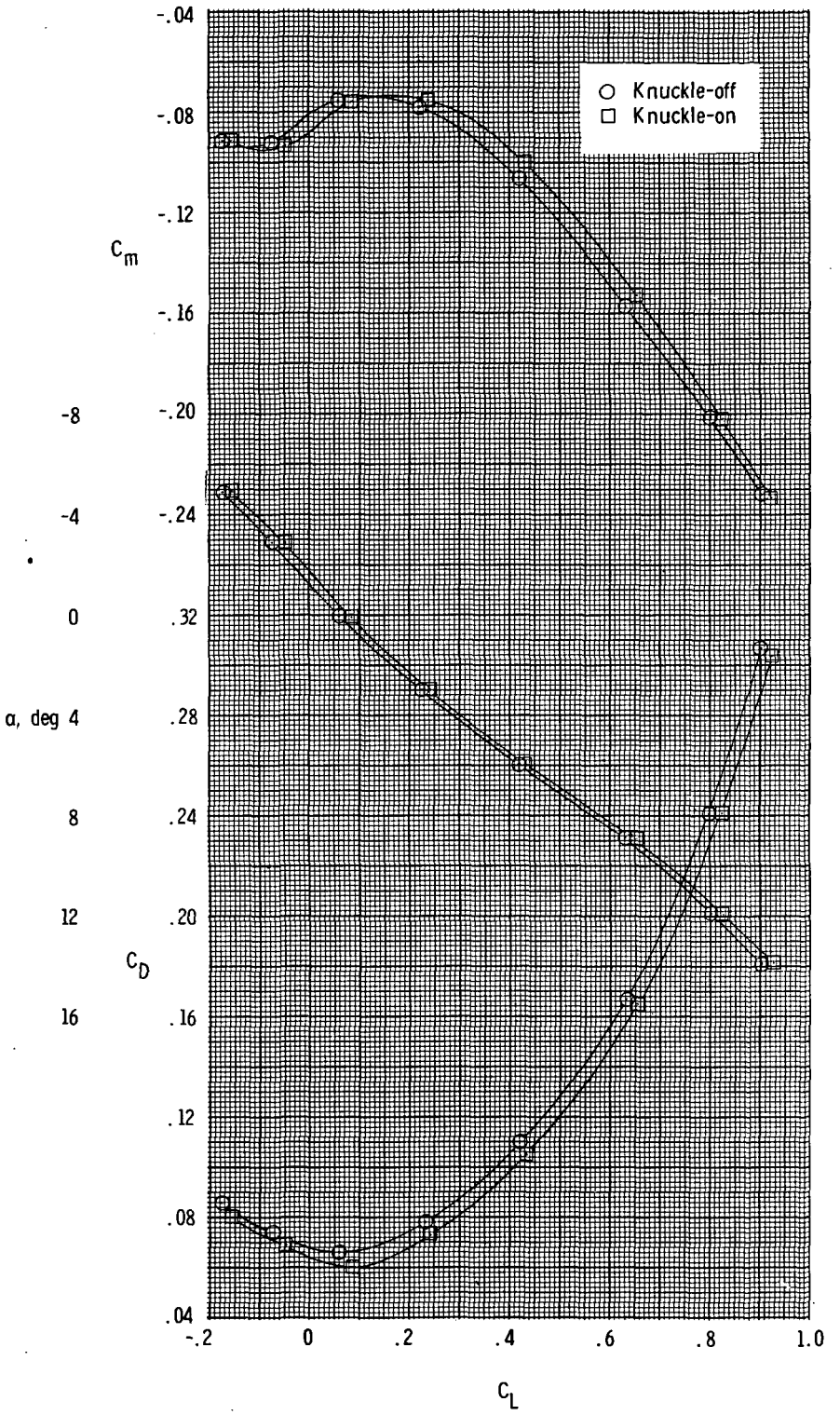

(a) M = 0.40.

Figure 18.- Effect of sting-knuckle interference on longitudinal aerodynamic characteristics, configuration 6; $\alpha = 0^{o}$; power-off.

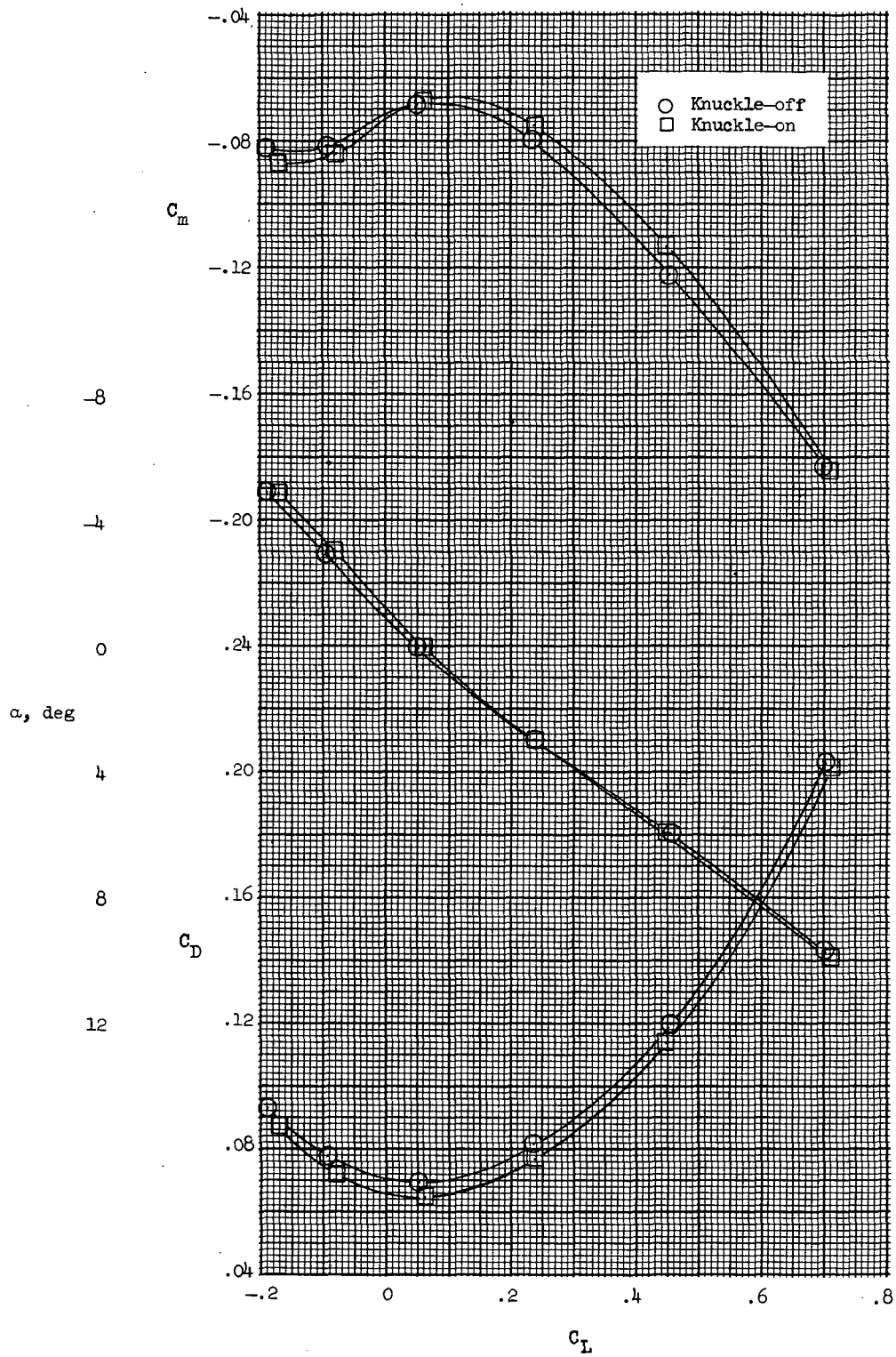

(b) M = 0.60.

Figure 18.- Continued.

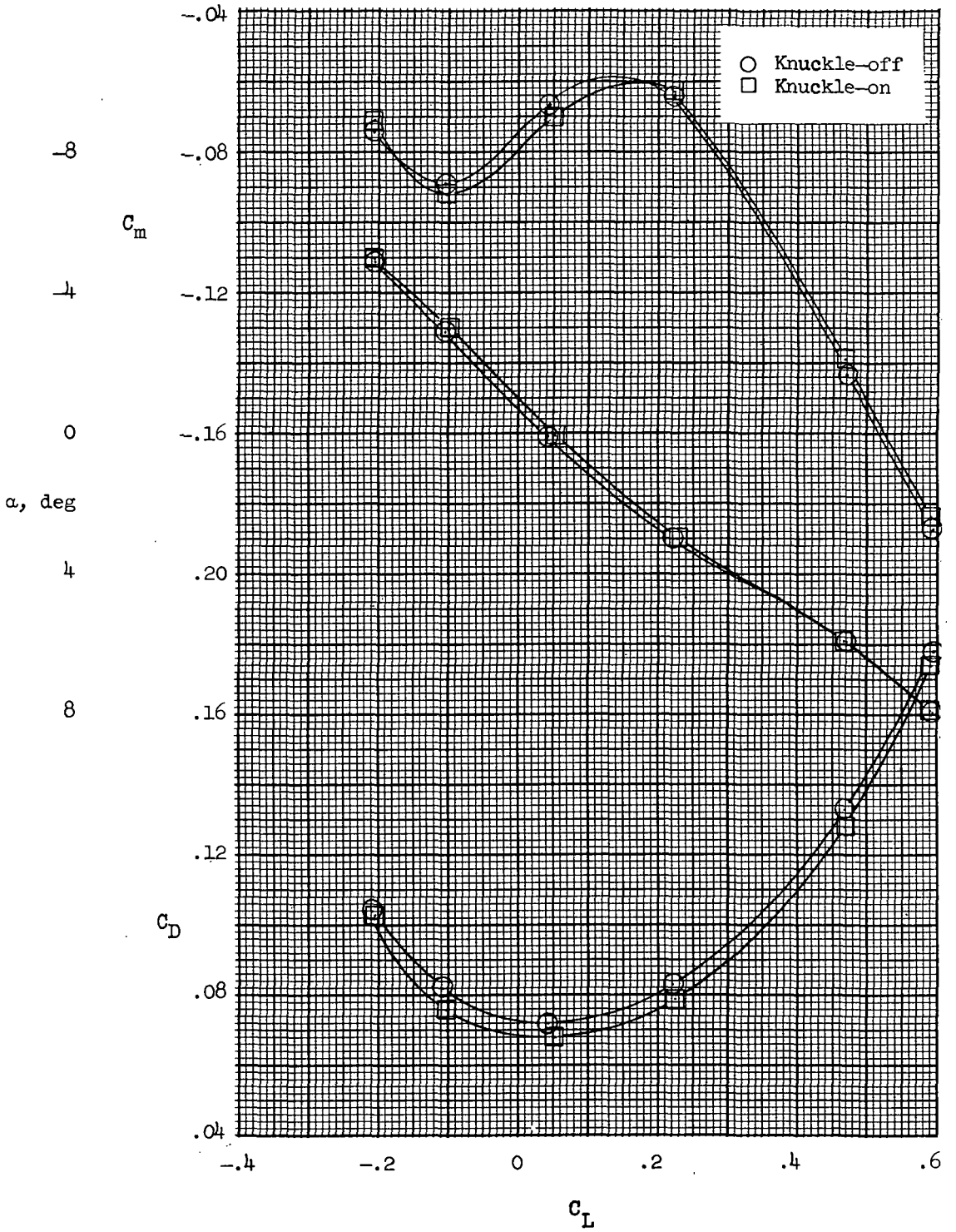

(c) M = 0.80.

Figure 18.- Continued.

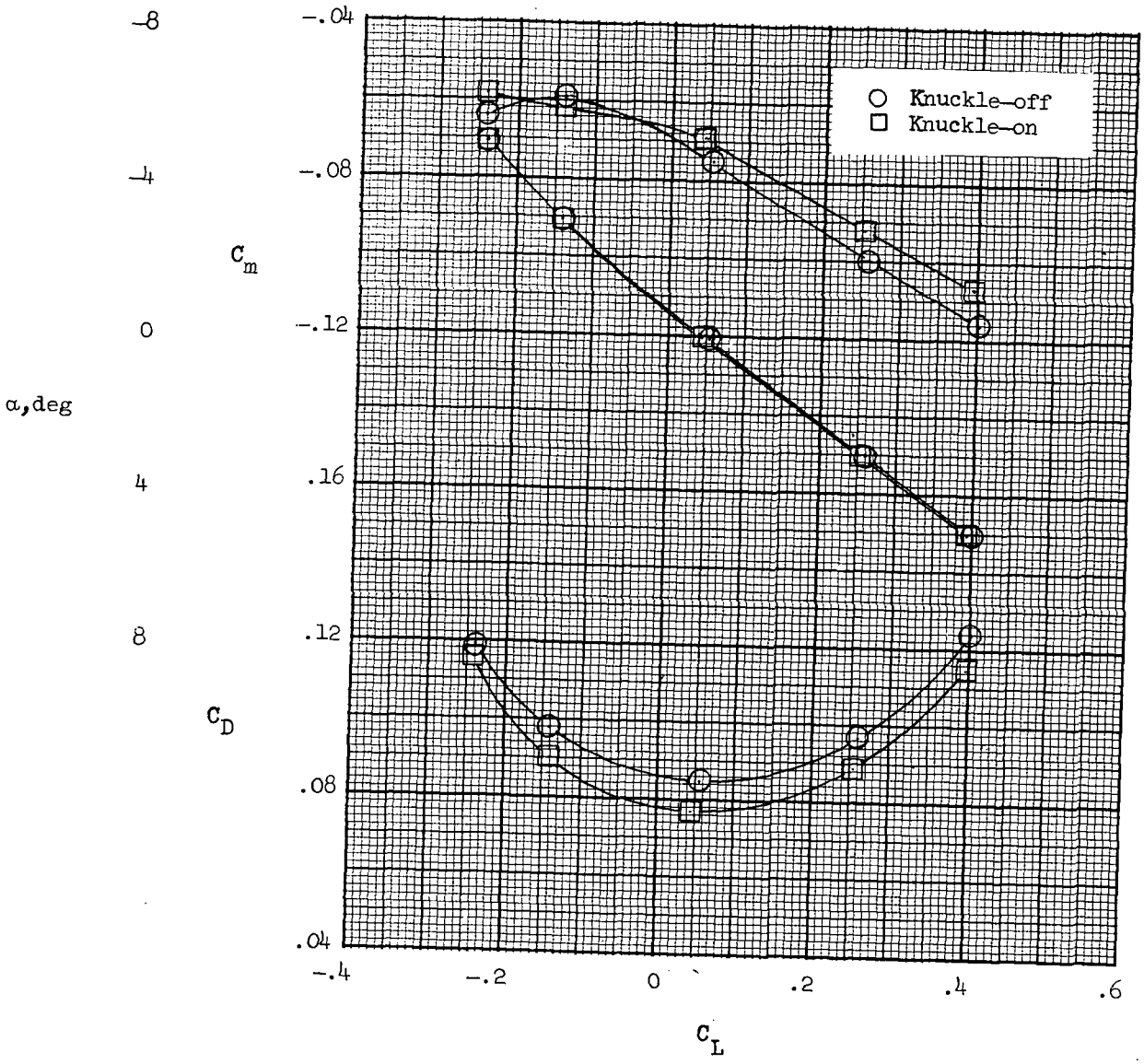

(d) M = 0.90.

Figure 18.- Concluded.

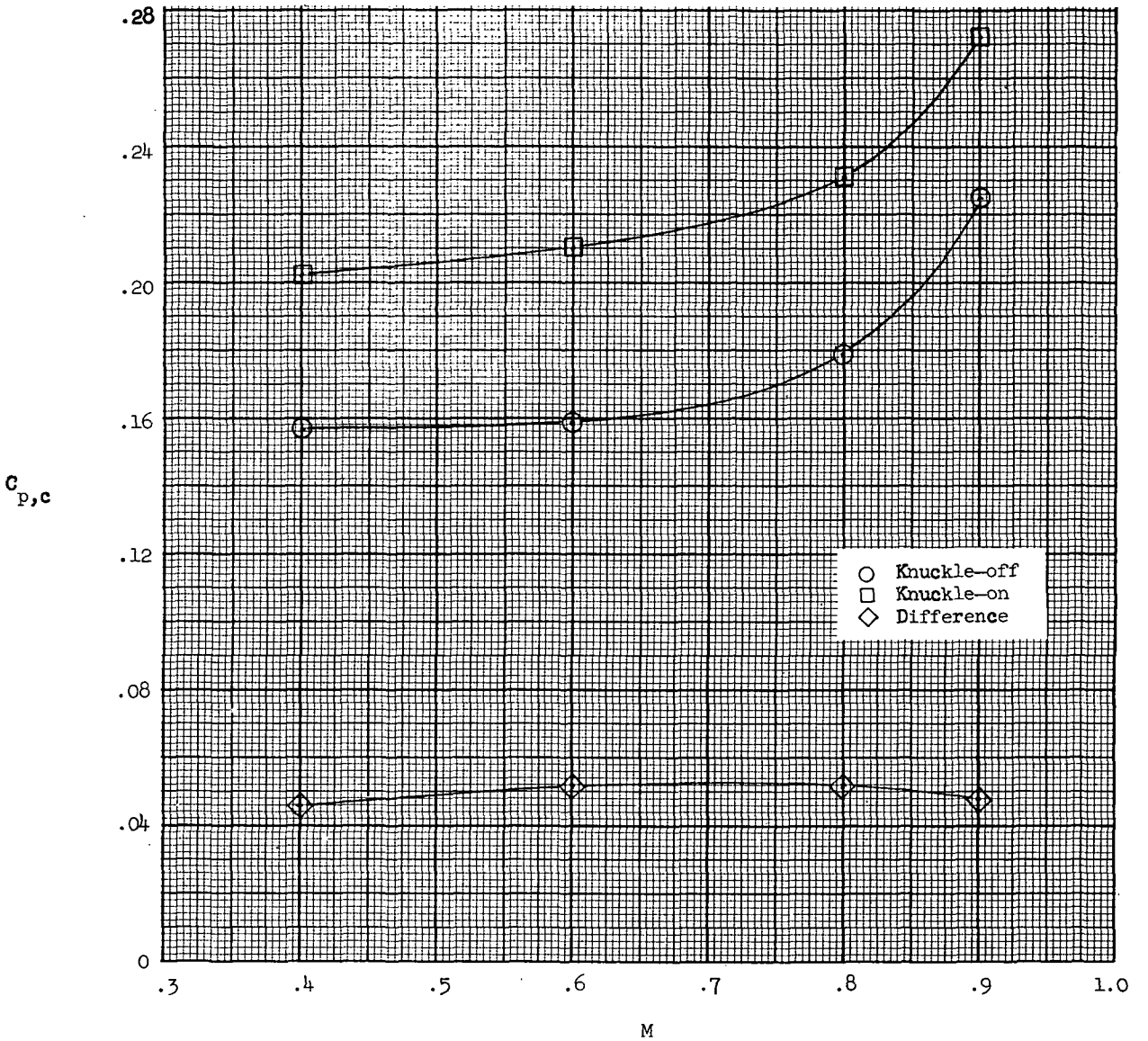

(a) $\alpha = 0^{o}$.

Figure 19.- Effect of sting-knuckle interference on fuselage-cavity pressure, configuration 6; power-off.

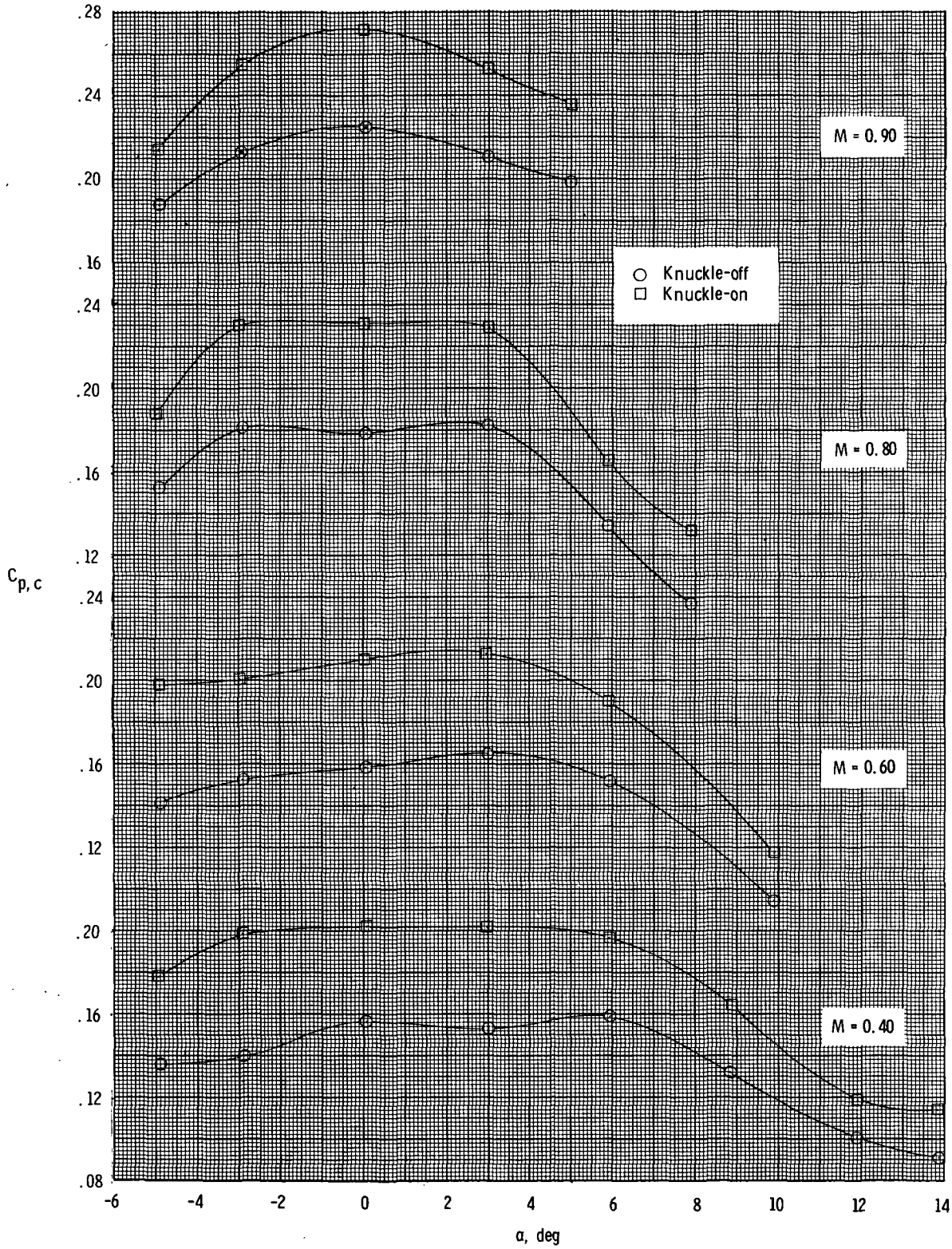

(b) Variable α.

Figure 19.- Concluded.

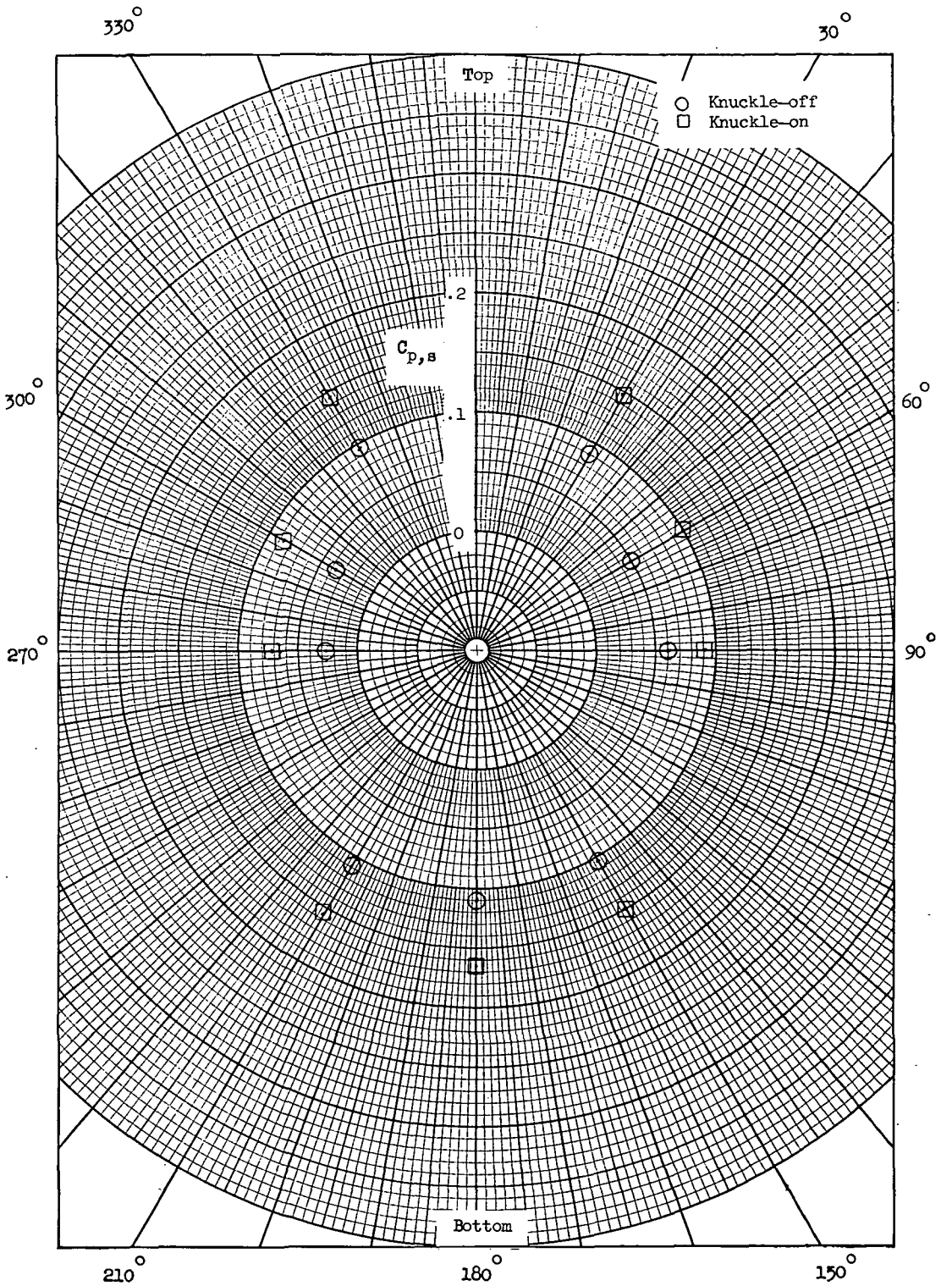

(a) M = 0.40.

Figure 20.- Effect of sting-knuckle on afterbody surface pressures, configuration 6; $\alpha = 0^{o}$; power-off; looking forward.

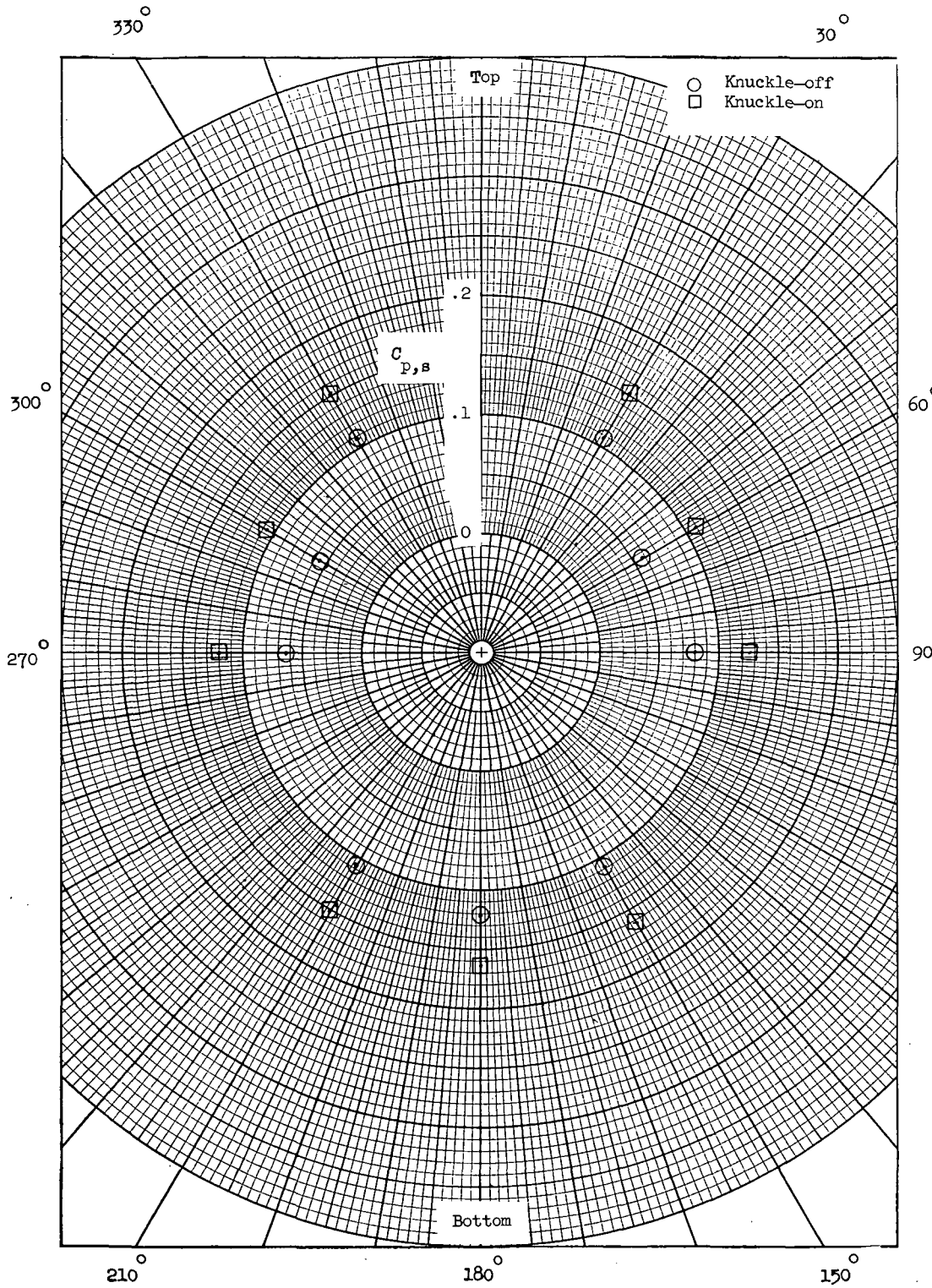

(b) M = 0.60.

Figure 20.- Continued.

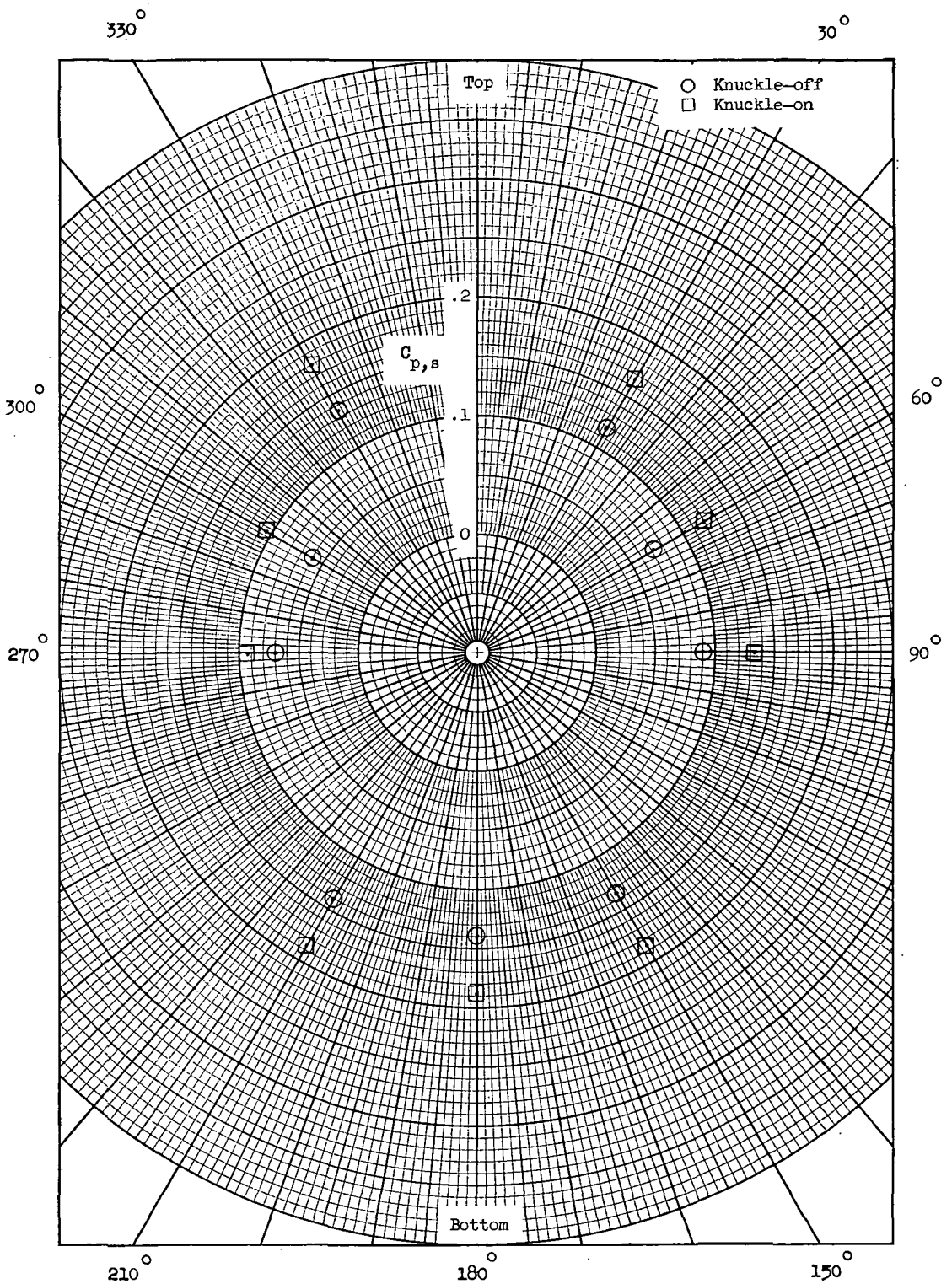

(c) M = 0.80.

Figure 20.- Continued.

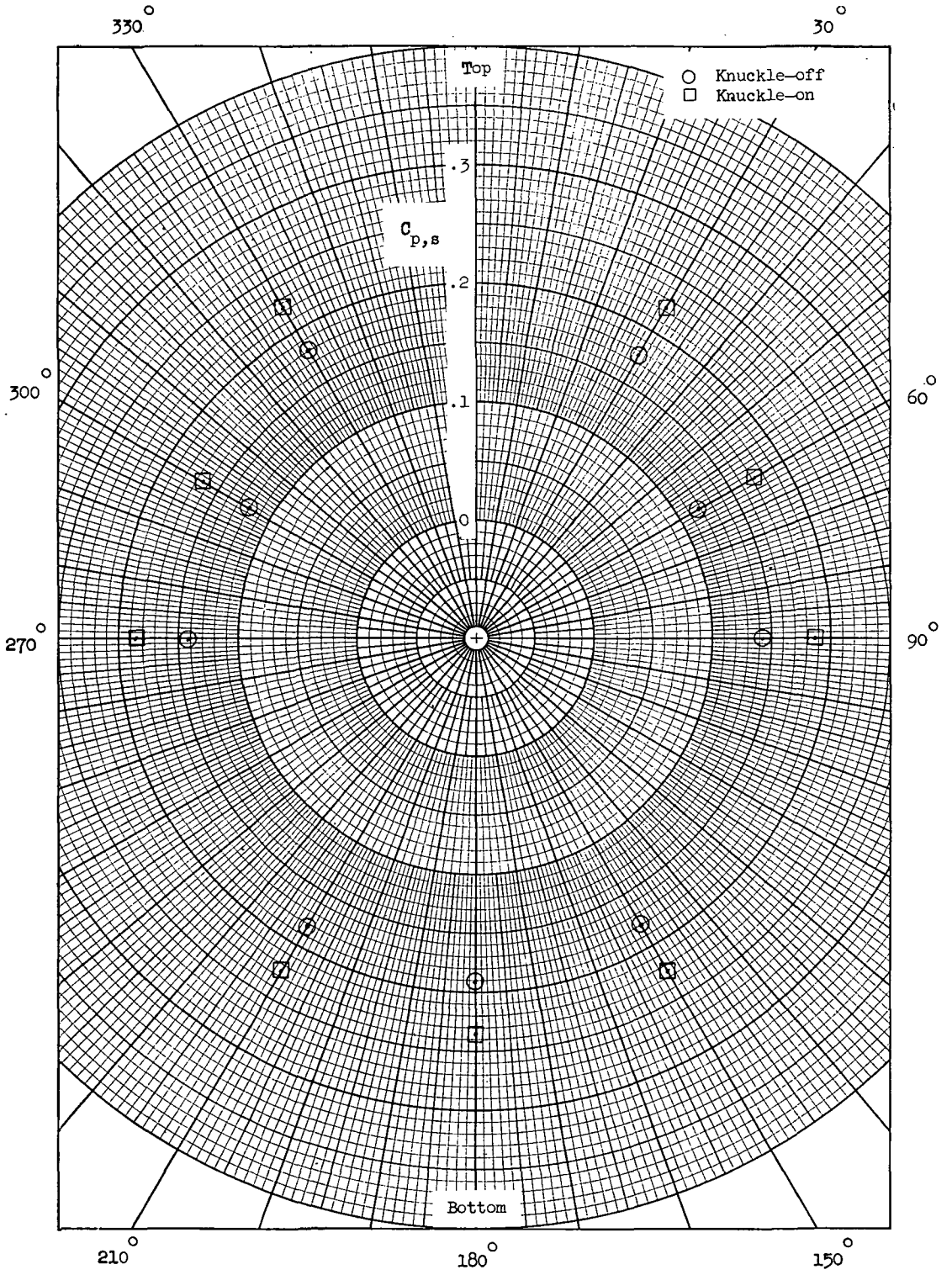

(d) M = 0.90.

Figure 20.- Concluded.

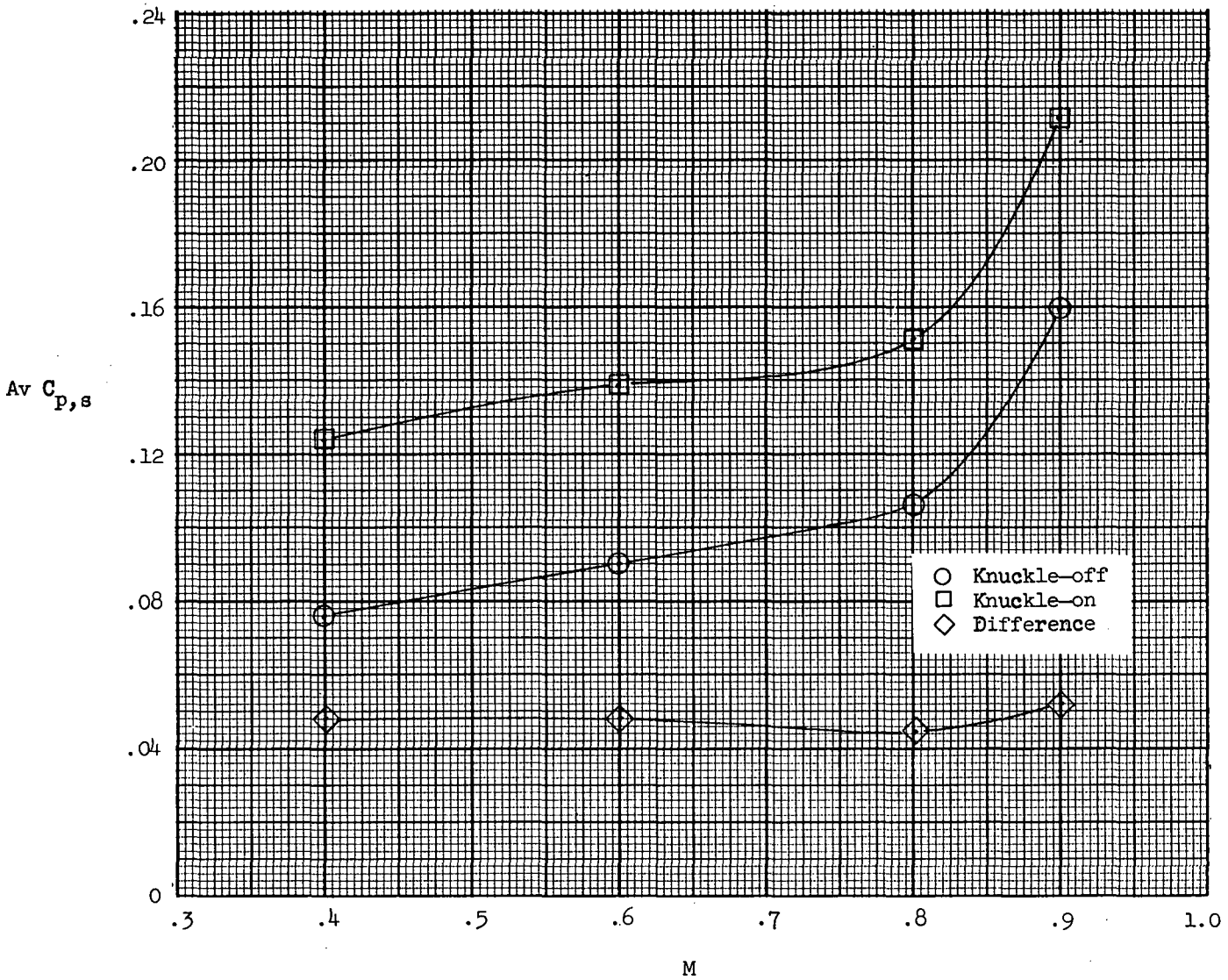

Figure 21.- Effect of sting-knuckle interference on averaged afterbody surface pressures at station 197.5, $\alpha = 0^{o}$; power-off.

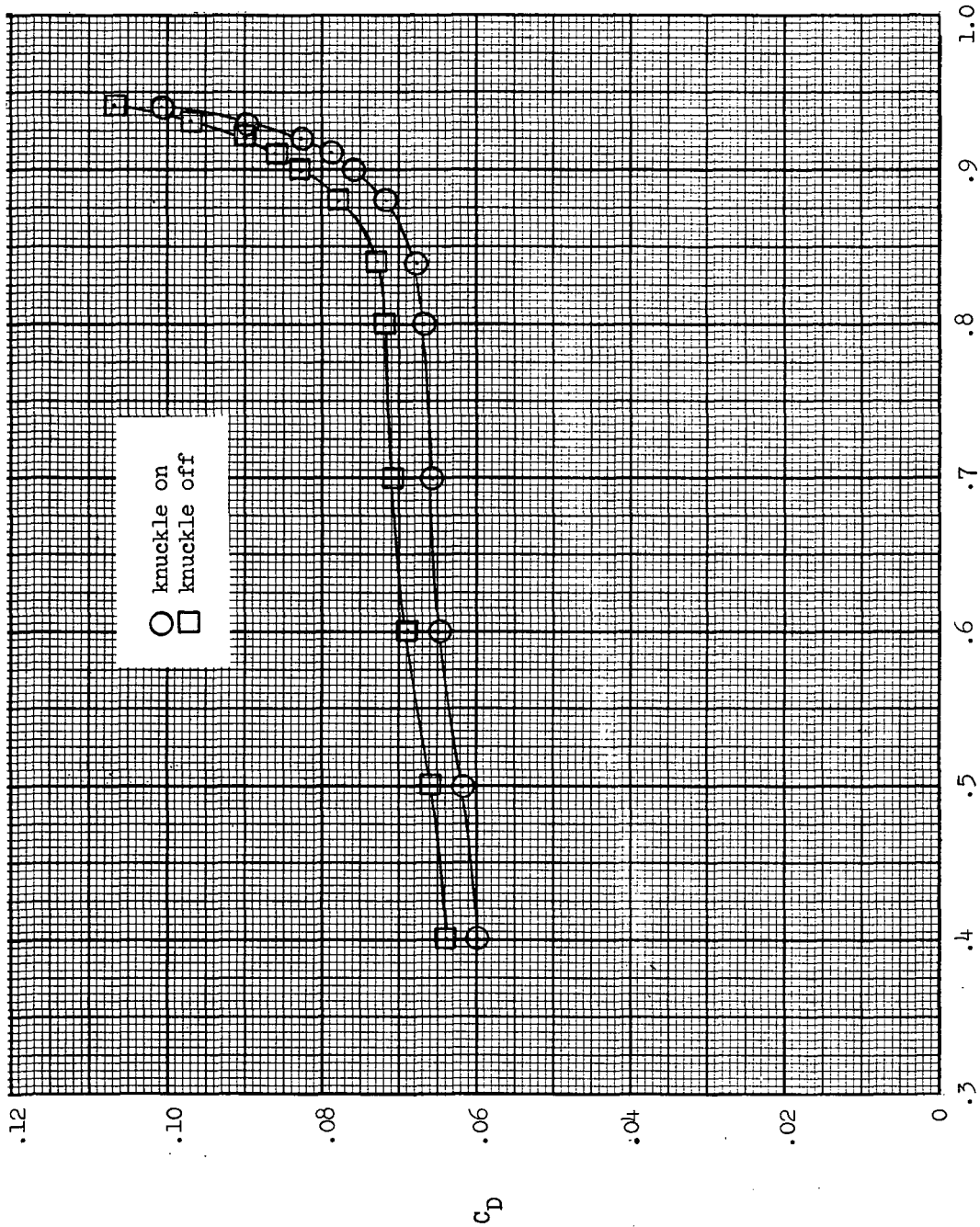

Figure 22.- Effect of knuckle on drag-rise characteristics, configuration 6; $\alpha = 0^{o}$.

NASA-Langley, 1973 — L-8500

NATIONAL AERONAUTICS AND SPACE ADMINISTRATION
WASHINGTON, D.C. 20546

OFFICIAL BUSINESS
PENALTY FOR PRIVATE USE $300

SPECIAL FOURTH-CLASS RATE
BOOK

POSTAGE AND FEES PAID
NATIONAL AERONAUTICS AND
SPACE ADMINISTRATION
451

U.S.MAIL

POSTMASTER : If Undeliverable (Section 158 Postal Manual) Do Not Return

"The aeronautical and space activities of the United States shall be conducted so as to contribute . . . to the expansion of human knowledge of phenomena in the atmosphere and space. The Administration shall provide for the widest practicable and appropriate dissemination of information concerning its activities and the results thereof."

—NATIONAL AERONAUTICS AND SPACE ACT OF 1958

NASA SCIENTIFIC AND TECHNICAL PUBLICATIONS

TECHNICAL REPORTS: Scientific and technical information considered important, complete, and a lasting contribution to existing knowledge.

TECHNICAL NOTES: Information less broad in scope but nevertheless of importance as a contribution to existing knowledge.

TECHNICAL MEMORANDUMS: Information receiving limited distribution because of preliminary data, security classification, or other reasons. Also includes conference proceedings with either limited or unlimited distribution.

CONTRACTOR REPORTS: Scientific and technical information generated under a NASA contract or grant and considered an important contribution to existing knowledge.

TECHNICAL TRANSLATIONS: Information published in a foreign language considered to merit NASA distribution in English.

SPECIAL PUBLICATIONS: Information derived from or of value to NASA activities. Publications include final reports of major projects, monographs, data compilations, handbooks, sourcebooks, and special bibliographies.

TECHNOLOGY UTILIZATION PUBLICATIONS: Information on technology used by NASA that may be of particular interest in commercial and other non-aerospace applications. Publications include Tech Briefs, Technology Utilization Reports and Technology Surveys.

Details on the availability of these publications may be obtained from:

SCIENTIFIC AND TECHNICAL INFORMATION OFFICE

NATIONAL AERONAUTICS AND SPACE ADMINISTRATION

Washington, D.C. 20546